BNL-99200-2013-TECH
C-A/AP/47;BNL-99200-2013-IR

Electron Cooling for RHIC

V. Parkhomchuk

April 2001

Collider Accelerator Department
Brookhaven National Laboratory

U.S. Department of Energy
USDOE Office of Science (SC)

DISCLAIMER

C-A/AP/47
April 2001

Electron Cooling for RHIC

V. Parkhomchuk
Budker Institute of Nuclear Physics
I. Ben-Zvi
Brookhaven National Laboratory

Collider-Accelerator Department
Brookhaven National Laboratory
Upton, NY 11973

C-A/AP/47
April 2001

Electron Cooling for RHIC

V. Parkhomchuk
Budker Institute of Nuclear Physics
I. Ben-Zvi
Brookhaven National Laboratory

Collider-Accelerator Department
Brookhaven National Laboratory
Upton, NY 11973

ELECTRON COOLING

FOR RHIC

Review of the Principles of Electron Cooling for the Relativistic Heavy Ion Collider (RHIC)

Principal Investigators:

Vasily Parkhomchuk
parkhomchuk@inp.nsk.su
Budker Institute of Nuclear Physics,
Novosibirsk, 630090

Ilan Ben-Zvi
ilan@bnl.gov
Collider-Accelerator Department
And
National Synchrotron Light Source
Brookhaven National Laboratory
Upton NY 11973-5000

ELECTRON COOLING FOR RHIC

Contents

INTRODUCTION

I.1 RHIC Gold-on-Gold collider parameters

The development of nuclear physics experimental research resulted in a sharp increase in the requirements for particle-beam quality. It is especially important to obtain beams of high density and low momentum spread. The luminosity of a collider is determined by the emittance ε of the bunches, the number of particles in the bunch N_i, the beta function at the interaction point β_{IP}, and the bunch repetition frequency f_b as

$$L = \frac{N_i \times N_i}{4\pi\varepsilon\beta_{IP}} f_b . \quad (1)$$

Cooling helps decrease the beam emittance, and decreasing the momentum spread Δp/p helps to achieve stronger focusing and smaller $\beta_{IP.}$ Without any cooling the normalized emittance of the ion beam increases by dilution at nonlinear elements of the transverse and longitudinal optics during injection and acceleration. If the ion source does not have a high brightness, it is impossible to reach maximal luminosity. For a luminosity limited by the beam-beam effect at the collision points equation (1) can be rewritten in the form:

$$L = \frac{(I_i / Z_i e)}{r_i \beta_{IP}} \gamma\beta\xi_{ii} , \quad (2)$$

where I_i is the ion beam DC current at ring, Z_i e is the ion charge, $r_i = (Z_i e)^2 / (A_i M_p)$ is the classical ion radius and ξ_{ii} is the beam-beam parameter at the IP:

$$\xi_{ii} = \frac{N_i r_i}{4\pi\varepsilon_{ni}} , \quad (3)$$

where $\varepsilon_{ni} = \gamma\beta\varepsilon_i$ is the ion beam's normalized r.m.s. transverse emittance. The ion beam current in large colliders is limited by losses in the vacuum tube that increase the heating of cryogenic equipment.

The Relativistic Heavy Ion Collider complex (**RHIC**) at Brookhaven consists of two intersecting rings in which counter rotating beams of particles collide head-on at up to six Interaction Points.

Table I.1. RHIC parameters for Gold-Gold ion collision

Variable	Units	Symbol	Value
Top Energy	(GeV/u)	E	100
No. Intersection Regions		n_{IP}	6
No. Bunches/ring		n_b	60
No. Particles/bunch		N_i	10^9
Revolution frequency	(kHz)	f_0	78.2
Frequency of repetition bunch (MHz)		f_b	4.692
Horizontal tune		Q_x	28.18
Vertical tune		Q_z	29.18
Transition energy		γ_{tr}	22.8
Transverse emittance r.m.s. (normalized)	(cm rad)	$\varepsilon_{nt}=\gamma\beta\varepsilon_t$	10^{-4}
Longitudinal emittance (Au)	(eV s)	ε_l	0.2
Bunch length r.m.s.	(cm)	σ_s	18
Beta function at the IP	(cm)	β_{IP}	200
Initial luminosity	(cm^{-2} s^{-1})	L_i	$2\cdot10^{27}$
Average Luminosity over 10 h		L_{av}	$2\cdot10^{26}$

The average luminosity over 10 hours is many times smaller then the initial peak luminosity because of the increase of the transverse and longitudinal emittances due to Intra Beam Scattering (IBS) and the beam-beam effect with external noise. The increasing longitudinal emittance leads to ions leaving the available longitudinal bucket area and thus to a decreasing number of ions, N_i.

Electron cooling can suppress or reverse the beam emittance growth and results in an increase of both peak luminosity and average luminosity. The continuous cooling may help to suppress nonlinear resonances due to the beam-beam interaction and therefore to achieve a higher beam-beam tune parameter, ξ_{ii}. Furthermore, cooling helps to reduce the beam tail that produces background at the IP detectors. Finally, cooling allows the accumulation of an intensive ion beam even when the injection chain does not produce an intensive beam.

I.2 Main features of electron cooling for heavy ion

G.I. Budker proposed electron cooling in 1965. In this cooling method, a friction force results from the relative motion of ions immersed in an electron beam, which is co-moving with the same average velocity of the ions. The energy of the chaotic motion of the ions is transferred to the cold electron 'gas'. To produce an electron beam with the same average velocity, the energy of the electron beam needs to be m_e/M_i times smaller than the ion energy; for example, cooling a 100-MeV proton beam requires an electron beam energy of only 50 keV. The first electron cooling experiments took place at the INP (Novosibirsk) in 1974 and demonstrated the high efficiency of this method.

The first cooling theory estimates used a plasma model of energy exchange in an electron-ion plasma. When an ion with a charge $Z_i e$ moves past an electron with velocity V at a distance ρ, the field of the ion, which is $Z_i e/\rho^2$, kicks the electron and changes its momentum by $\Delta p_e = Z_i e^2/\rho^2 \times 2\rho/V$. The ion energy loss is $\Delta p_e^2/(2m_e)$. Using the small-displacement (Born's) approximation for electron motion the friction force, integrated over the range of distances, can be written in the form:

$$F = \frac{1}{V}\frac{dE}{dt} = \int_{\rho\min}^{\rho\max} \frac{2Z_i^2 e^4 n_e}{m_e V^2 \rho^2} 2\pi\rho d\rho = \frac{4\pi Z_i^2 e^4 n_e}{m_e V^2} \ln\left(\frac{\rho_{\max}}{\rho_{\min}}\right), \quad (4)$$

where ρ_{max} and ρ_{min} are the maximal and minimal impact distances. Let us consider an electron beam with a density that is not too high. This would be defined as the plasma frequency being smaller than the inverse time of flight in the cooling section, or $\omega_e = c\sqrt{4\pi n_e r_e} << 1/\tau$. (in the beam's reference system $\tau = l_{cooling}/(\gamma\beta c)$). Then the maximum impact distance is determined by the path of ions in the electron beam,

$$\rho_{\max} = V\tau \quad (5)$$

and the minimal impact distance is determined by the condition that the displacement of the electrons during the interaction time $\tau_i = \rho/V$, where $\rho = V\tau_i \approx Z_i e^2/(\rho^2 m_e)\tau_i^2$, is given by:

$$\rho_{\min} = \frac{Z_i e^2}{m_e V^2} = \frac{Z_i r_e}{(V/c)^2}. \quad (6)$$

When the electrons have their own chaotic motion with a velocity distribution $f(\vec{V}_e)d^3V_e$, the calculation of the friction force requires averaging the friction force over the distribution:

$$\vec{F} = \int \vec{F}(\vec{V} - \vec{V}_e) f(\vec{V}_e) d^3V_e. \quad (7)$$

For example, if the distribution $f(\vec{V}_e)$ corresponds to a uniform sphere in velocity space, $f(\vec{V}_e) = const$ for $|\vec{V}_e| < V_c$, then the friction force grows linearly from center of the electron velocity distribution to the edge, and outside it decreases as V^{-2}. The cooling rate reaches a maximal value which is given for a small ion velocity, contained inside the electron velocity distribution $V < V_c$, by:

$$\lambda_{\max} = \frac{4\pi e^4 Z_i^2}{m_e M_i V_c^3} \ln\left(\frac{\rho_{\max}}{\rho_{\min}}\right) \quad (8)$$

For high ion velocities with $V > V_c$ the cooling decrement drops as V^{-3} :

$$\lambda = \frac{4\pi e^4 Z_i^2}{m_e M_i V^3} \ln\left(\frac{\rho_{\max}}{\rho_{\min}}\right) \quad (9)$$

In the first experiment at NAP-M, a 65-MeV proton beam was cooled by an electron beam with an energy of 35 keV. The temperature was E_{te}=0.2 eV, two times higher energy than the thermal motion of the electrons due to the electron-gun's cathode temperature (1000 K, 0.1 eV). The thermal velocity of the electrons with this energy was

$V_e = 2.3 \cdot 10^7$ cm/s. This results in a cooling time of 3 s for a velocity, given at beam reference system, of less than $2.3 \cdot 10^7$ cm/s.

In the NAP-M experiment it was discovered that the cooling time continued to decrease for a low transverse ions velocity $V<V_c$, and in fact it turned out to be less than 0.1 s instead of 3 s. Such a dramatic increase in cooling efficiency was a result of the combined effect of two factors: first, the presence of a longitudinal magnetic field in the cooling section, and second, an extremely low spread in the longitudinal electron velocities after acceleration. The longitudinal magnetic field was used to transport the electron beam from the cathode to the proton beam cooling section and further down to the electron beam collector. In the language of electron cooling, the magnetic field ``magnetizes" the transverse electrons motion. It means that the ions interact with 'cool' electrons, having a Larmor circle with a relatively small radius, $\rho_L=mV_c/eB$, where B is the magnetic field (for NAP $\rho_L=10^{-3}$ cm), rather than with hot (and fast) free electrons. This phenomenon resulted in both an enhancement of the cooling rate and cooling of the ions to temperatures many times lower than the cathode temperature 1500^o K. Thus, NAP-M obtained a proton longitudinal temperature of about 1^o K.

Figure I.1 shows measured results of the cooling rate versus the electron beam density in the beam reference system for an ion velocity of $5 \cdot 10^6$ cm/s in various rings.

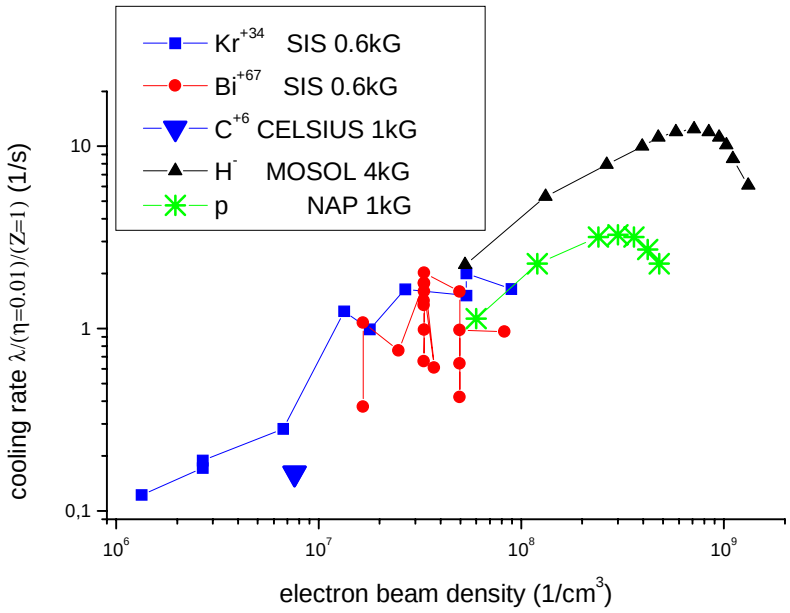

Figure I.1. Experimental cooling rate data. For comparison between the various machines, the data were normalized for a single ion charge and for η=0.01 (the fraction of the ion ring circumference occupied by the cooling electron beam).

If we were to estimate the cooling rate at RHIC using equation 9 only on the basis of the experimental data of figure 0.1, the cooling rate for gold ions Au^{79} would be (taking $n_e = 10^8$ cm^{-3} , $V=4 \cdot 10^7$ cm/s, $Z_i=79$, $A_i=197$, $\eta=0.0078$) :

λ=8 $(5\cdot10^6 /4\cdot10^7)^3$ $(79^2/197)$ (0.0078)/0.01= 0.5 s^{-1}, which corresponds to a 200 seconds cooling time in the laboratory's frame of reference, which is a good rate for cooling.

However, by introducing electron cooling have opened an additional channel of ion losses through electron ion recombination in the cooler section. The capture lifetime of Bi^{67} ion at SIS cooler for an electron beam density of 10^8 cm^{-3} (η_{eSIS} =0.019) was about τ_{lifeBi}=6.3 s. At RHIC the Au ion capture lifetime at laboratory's reference system will be $\tau_{lifeAu}=\tau_{lifeBi}\cdot(67/79)^2\cdot(0.0078/0.019)*\gamma$=1000 s. Such a short lifetime would limit the use of electron cooling at RHIC, which has an operational storage time of about 10 hours. Therefore we use the fact that the efficiency of capture is inversely proportional to the transverse velocity of the electron motion in the cooling section, and use that for increasing the ion beam's lifetime.

Table I.2. Initial parameters for the electron cooling system for RHIC

Parameter	**Symbol**	**Value**	**Units**
Electron beam energy	E_e	50	MeV
Peak electron beam current	J_e	1	A
Length of electron bunch	L_e	50	cm
Cooler fraction of ring circumference	η_e	0.0078	
Number of electron at bunch	N_e	10^{10}	
DC electron current	$Je_{DC}=e*N_e*f_b$	7.4	mA
Beta function at cooling section	β_x	60	m
Ion beam radius	$a_e=\sqrt{(\varepsilon_{nt}*\beta_x/\gamma\beta)}$	0.08	cm
Ion beam divergence at cooling sect.	$\theta=\sqrt{(\varepsilon_{nt}/(\beta_x\beta_\gamma))}$	$1.3\cdot10^{-5}$	rad
Ion transverse velocity (ion's reference system)	$V_i=\gamma\beta_c\theta$	$3.8\cdot10^7$	cm/s
Electron beam density (ion's reference system)	n_e	10^8	cm^{-3}

To make the capture lifetime $\tau_{lifeAu}=10^5$ s the transverse velocity of electrons must be increased by a factor of 100 (from 1.8 10^7 cm/s to 1.8 10^9 cm/s), thus the temperature of electron beam should be increased from 0.1 eV (cathode temperature) to 1000 eV (temperature of electron into cooling section). Now, this very high transverse velocity may decrease the efficiency of the cooling. Thus, the only way to use electron cooling under this condition is to use strong magnetization cooling, as demonstrated at the cooling experiment on the NAP-M storage ring at BINP. The increase in the transverse velocity should be compensated by an increase of the magnetic field along the cooling section. The Larmor circle radius at a magnetic field of B=10 kG=1T for electrons with a transverse velocity of $1.8\cdot10^9$ cm/s is:

$$\rho_L = \frac{m_e c V_e}{eB} = 0.011\,\text{cm} \quad (10)$$

Since this Larmor radius is several times smaller than the radius of both beams, a_e=0.07 cm, that gives hope to not losing too much cooling rate. What the cooling time which is really needed for the suppression of IBS, beam-beam interaction and other sources of noise is will remain an open question up to a real cooling experiment. The cooling time of 200 s looks very powerful, and it is hard to believe that fast heating effects exist at RHIC such that can increase the beam emittance in 200 s.

1 MAIN SCENARIO FOR ELECTRON COOLING

In this section we cover the subjects of continuous cooling at the collider's storage state, at beam injection energy and the usage of cooling for accumulation of beam.

1.1. Continuous cooling at the collider's storage energy

This report provides a preliminary study of the beneficial effect of electron cooling on RHIC luminosity for gold - gold collisions. Various parameters are not optimized at this point; therefore we can expect changes as the work progresses. We will show how the beneficial effect of electron cooling changes when we vary RHIC parameters for a gold-ion beam. Electron cooling will help to optimize RHIC's parameters for various experiments. For some experiments it may be necessary to have a maximal integral luminosity over the storage period, but other experiments may require, for example, a constant luminosity over the storage period.
The basic sets of the parameters used in the Cooling Scenario for the RHIC gold-ion beam are listed in the table below:

Table 1.1. GOLD nominal beam parameters at various stages

	Units	Injection	Store start	Store end
Nominal beam int. N_i	10^9	1.0	1.0	
Transverse emittance ε_{ni}	95% π*μm, normalized	10	15	40
RMS bunch length σ_s	m	0.47	0.12	0.2
RMS momentum spread	0.001	0.27	0.53	0.9

The following results are taken from a simulation program. We will compare various beam parameters as a function of time at RHIC storage (top) energy, without cooling and with cooling with various electron currents. A single particle Mathcad code is used for the simulation of cooling. The advantage of this code is a very fast response, the disadvantage - large fluctuation near equilibrium. This version is useful for fast testing of of the influence of various parameters

The simulation of beam heating (increase in transverse and longitudinal ion beam emittances and the associated losses of ions) is based on the simplest IBS model using a random oscillation of the colliding ion beam at the interaction point with an amplitude of 0.1 microns. Ions are lost by escaping the longitudinal bucket area, by dissociation at Interaction Points and pair production with a cross section of 212 barns, and by capture of electrons at the electron cooler.

In the simulation the fraction η of ions held in the bunch is taken as the ratio of the bucket area to the emittance, $\eta=2*\varepsilon_{lon0}/(\varepsilon_{lon}+\varepsilon_{lon0})$, or as 1 when all the ions are contained in the bucket. When cooling is applied and the longitudinal emittance is decreasing, $\varepsilon_{lon}<\varepsilon_{lon0}$

this coefficient equals 1. With the same parameters it is possible to see an increase in the number of ions as a result of capture of coasting ions into the RF bucket. Ions may escape the bucket at some particular time. When the ions escape the bucket they are not immediately lost, but they do not take part in luminosity production. Electron cooling may return some part of these ions to the RF bucket. More information about the electron beam parameters is embedded in the Mathcad rep4a1a.mcd file.

The performance of RHIC under cooling. Given the mechanisms IBS, electron cooling, beam dissociation and recombination, we can now calculate the performance of RHIC at storage energy with a particular electron cooling current. We take the following parameters for electron cooling:

Table 1.2. List of basic parameters list used for the simulation of electron cooling in this section

Number of electron in a single cooling bunch		N_e= 0---10^{11}
Electron bunch length r.m.s.	[cm]	σ_s =20
Frequency of repetition ion bunches	[MHz]	f_b=4.6
Average electron current	[mA]	Iav=0---74
Peak electron current	[A]	I_{peak}= 0--- 9.6
Magnet field at cooling section	[kG]	B=10
Transverse electron temperature in beam's reference system	[eV]	$T_\perp$=1000
Electron beam diameter	[mm]	a=2

The results of the simulations are summarized in Figure 1.1.1. The luminosity at a single Interaction Point is defined as:

$$L = \frac{N_i^2 \gamma \beta}{4\pi \varepsilon_{ni} \beta_{IP}} f_b \ , \quad (1)$$

where β_{IP} is the beta function at the collision point. With no cooling there is an emittance increase of about a factor of 2 to 3 during a 10-hour storage and the luminosity decays in about 4 hours. This is in agreement with the nominal values given in the RHIC Design Manual and an effect of Intra-Beam Scattering (IBS). The details of the model used for evolving the beam parameters due to IBS and to beam noise can be found in Section 6d

The observation that a very low cooling current (Ne=10^{10}) has a useful effect on the RHIC luminosity is a pleasant surprise. The luminosity is nearly constant over a time of 10 hours. While cooling with an increasingly intense current we obtain the faster increase in luminosity and then the faster decay. The decay is due mostly to losses of ions to disintegration by the ion-ion collision. For such a fast cooling and the resultant losses the optimum average luminosity calls for a shorter RHIC cycle.

.

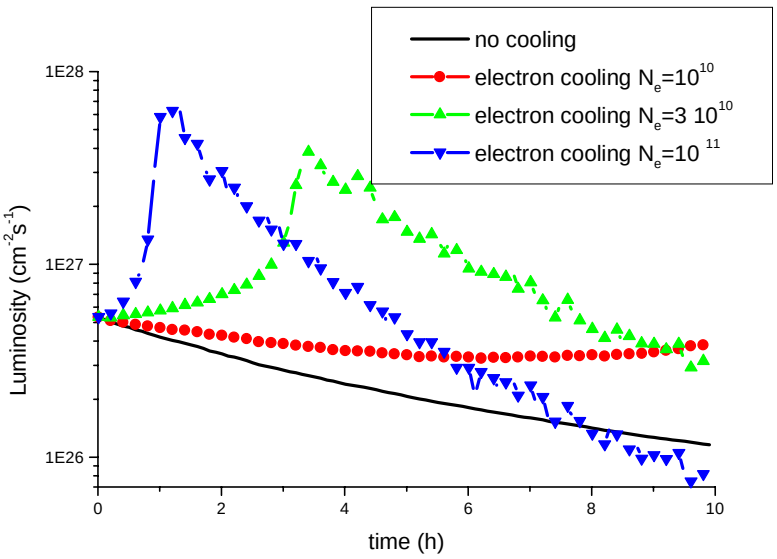

Figure 1.1. The luminosity at a single IP versus time for different cooling current.

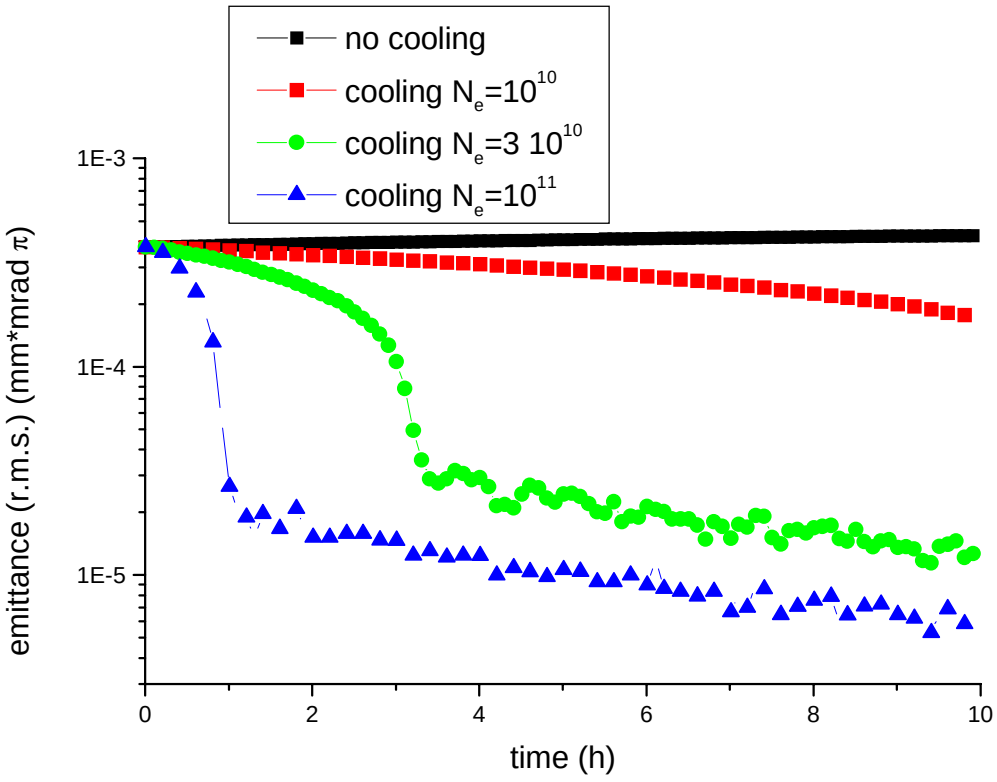

Figure 1.2. The transverse ion beam emittance versus time for various cooling currents.

Figure 1.2 shows the contribution of the transverse beam emittance to the development of the luminosity show in Figure 1.1. An equilibrium between the IBS and cooling processes takes place at an ion beam emittance of εn_{ieq}=0.3-0.1 mm*mrad. The large initial the ion beam emittance of RHIC, 4 mm*mrad leads to a delay of the cooling take-off. A preliminary cooling at injection energy would help to avoid this delay and to start from the higher luminosity. If this were the case, the top energy electron cooling, used for obtaining an IBS–cooling equilibrium, would require a lower electron current.

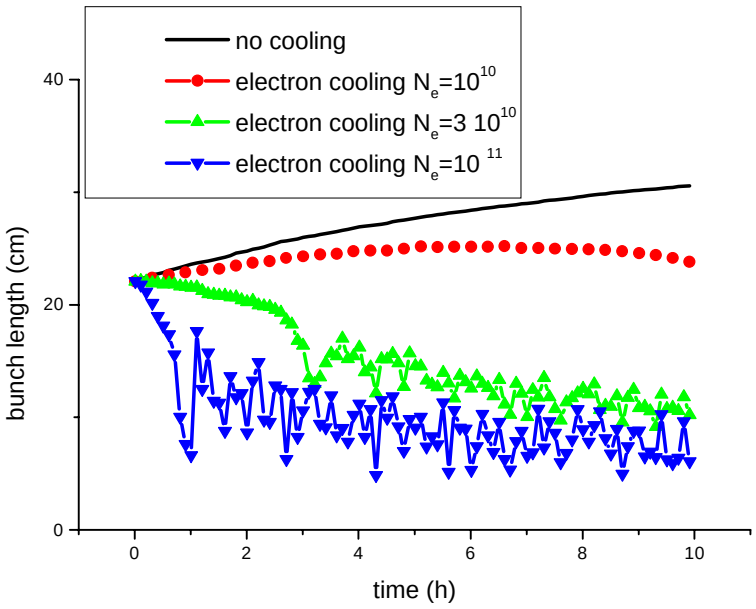

Figure 1.3. The longitudinal bunch length versus time for various cooling currents.

Figure 1.3 shows the development of the bunch length. With no electron cooling we observe a steady growth of the bunch length. Only moderate cooling is necessary to keep the bunch length constant. Cooling with high electron beam intensity actually increases the intensity of IBS and does not reduce the bunch length effectively. For an optimal cooling system we should redistributed the cooling rate by sweeping the electron beam energy with a fixed bunch length, so as not to allow the ion bunch length to grow.

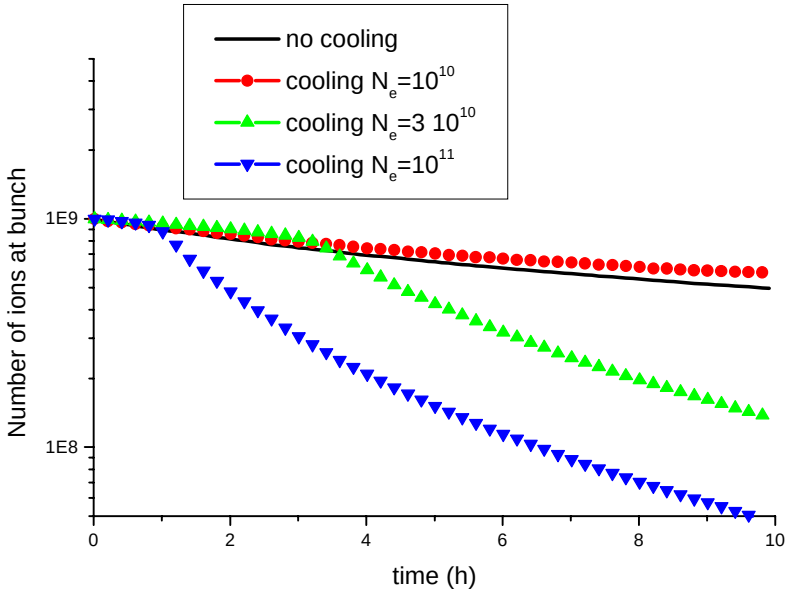

Figure 1.4. The number of ions in a single bunch versus time for various cooling currents.

Figure 1.4 shows the number of ions as a function of time. While moderate cooling reduces particle losses, strong cooling produces large losses due to ion-ion collisions. However, these are "good" losses.

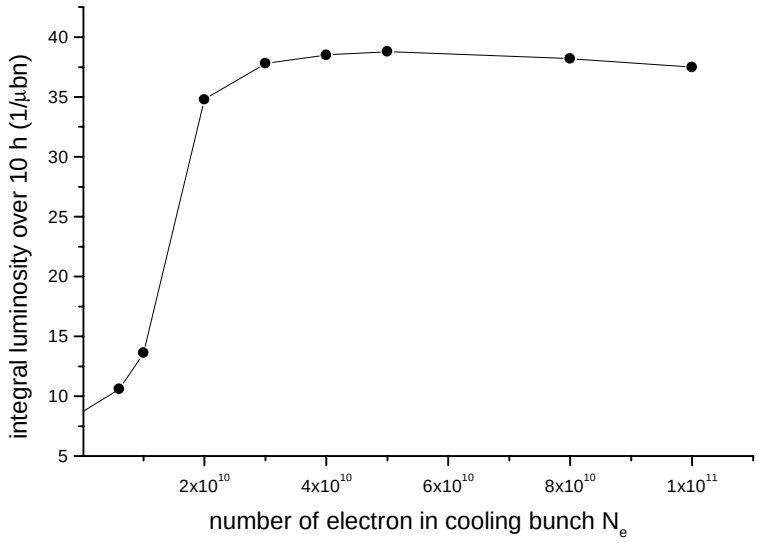

Figure 1.5. The Integrated luminosity over 10 hours versus cooling current (given as the number of electrons per cooling bunch).

Figure 1.5 shows that after reaching an electron bunch intensity N_e=2 10^{10} the more intensive cooling does not benefit the integrated luminosity over a 10 hours run period. The disintegration cross section σ_{tot}=212 nb limits the integrated luminosity through:

$$\left(\int L dt\right)_{max} = \frac{N_i n_b}{n_{IP}\sigma_{tot}}, \quad (2)$$

where n_b=60 is the number of bunches in the storage ring, and n_{IP}=6 is the number of interaction points delivering this luminosity. From equation 2 we can see that the maximal integrated luminosity (over time $0-\infty$) equals 47 1/μbn. An integrated luminosity of 38 1/μbn on figure 1.5 means that 80% of the ions were disintegrated in IP collisions.

The parameter that measures the intensity of the interaction in the IP through the space charge of the ion bunches is the tune shift parameter at a single interaction point:

$$\xi_{ii} = \frac{N_i r_i}{4\pi\varepsilon_{ni}}. \quad (3)$$

Figure 1.6 shows the variation of the tune shift parameter under cooling.

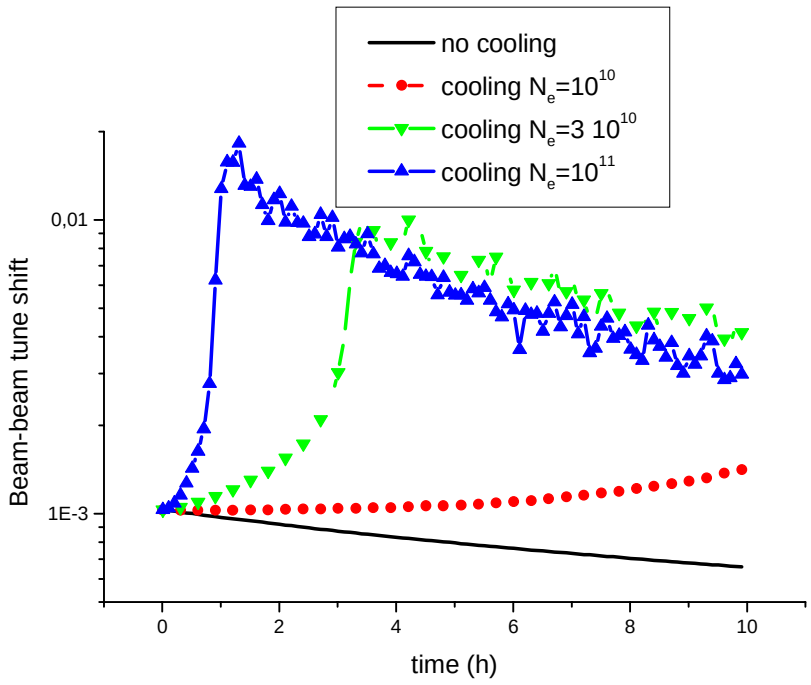

Figure 1.6. The beam-beam tune shift parameter at a single IP versus storage time.

From figure 1.6 we can see that without cooling the initial tune shift is very low and decreases as a function of storage time. Cooling, by decreasing the emittance of ion beam, increases the tune shift up to 0.01. The current state-of-the-art simulation code does not predict any problems with this value of tune shift. The simulation results of the ion-ion interaction can be found below in a special section.

Cooling dependence on initial RHIC parameters. For a proper optimization it is important to have information on the dependence of the results on the initial parameters of RHIC. The initial storage emittance is an important parameter for optimization. Figure 1.7 shows the luminosity with and without cooling (for N_e=3 10^{10}) for a few initial ion beam emittance values, ε_{ni} =4,1.3,0.4 mm*mrad. From figure 1.7 we can see that a large initial emittance leads to the delay in the onset of equilibrium between IBS and cooling. An emittance of less than 1 mm*mrad does not change very much the result since it is close to the equilibrium.

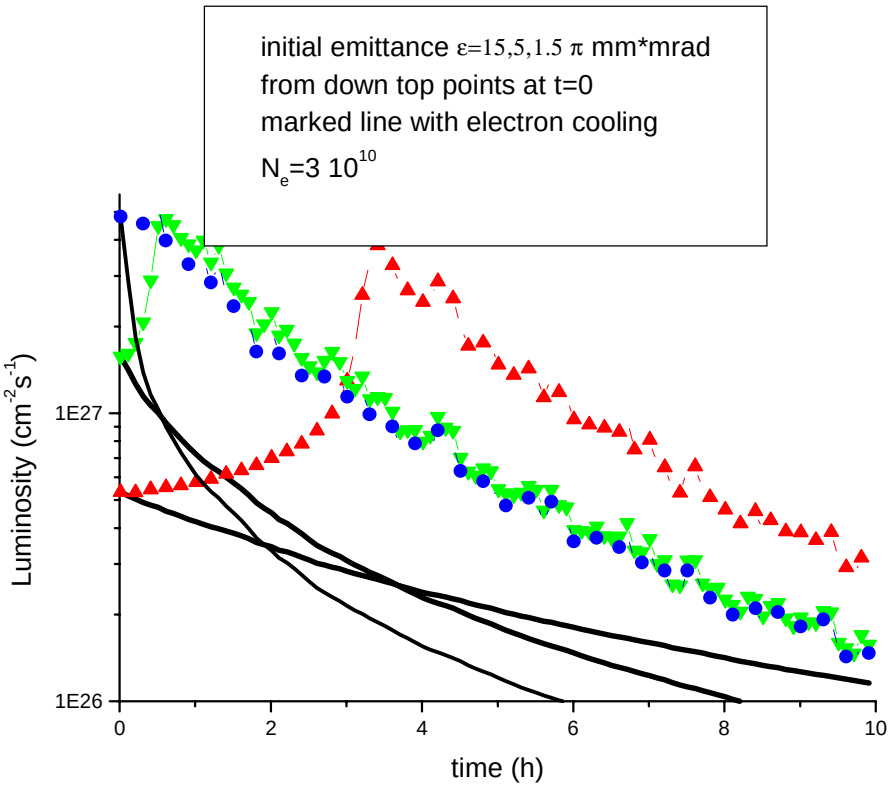

Figure 1.7. The luminosity versus time with and without cooling for 3 different start storage emittances.

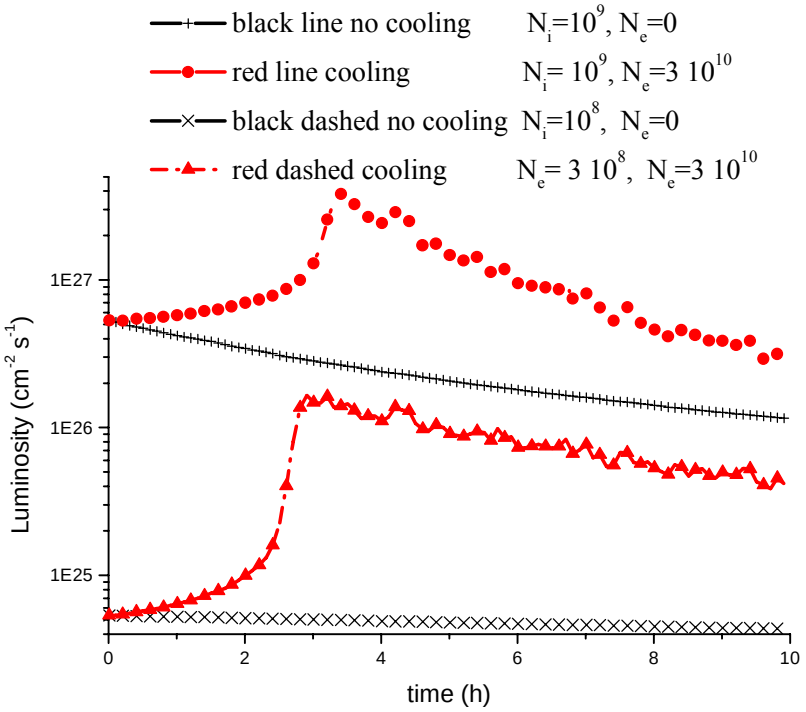

Figure 1.8. The luminosity with and without cooling, for various initial numbers of ions per bunch.

Figure 1.1.8 illustrates that the electron cooling has a large luminosity gain for a low number of ions per bunch, due to a less intensive IBS process. Without cooling the luminosity scales as N^2_i , but with cooling, the luminosity scaling is closer to N_i .

1.2. Cooling at beam injection energy

In this section we provide a preliminary study of electron cooling at RHIC injection. This regime is interesting for the preparation of the ion bunch parameters before storage at the top energy. During injection, the use of cooling can facilitate the accumulation of some ions species that can not be easily delivered by the injection chain. Examples may be rare ions or polarized ions that have a low injection current.

The results of the following calculations are taken from a simulation program similar to the program used for analyzing the main scenario (cooling at storage) (rep4inj.mcd). In this section, we observe various beam parameters as a function of time at RHIC injection energy, with no electron cooling applied, and with electron cooling.

The cooling at injection energy of RHIC (10 GeV/u ions, 5 MeV electrons) requires almost a DC electron beam because the ion bunch length is very large. The frequency of bunch rotation does not correspond to a harmonic frequency of the electron linac for cooling at the top energy (50 MeV). The difference in frequency is $\Delta f/f=1/(2\gamma^2)=0.5\%$.

The simplest solution to the problem of bunch synchronization is to use a separate accelerator system adapted to cooling at injection energy. The cooling calculation used the following parameters:

Table 1.3. Parameters for cooling calculation

Electron bunch length	1.1-m r.m.s.
Ion bunch length	1.1-m r.m.s.
Number of Ion bunches	60
Average electron cooling current	15 mA
Peak electron cooling current	0.3 A

As may be seen from the figures below, the ion losses during a 1000 s cooling time is near 20% and IBS induced emittance growth no longer limits the beam storage at injection. The accumulation of ion current under these conditions looks reasonably easy. It is possible to repeat injection at time intervals of about 50-100 s. Figure 1.9 shows the transverse normalized r.m.s. beam emittance versus storage time at injection energy at RHIC with and without cooling electron bunches having intensities of $N_e=10^{10}$ and $N_e = 2*10^{10}$. The cooling electron beam has the following parameters: An r.m.s. bunch of length σ=1.1 m, a repetition frequency 4.6 MHz, average currents of 7.5 and 15 mA (all other parameters are to be found in rep4inj.mcd).

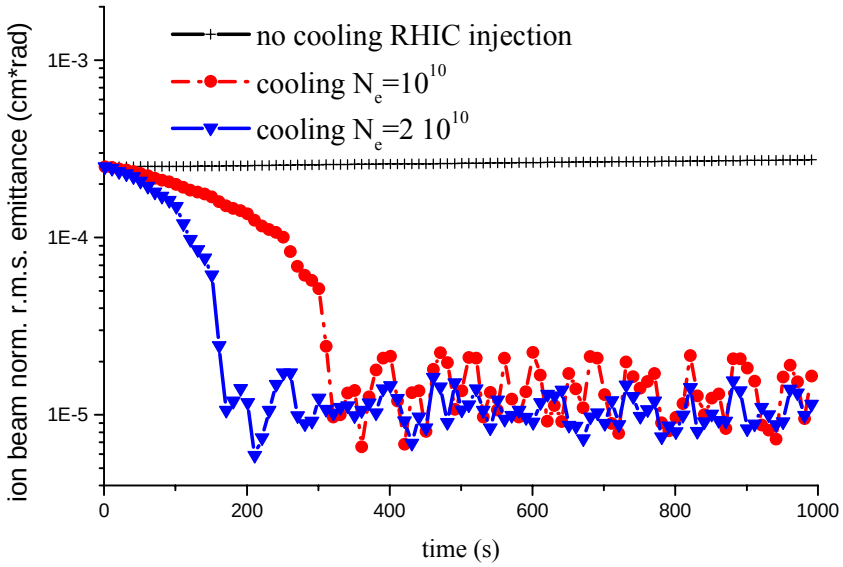

Figure 1.9. The transverse ion emittance (r.m.s. normalized) versus storage time at the injection energy.

Without cooling, the initial emittance increases from 2.5 mm*mrad to 2.7 mm*mrad and the bunch length from 1.1 m to 1.11 m . Cooling was made with redistribution of the cooling rate so that longitudinally the beam is not cooled, to reduce IBS. For cooling at injection energy, the electron beam temperature can be about 100 eV and the magnetic field of the cooling solenoid may be reduced down to 1 kG (instead of 10 kG required at

the top energy.) As a result of the decreased field the losses on injection increase but for a cooling time of 1000 s the loss is not significant. Figure 1.10 shows the number of ions in the bunch versus time under this condition.

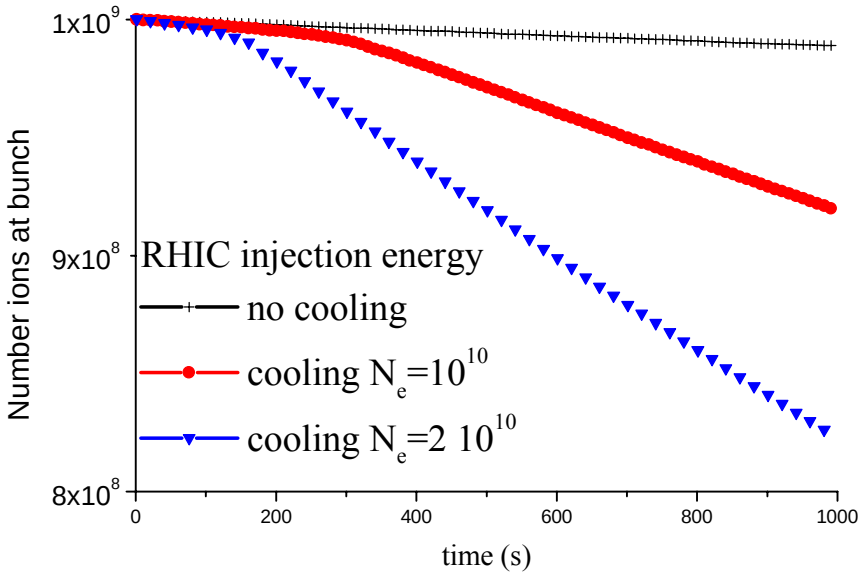

Figure 1.10. The number of ions in a bunch versus storage time at injection energy.

From figures 1.10 one can see that the ion losses over a period of 1000 s are nearly 20%. For injection, this loss is not very significant. The loss can further be suppressed by decreasing the electron current after cooling specific bunches. For just the compensation of IBS after cooling all that is really needed is an electron cooling intensity a few orders of magnitude less than that required for initial cooling.

Conclusions for the cooling scenario section

The results shown above have only illustrated various possibilities of using electron cooling at injection and at top energy of RHIC. From these results we can see that electron cooling can effectively suppress IBS and other noise heating processes in RHIC at the top energy in times of the order of 2000 s and at injection energy in times ranging from 100 s to 200 s. The equilibrium momentum spread and transverse ion beam emittance are considerably lower than the values necessary for RHIC. The optimization of cooling parameters is expected to continue up to commissioning time of the RHIC coolers.

A few words concerning the attached Mathcad2000 files
Rep4a1a.mcd (for top energy) and repinj.mcd (for the injection energy) provide readers with the possibility of trying various sets of parameters for optimization of some special cases. However, the set of parameters provided at this point can be used for discussions of the conceptual design of the electron coolers for RHIC.

2. LUMINOSITY UNDER COOLING

2.1 Beam Parameters at the Interaction Points

At RHIC, collisions take place at n_{IP}=6 Interaction Points. For simplifying the discussions below, we will assume equivalency of all the IPs, with parameters listed in the table 2.1:

Table 2.1 RHIC parameters used in various calculations

Parameter	**Symbol**	**Value**	**Units**
Beta function at IP	β_{IP}	2	m
Crossing angle		0	Radians
Number of ions per bunch	N_i	10^9	
Number of bunches in the ring	n_b	60	
Initial ion r.m.s. normalized emittance	ε_{ni}	3.7	mm·mrad
Initial r.m.s. bunch length	σ_s	22	cm
Initial momentum spread	σ_p	$1.46 \cdot 10^{-3}$	

2.2. Beam-beam interaction

The main beam-beam parameter for the interaction is the linear tune shift at the IP:

$$\xi_{ii} = \frac{N_i r_i}{4\pi\varepsilon n_i} \quad (1)$$

This parameter is a measure of the strength of nonlinear resonances which cause a diffusion of ions to large amplitude oscillations. The beam-beam parameter for RHIC storage at top energy is $\xi_{ii}=3.8 \cdot 10^{-3}$. The result of a simulation made at BINP shows that the power of these resonances for the proper ring lattice becomes significant if $\xi_{ii}>0.05$. Any low-power cooling is useful for preventing the blowup of the beam during collisions of ion bunches for a small tune-shift. Experience with electron-positron colliders shows that increased cooling helps to reach a higher tune shift and luminosity. The Figure 2.1 shows measurement results of the maximal tune shift in the collider VEPP2M at an energy range 300-700 MeV [1] when the syhrotron radiation cooling changes significantly by changing the radiated power.

The maximal beam-beam tune-shift as a function of the number of turns in one cooling time may be estimated by a simple power fitting approximation (Skrinsky formula):

$$\xi_{ii\max} = \frac{2}{N_{cooling}^{1/3}}. \quad (2)$$

The solid line in the figure shows calculation according this line.

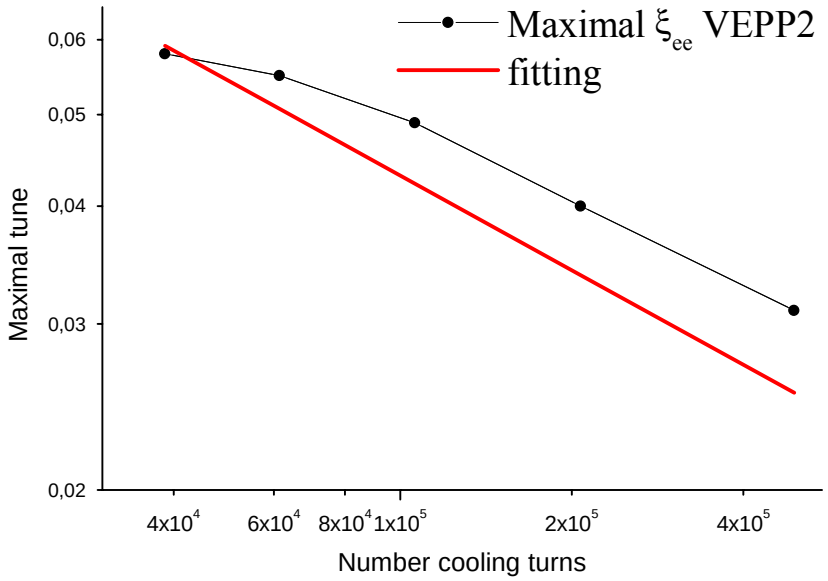

Figure 2.1. Measurements of the maximal ξ_{ee} in VEPP2 as a function of the number of turns per cooling time for electron cooling of the transverse oscillations. The solid line represents the Skrinsky estimating formula.

If we apply this estimate to RHIC, it means that for reaching a tune parameter of 0.005 per a single IP (with 6 IP in the ring), the number of turns per cooling time for RHIC should be less than:

$$N_{RHIC} = \left(\frac{2}{0.005}\right)^3 \frac{1}{6} = 10^7 \,(turns)$$

That corresponds to a cooling time:

$$\tau_{cooling} = \frac{N_{turns}}{f_0} = 136\,(s)$$

The electron cooling of Gold ions can reach this cooling time for a single-ion motion. But what is more important is that the electron cooling system cools coherent fluctuations much faster, in fact faster by many orders of magnitude than that for the single-particle motion. The cooling of small coherent fluctuations of a sample containing N_{sample} ions is N_{sample} times faster than the cooling of a single particle. As a result, the fluctuation generated by the beam-beam interaction will be damped very fast. This consideration gives hope to reach a high beam-beam tune-shift, but this will be the subject of a separate investigation.

[1] P.M. Ivanov, I.A. Koop, E.A. Perevedentsev, Yu. M. Shatunov, I.B. Vaserman, Luminosity and beam - beam effects on the electron-positron storage ring VEPP-2M with superconducting wiggler magnet, Third advanced ICFA beam dynamics workshop on beam-beam effects in circular colliders, Novosibirsk, 1989, pp. 26-33.

2.3 Noise and beam-beam

Diverse sources of noise produce random fluctuations of the orbit position at the Interaction Point. Kicker magnets, electrostatic plates, or high frequency vibrations of quadrupole magnets or the vacuum chamber can produce these noises. As a result, the ion bunch receives a random kick at the IP, with an amplitude proportional to the deflection of the counter rotating bunch from the central position x:

$$\Delta\theta(x) = 2\pi\xi_{ii}\frac{x}{\beta_{IP}} \quad (3)$$

This kick produces coherent oscillations of the ion bunch, which persist over the decoherence-time of RHIC. This energy is transferred to the chaotic thermal motion of ions. However, with electron cooling, the energy of this decaying coherent oscillation is damped by a coherent interaction with the cooling electron beam. If we neglect coherent damping, the heating rate of the beam emittance by this process is equal to:

$$\frac{d\varepsilon_i}{dt} = f_0 n_{IP}\frac{(2\pi\xi_{ii})^2}{\beta_{IP}}\left\langle x^2\right\rangle \quad (4)$$

As the process of cooling proceeds, the density of the ion beam increases and ξ_{ii} increases until such a time that an equilibrium state is reached, when the cooling is equal to this heating source. The simulation code rep4a1a.mcd takes this process into account.

The decay time of the coherent oscillation after a single kick can be estimated as follows [1]. A tune spread is generated equal to:

$$\Delta Q \approx 0.2\xi_{ii} n_{IP} \quad (5)$$

and this leads to a damping of the coherent oscillation in a number of turns given by

$$N_{decoh} = \frac{1}{\Delta Q} \approx 1000(turn) \quad (6)$$

The requirement to the coherent cooling rate comes from this number of turns necessary to damp the coherent oscillation.

[1] V. Lebedev, V. Parkhomchuk, V. Shiltsev, G. Stupakov, Emittance growth due to noise and its suppression with feedback system in large hadron colliders, Particle Accelerators, V**44**, pp.147-264,
(1994)

2.4 Simulation of beam-beam effects for the gold ion collisions at RHIC.

We used a ‘weak-strong’ model, where the ‘strong’ bunch has the initial conditions during all the simulation time, and the ‘weak’ one is represented by 1000 macroparticles, which are tracked independently. The other simulation parameters are listed below:

- The betatron tunes are: Q_x=28.18, Q_y=29.18, synchrotron tune is Q_s=0.006. 6–fold symmetry of the ring. Simple linear transport map between the Interaction Points: tune advances are 4.6967, 4.8633, 0.001, respectively. No radiation damping and noises were accounted.

- Initial emittances (both horizontal and vertical) are 10^{-6} cm · rad, bunch length is 10 cm, energy spread is $4 \cdot 10^{-4}$, β-functions (both horizontal and vertical) at the IPs are 36 cm.
- The 'strong' bunch at the IPs is divided longitudinally into 3 slices, in order to account the hour-glass effect. Since $\sigma_L << \beta^*$, 3 slices seems to be quite enough. The space charge parameter per one IP is $\xi = -0.01$, the minus sign is due to the equal signs of charges of the colliding beams.
- Without the 'noise' effects we do not observe any extensive degradation of the 'weak' beam during a few million turns. In order to see the effect we introduced (at one IP out of the six) a noise in the separation between the colliding bunches. The noise amplitude was chosen intentionally to be at a higher level in order to obtain visible results during the computing-power limited number of turns (a few millions). We used the Ornstein-Uhlenbeck process with an amplitude $\Delta = 2$ μm and 'memory' $N = 100$ turns, in both transverse directions (X and Y) independently. The separation on the i-th turn is calculated by the following recursive formula:

  $$S_i = S_{i-1} \cdot (1 - 1/N) + \Delta \cdot g \cdot (2/N - 1/N^2)^{1/2}$$

  where g is the random Gaussian number with zero mean and unity variance.

The electron cooler is placed at the point where $\beta_x = \beta_y = 60$ m. Since the actual length of the device is much smaller, we can neglect the phase advances between the cooler edges and represent it as a single kick (transverse and longitudinal), which depends on the particle's 6-D coordinates. In our model, we used the following expression for the cooling force (in the beam's rest frame):

$$F_i = -A \cdot V_i / (V^2_{eff} + V^2)^{3/2}$$

where i=x,y,z. The value of V_{eff} was set to be $0.002 \cdot c$. The value of $D = A/V^3_{eff}$ (that is the decrement for particles with about-zero amplitudes) was scanned in the range from 0 to $6 \cdot 10^{-7}$, step is $2 \cdot 10^{-7}$. These values are larger than the design values, but we were forced to increase them for matching with the high level of noises. We hope that our results can be scaled to the normal conditions, e.g. smaller noises and smaller cooling decrements.

The tracking process was divided into 5 steps (or stages), one million turns per step. The data gathered (luminosity, emittances, distribution) are averaged over all the particles, all the turns (that is 10^9 particle-turns) for each step independently, so we get 5 'frames' of the evolution of the 'weak' beam. The obtained results are presented in Figure 2.2 (luminosity), Figures 2.3–5 (emittances) and Figure 2.6 (distribution in the space of normalized betatron amplitudes).

As may be seen from these results, the cooling corresponding to $D = 2 \cdot 10^{-7}$ compensates the emittance growth due to the bunch separation noises, and a further increase in the cooling strength results in a shrinking of the ion beam and an increase of luminosity. It is important to note that the nonlinear beam-beam resonances are not visible in these simulations and all the observed effects can be estimated analytically. More detailed simulations with an increased number of tracked particles and number of turns, more realistic noises and other "noise" effects could be useful. However, that will require much more computing resources. Nevertheless, even our simplified model demonstrates clearly the advantages of the cooling device.

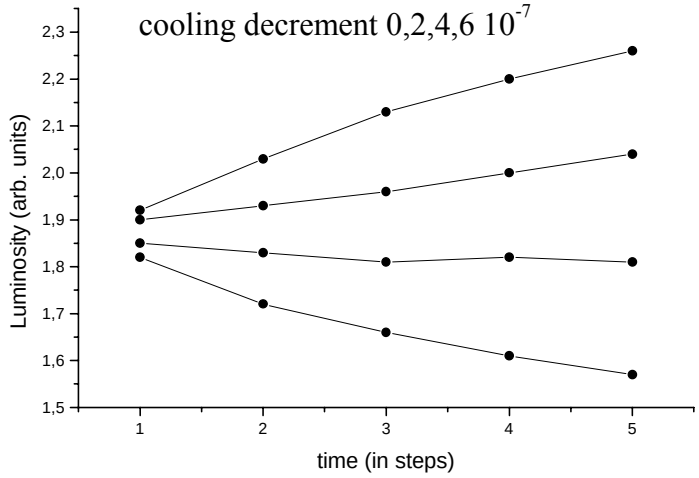

Figure 2.2. Luminosity vs time for different cooling decrement.

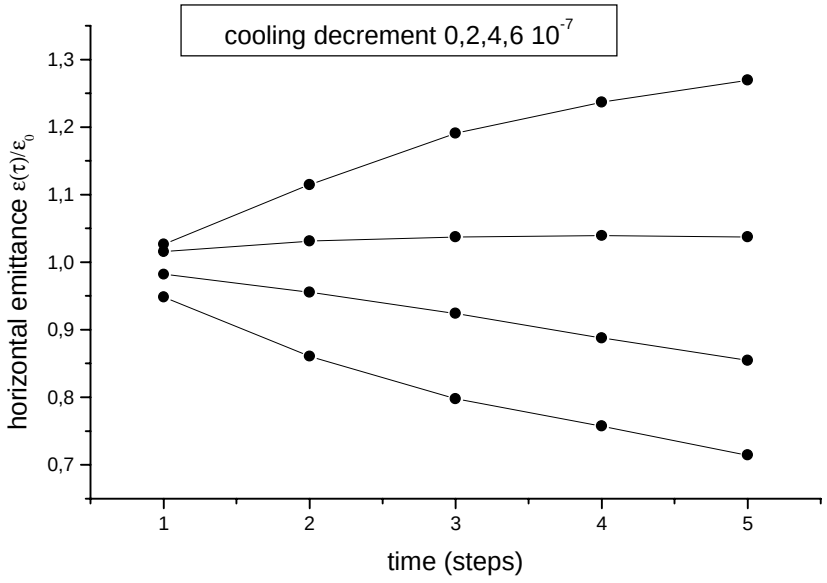

Figure 2.3. Horizontal emittance vs time for different cooling decrement.

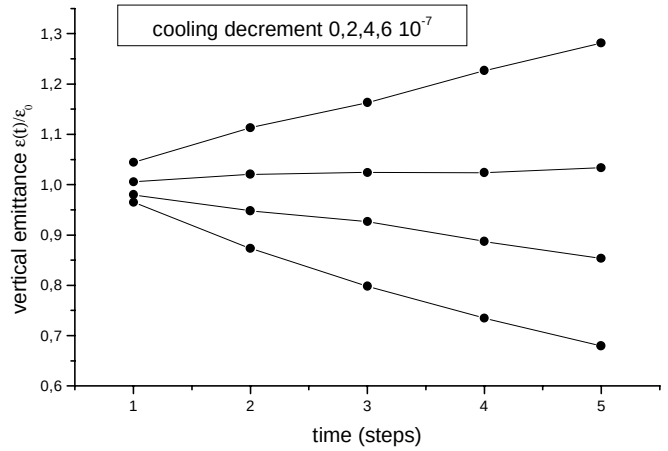

Figure 2.4. Vertical emittance vs time for different cooling decrement.

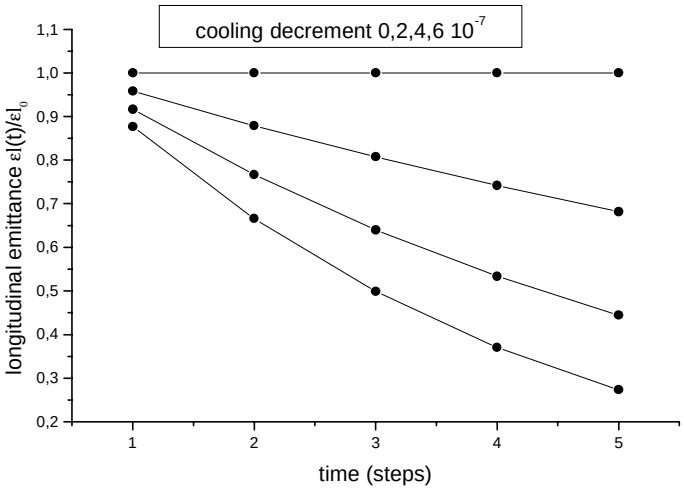

Figure 2.5. Longitudinal emittance vs time for different cooling decrement.

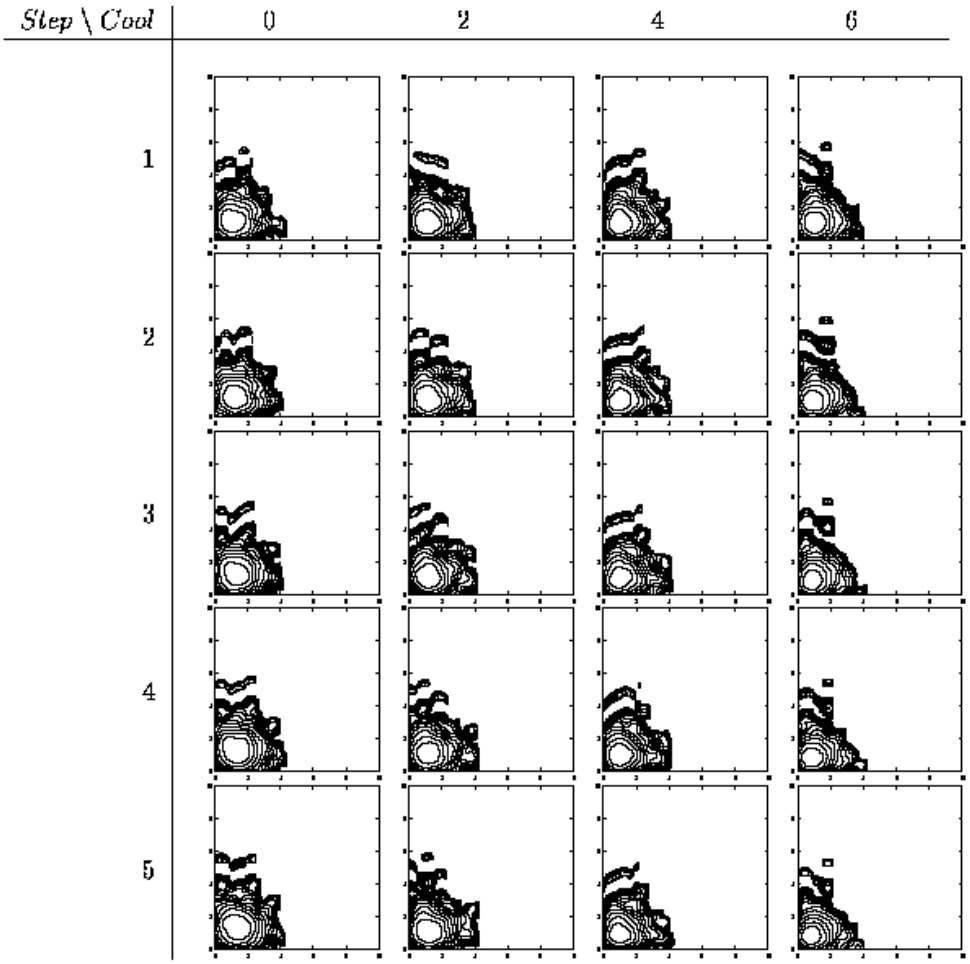

Figure 2.6. Contours of x-y distribution of ion beam for different cooling rate at different moment of time (step).

2.5 Recombination and dissociation ion losses

The capture of electrons by high charge ions is an additional source of losses in the ion beam. The recombination rate is a strong function of the transverse temperature of the electron beam. Figure 2.7 shows how critical this temperature is for losses. This calculation was made without taking into account the dissociation losses at IP.

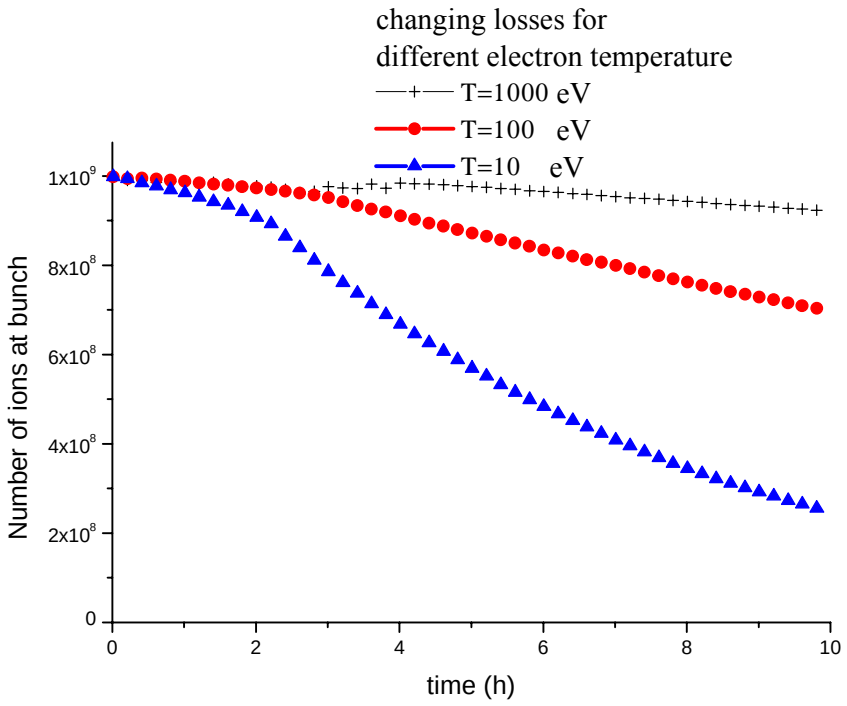

Figure 2.7. The number of ions plotted versus storage time for various transverse temperatures of the electron beam.

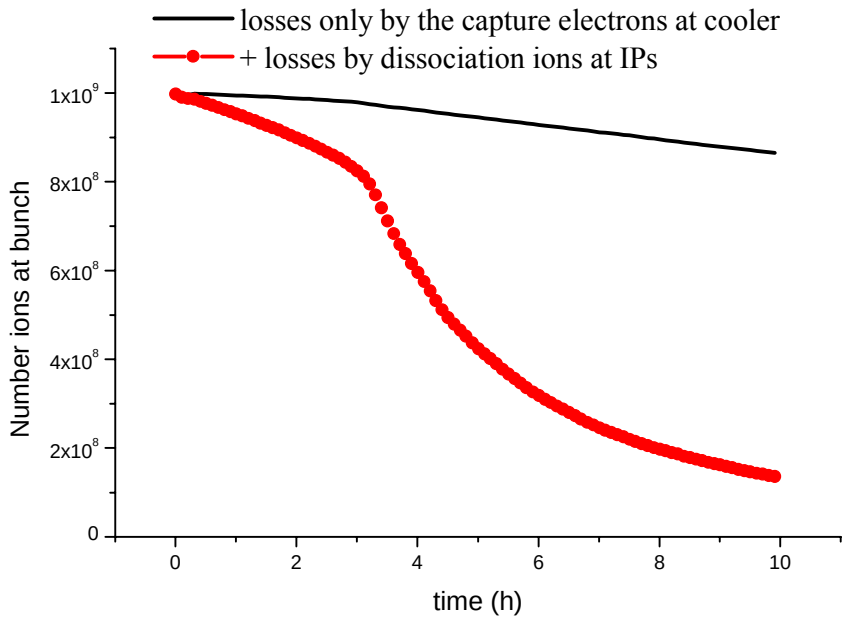

Figure 2.8. Number of ions versus storage time: the black line represents electron capture from cooler only, red line represents both electron capture and ion dissociation in the IP.

For the RHIC parameters, the processes of ion dissociation in high-energy collisions at the IP have a large cross section, about 212 nb. Figure 2.8 shows a comparison of loss rates in these two channels. At a transverse electron temperature of 1000 eV the capture of electrons in the cooler adds less than 10% to the losses. For a temperature of 100 eV the capture losses are close in value to the dissociation channel.

3. THE TECHNICAL APPROACH FOR THE ELECTRON COOLING SYSTEM

3.1 The parameters of the cooling electron beam

3.1.1 Cooling section length

There are a few reasons why the cooling section for RHIC should have a large length:

a. The magnetization cooling requires a long interaction time in the beam's reference frame.

The interaction time τ should satisfy $\omega_L\tau >>1$ (where $\omega_L=eB/m_ec$ is the Larmor frequency of the electron's motion in the magnetic field B), and $\rho_{max}=V\tau >>\rho_L=m_eV_\perp c/(eB)$, where ρ_L is the Larmor radius and $\tau =l_{cool}/(\gamma\beta c)$ is the time of flight through the cooling section of length l_{cool}.

b. A longer cooling length allows using a smaller electron beam current. A high electron current for cooling complicates the injection chain and increases the cost of the equipment.

c. The cooling time is proportional to the ion's transverse velocity to the third power and inversely proportional to the density of electron beam. A larger value of the ion's beta function in the cooling section decreases the transverse ions velocity. Thus, an increase in β_{cool} leads to a decrease in cooling time as $\beta_{cool}^{-1/2}$.

d. The damping decrement of coherent ion beam fluctuations is proportional to τ^4. If the cooling parameter is far from being dangerously large, it is advantageous to have faster coherent cooling by increasing the length of the cooling section.

The long straight sections near the RHIC interaction points permits to have a cooling solenoid length of about l_{cool}=30 m, a value that will be adopted in this report.

The magnetic field necessary for obtaining a long beam lifetime due to radiative electron capture is estimated in the introduction as 1 Tesla. Figure 3.1 shows that a magnetic field 1 kG over a store time of 10 h is not enough for cooling the ion beam, but with a magnetic field of 10 kG the luminosity is increased significantly after few hours cooling. The difference between 10 kG and 5 kG is not too large. In any case, the solenoid of the cooling section should be superconducting (due to the length and high magnetic field), thus we might as well use a field of 10 kG.

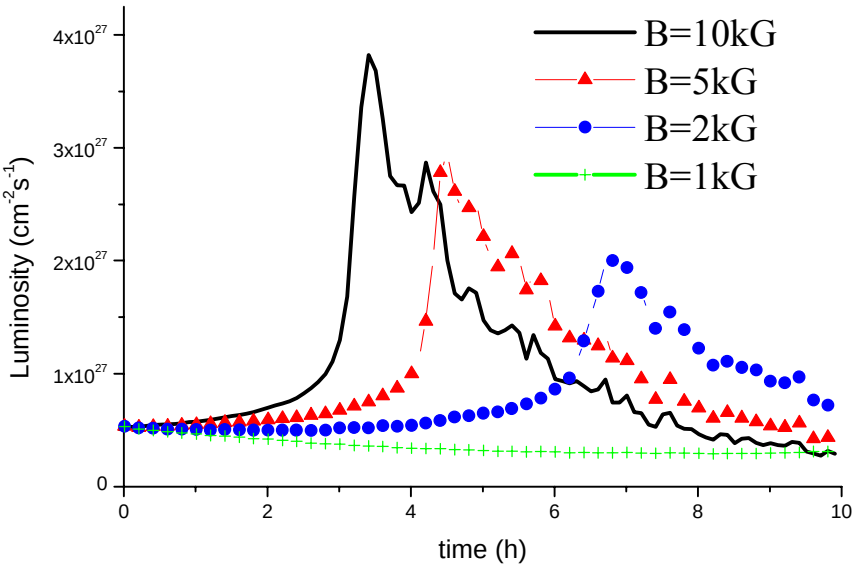

Figure 3.1. Luminosity vs. storage time for various magnetic fields of the cooling section.

The action of this solenoid on the ion motion at RHIC should be the subject of another study, which must consider the necessity to have anti-solenoids for compensation of the coupling of the two transverse planes. In many electron cooled ion storage rings the anti solenoid was included, but in practice it doesn't produce a big difference in performance. The question of the solenoid should definitely be discussed in the framework of cooling a polarized proton beam in RHIC. For systems with polarization, the position of the solenoid relative to the IPs is very important.

The main requirement imposed on the solenoid's design by the electron cooling mechanism is the parallelism of the magnetic field lines along the beam's orbit. This allowed divergence should be of the order of the angular spread of the ion beam:

$$\Delta\theta = \sqrt{\frac{\varepsilon n_i}{\beta\gamma\beta_{cool}}} = 12510^{5}$$

Precision of this cooling section field at a level of 10^{-5} means the accuracy near 0.01 mm at a distance of 1 m, which is a challenging but doable accuracy. It may be accomplished economically by using trim coils distributed along the cooling section to compensate transverse field components. The main challenge in this procedure is a precise measurement of the field direction. This has been achieved by sensing laser light reflected by a mirror mounted on a small permanent magnet bar. [1,2].

[1] L. Arapov, N. Dikansky, V. Kokoulin, V. Kudelainen, V, Lebedev, V. Parkhomchuk, B. Smirnov, B. Sukhina, Precise solenoid for electron cooling, 13 International conference on high energy accelerators v.1 p.341-343 1986.

[2] BINP FNAL team, Measuring direction of magnet line. Report will be at Russian conference 2000

3.1.2 Electron Beam Parameters

For electron cooling of RHIC gold beams it is necessary to have an electron beam with an energy of 52 MeV, a peak current of up to 0.1 A, an energy spread of $\Delta\gamma/\gamma=10^{-4}$ and a transverse momentum spread of $\Delta p/p=10^{-4}$. In addition to these requirements, the following physics problems must be addressed.

The first problem is matching the length of the electron bunch. Electron bunches from a linear accelerator are very short (L_{bunch}~1 cm). However, we need bunches with a length of about 30 cm. At the same time, increasing the electron bunch length must not lead to an increase in the energy spread by dilution of the longitudinal phase space.

Also, the electron beam from the linear accelerator has an intrinsic energy spread that may be too high for cooling. Thus we may adopt the following strategy: The electron beam will be transformed in longitudinal phase space to produce a longer bunch with the necessary low energy spread. Then the beam, which still may be shorter than the ion beam, will be swept in phase to produce coverage of the whole ion bunch. This strategy has certain advantages; one of them is the ability to control the ion bunch longitudinal density distribution. This topic will be discussed in detail later on.

Another problem is introduced by the high value of the cooling section solenoid's magnetic field (about 1T). The electrons may acquire a high additional transverse momentum upon entering the solenoid. This effect must be corrected by special optics.

3.2 Schematic layout of the cooling system next to a RHIC interaction point

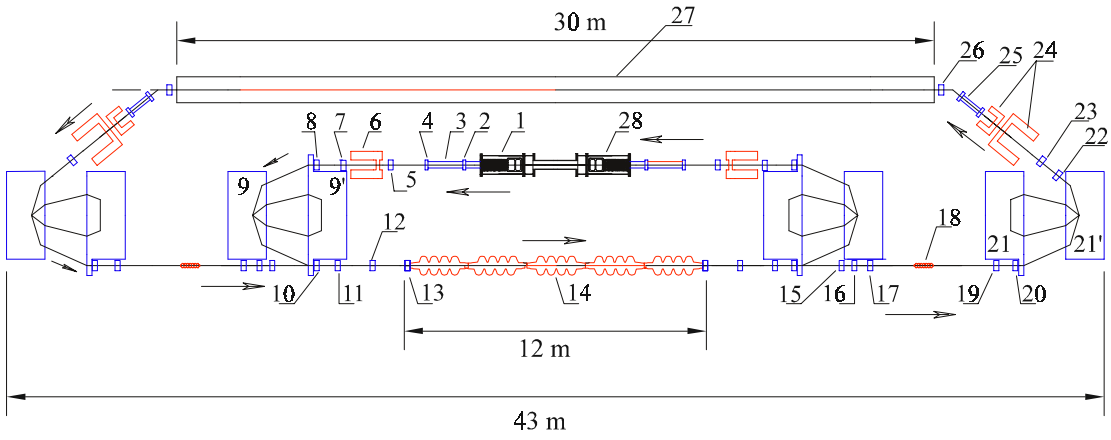

Figure 3.2. The scheme of cooling system.

The electron cooling equipment comprises the following key elements:

1 – A 2 MeV injector with a magnetized cathode (the magnetic field on the cathode of the injector is ~100 G).
3 – A solenoid extension of the longitudinal magnetic field of the injector (100 G).
2,4 –Skew quadrupoles for the transformation of the magnetized beam into a flat beam
6 – Energy modulating cavity for reducing the electron bunch length from 4 ns to 0.06 ns. It consists of two 70 MHz RF-cavity (the gap voltage is 350 kV) and one 210 MHz (36 kV) RF-cavity.
5,7,8 – Electron optical elements of the bunching system.
9,9' – Magnetic compressor (an α-magnet, with a bending radius of 1m).
10,11,12,13 – Electron optical elements of the bunching system.
14 – RF linac structure (350 MHz LEP structure).
15 – A bending magnet for a compensation of the action of the last high-energy (50 MeV) bending magnet (9").
18 –Third harmonic of the RF linac (1.05 GHz), for compensation of the non-linearity of fundamental accelerating field.
16,17,19,20,22,23 – Electron optical elements of the debunching system.
21,21' –Magnetic de-compressor (an α-magnet, with a bending radius of 1m).
24 –RF-cavity for eliminating the linear energy chirp. It consists of 80 MHz RF cavity (the gap voltage is 4.6 MV) and 240 MHz (0.24 kV). This cavity should be superconducting.
25 – Transfer optics from a flat to a round beam electron beam, for injection into the main solenoid.
26 –Bending magnet.
27 –Main solenoid (10^4 G).
28 –Beam-dump or system of beam recuperation.

The electron beam from the injector electron gun (2 MeV) with a magnetized cathode (100 G) is transformed to a flat beam ($\varepsilon_{nx}=2.1\cdot10^{-2}$ cm·rad, $\varepsilon_{ny}=7\cdot10^{-4}$ cm·rad). After that, the bunch passes through a bunching section. This section consists of an energy-modulating RF cavity and an α-magnet magnetic-compressor. The length of the electron bunch is decreased to the suitable length for acceleration ($\sigma_z=1.8$ cm). In the main linac, the bunch is accelerated to the full energy (52 MeV). The acceleration is done at a phase of $\theta= -10°$ in order to achieve the linear dependence between the longitudinal momentum and the position of the electron in the bunch (chirp). This chirp is used for further debunching. The length of the electron beam is increased in the debunching magnet structure up to 10-40 cm, allowing optimization of the cooling. After debunching, the electron beam passes a system of RF cavities designed for reduction of its momentum spread. Before going into a cooling solenoid the electron beam is transformed from a flat to a round beam. After the cooling section, the beam returns to

the debunching system with the necessary modulation of energy for optimization of the bunch length and energy recovery at the main linac. The electron beam with a residual energy of 2 MeV is terminated in a beam dump.

An initial analysis of electron optics has been made using the thin-lens approximation. The betatron and dispersion function are shown in Figures 3.3 to 3.5. The detailed calculation of optic scheme for electron can be completed after a choice of parameters of electron transport system is made.

In the RF linac structure it is useful to use a special procedure for evaluation of betatron function. The motion of particle at acceleration can be written as

$$\frac{d^2x}{ds^2}+\frac{1}{\gamma(s)}\frac{d\gamma}{ds}\frac{dx}{ds}=0 \qquad (v/c\approx 1). \tag{1}$$

If we use the Ansatz:

$$x(s)=Aw_\gamma(s)\cos\left(\int_0^s\frac{ds'}{\gamma(s')w_\gamma^{\,2}(s')}+\varphi_0\right) . \tag{2}$$

Then the differential equation becomes:

$$\frac{d^2w_\gamma}{ds^2}+\frac{1}{\gamma(s)}\frac{d\gamma}{ds}\frac{dw_\gamma}{ds}-\frac{1}{\gamma^2 w_\gamma^{\,3}}=0 , \tag{3}$$

which is similar to usual envelop equation. Thus one can calculate the dynamic variable w_γ for a given $\gamma(s)$ and then calculate $\beta(s)$ as:

$$\beta(s)=\gamma(s)w_\gamma(s)^2 . \tag{4}$$

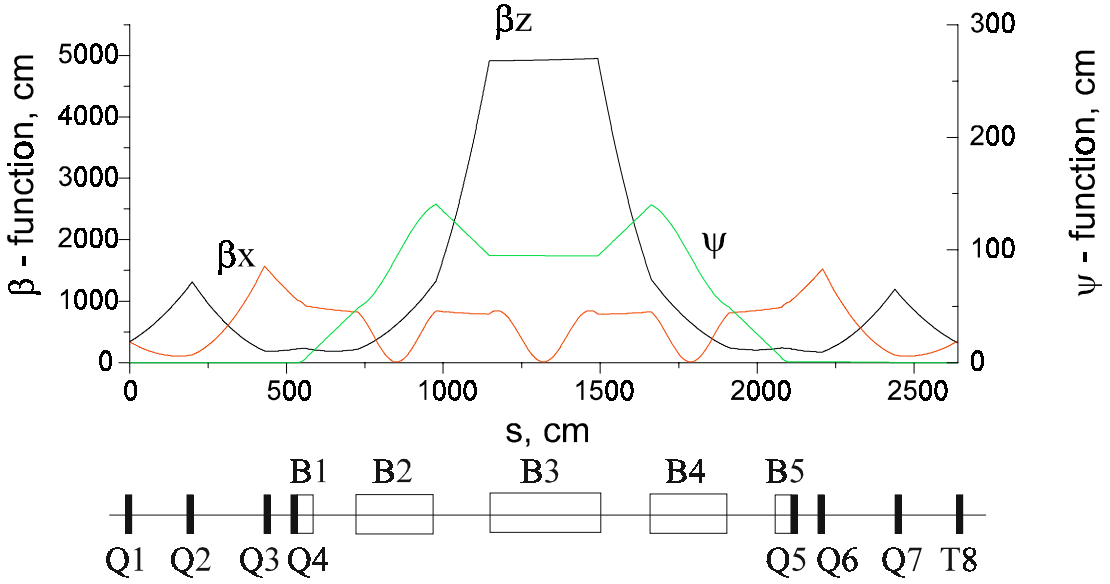

Figure 3.3. The sketch of betatron and dispersion functions from element 4 to

element 13.

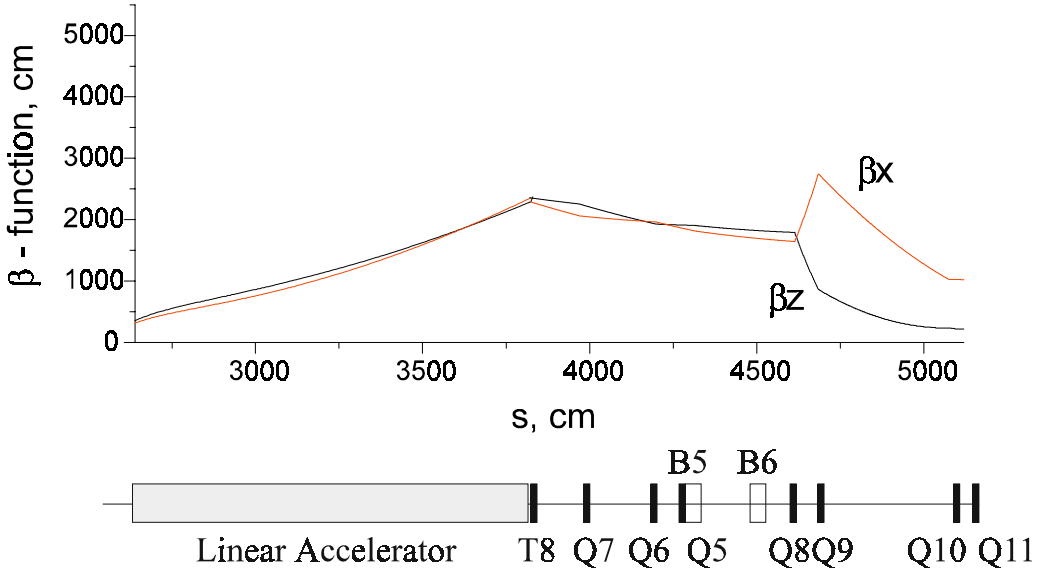

Figure 3.4. The sketch of betatron and dispersion functions from element 13 to element 21.

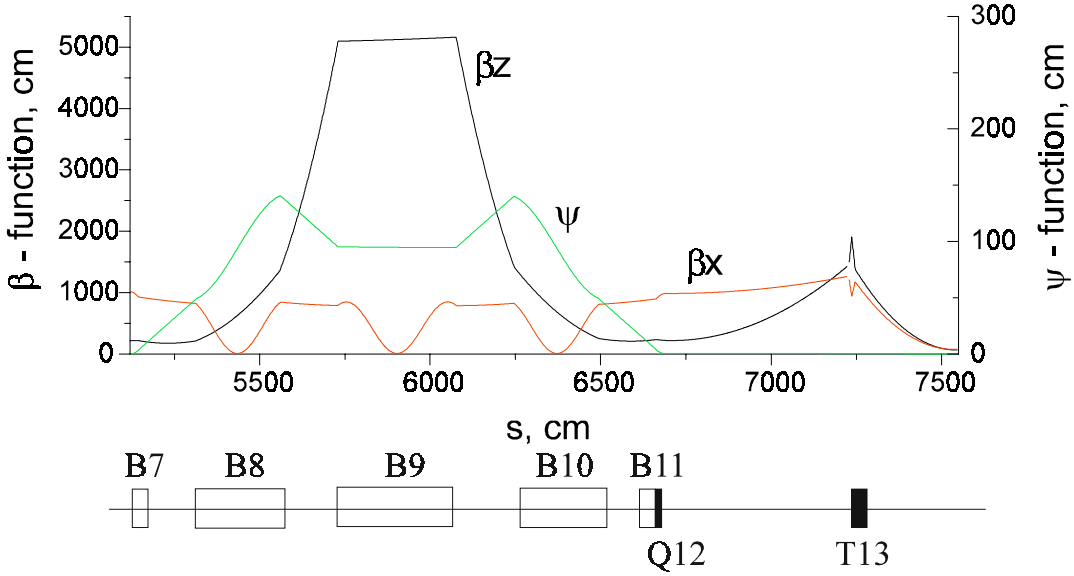

Figure 3.5. The sketch of betatron and dispersion functions from element 21 to

element 25.

Table 3.1. The parameters of optic elements for part of cooling section corresponding injection energy of electrons (2 MeV).

Element	Length, cm	Focal length, cm	Magnetic field, G		
Quadrupole	1	169		tilt. 45	2
Quadrupole	1	-338		Q1, tilt. 45	4
Quadrupole	1	228		Q1a	
Drift	200				
Quadrupole	1	-182		Q2	5
Drift	230				
Quadrupole	1	191		Q3	7
Drift	105				
Quadrupole	1	-541		Q4	8
Magnet	24.8		89	B1	9
Drift	168				
Magnet	248		89	B2	
Drift	168				
Magnet	347		89	B3	
Drift	168				
Magnet	248		89	B4	
Drift	168				
Magnet	24.8		89	B5	
Quadrupole	1	-541		Q5	10
Drift	105				
Quadrupole	1	191		Q6	11
Drift	230				
Quadrupole	1	-182		Q7	12
Drift	200				
Quadrupole	1	-24.8		T8	13
Drift	2				
Quadrupole	1	11.9			
Drift	2				
Quadrupole	1	-23.9			

Table 3.2. The parameters of optic elements for part of cooling section corresponding cooling energy of electrons (50 MeV).

Element	Length, cm	Focal length, cm	Magnetic field, G		
Drift	200				
Magnet	24.8		-89	B6	15
Drift	50				
Quadrupole	1	-239		Q8	16
Drift	70				
Quadrupole	1	239		Q9	17
Drift	390				
Quadrupole	1	-701		Q10	19
Drift	50				
Quadrupole	1	2400		Q11	20
Magnet	24.8		1750	B7	21
Drift	168				
Magnet	248		1750	B8	
Drift	168				
Magnet	347		1750	B9	
Drift	168				
Magnet	248		1750	B10	
Drift	168				
Magnet	24.8		1750	B11	
Quadrupole	1	2400		Q12	22
Drift	535				
Quadrupole	1	68.7		T13	23
Drift	9				
Quadrupole	1	-34.3			
Drift	9				
Quadrupole	1	68.7			
Drift	300				

3.3. Electron gun in DC accelerator (2 MeV).

The electron gun design for the 52-MeV electron cooler consists of a high-voltage (2 MV) power supply (PS), controls electronics, and a DC accelerator tube (Figure 3.6). The whole gun is embedded into a high-pressure vessel containing SF_6 ($\approx 10^6$ Pa). One can find some similar devices in [1]...[4]. Its expected parameters are as follows:

Table 3.3. Electron gun parameters.

Electron energy (kinetic), MeV		2
Relative energy spread		10^{-3}
Average current, mA	up to	120
Peak current, A		5
Pulse duration, ns		4

The design of the high-voltage power supply is based on an AC-transformer with a gap in the core to insulate the high voltage from the ground. The operating frequency is chosen to be ~ 1kHz. The low-voltage coil is water-cooled. The inner surface of the high-pressure vessel should be copper-coated to reduce the power loss. Each rectifier cell contains a coil and high-voltage rectifier. A slow feedback system is used to maintain an exact average-voltage. Ripple is reduced by a fast feedback system with a series transformer.

The accelerating tube consists of ceramic rings with brazed electrodes. The tube also serves as a vacuum chamber. A voltage divider is connected to the electrodes. A LaB_6 cathode-grid unit is used as an electron emitter. Its diameter is 25 mm and its expected current density is 1.4 A/cm^2 (partially absorbed by the grid). The cathode should be slightly concave to reduce the temperature dependence on the cathode-to-grid distance. So, some compression inside the gun is necessary. It means that the magnitude of the magnetic field at the cathode should be lower than its value further along the beam direction. The cathode-to-grid distance is chosen to be 0.5 mm; the voltage necessary to control the current is ≈ 100 V including the locking voltage. No serious technical problems are expected in designing a 100 V, 7 A, 4 ns, and 6 MHz controlled pulser.

Other possibilities for the emitter are: (i) a conventional gridded oxide cathode, (ii) an oxide cathode with a modulating electrode, or (iii) a photo-cathode. A gridded oxide cathode (i) is analogous to the proposed LaB_6 one, but it has significantly lower temperature (advantage) and much greater sensitivity to organic vapor (drawback). This choice should be made if one is absolutely sure in absence of organic matter in the vacuum system. Note that the cathode area hardly can be reduced significantly. If the mentioned above set of parameters is admitted, the power coming to the grid with the electrons is ≈ 3.5 W. If the area of the grid is reduced, it can be overheated.

A gridless cathode with a modulating electrode at some distance comparable to the cathode diameter (ii) is much more simple and its area can be much less as there's no problem with grid overheating in this case. Unfortunately, it claims much higher voltage of the pulser (several kV typically). It's nearly impossible to design a pulser providing, for example, 3 kV 4 ns 5 A pulses with the repetition rate 6 MHz at the current state of the art.

The third possibility (iii) requires a high-efficiency (~ 1%) photo-cathode and a 30 W average power pulsed laser. Note that the length of its optical resonator is to be ≈ 25 m to provide 6 MHz repetition rate. In this case the whole design of the injector ought to be revised as much shorter pulses of much higher current can be obtained (advantage). It's also known that the life time of such cathodes is too small (typically, several hours), so a cathode preparation unit should be included in the gun (drawback).

Both 0.01 T solenoids should be designed to provide the uniform field along the entire axis with the exception of the near-cathode region. There the field should be ≈ 1.5 times less to permit the appropriate beam compression. The expected current density is ≈ 10^4 A/m, thus the cooling requirement are fulfilled. A quadrupole lens over the second solenoid is necessary to convert the round beam into a flat beam outside the magnetic field.

The control electronics should contain a set of controlled power supplies for filament, bias, and the pulser. The requirement for the timing jitter of the pulser trigger is less than 0.3 ns. One should pay particular attention to the cooling of the gun. The expected power dissipation is ~ 300 W in the cathode and ~ 30 kW in the high-voltage power supply.

References

[1] M.L. Sundquist, R.D. Rathmell, and J.E. Raatz. NIM A287 (1990) 87-89.

[2] J.E. Raatz, R.D. Rathmell, P.H. Stelson and N.F. Ziegler. NIM A244 (1986) 104-106.

[3] Industrial electron accelerators of ELV type. http://www.inp.nsk.su/products/indaccel/elv.en.shtml.

[4] B.B.Baklakov, A.M.Batrakov, et al. Status of the Free Electron Laser for the Siberian Centre for Photochemical Research. SR'2000, Novosibirsk, Russia (oral, to be published in the SR'2000 Proceedings in NIM).

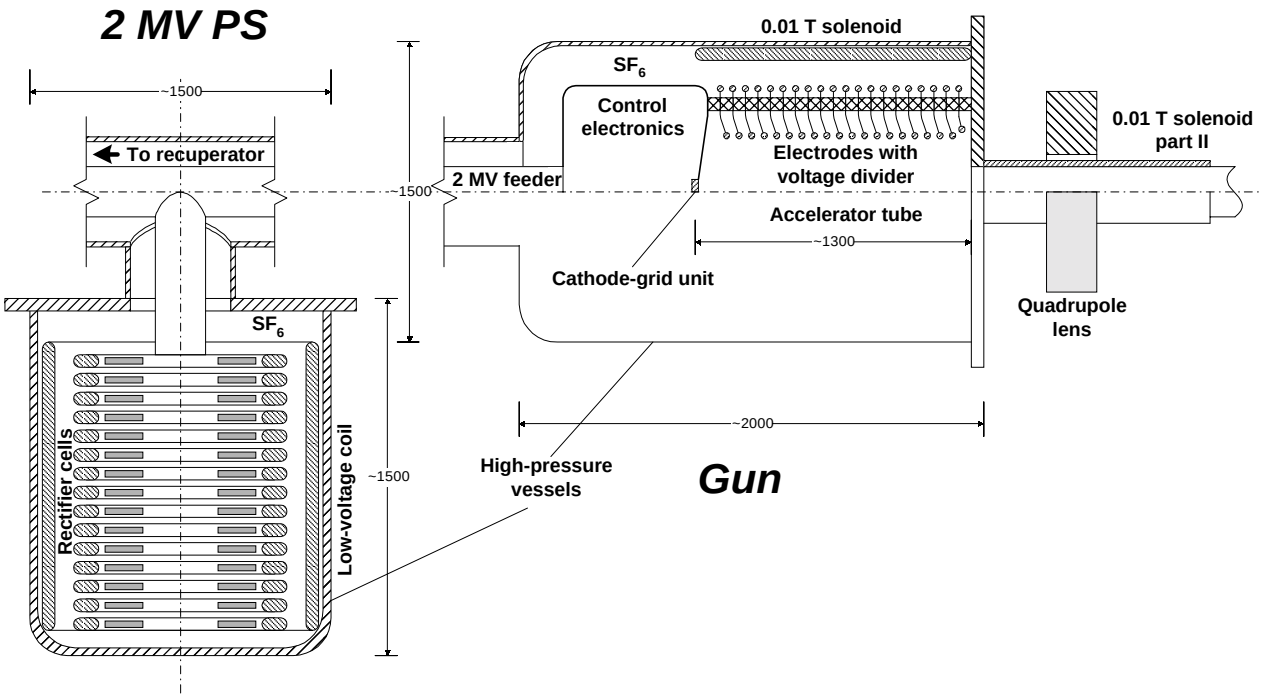

Figure 3.6. Schematic drawing of a 2-MeV electron gun.

3.4. Bunching system

The RF acceleration of a high-charge bunch requires longitudinal bunch compression. The proposed scheme (see Figure 3.7) compress the 2 MeV, 1.6 nC bunch (10^{11} – electron in a single bunch) from 4 ns to 0.06 ns. The number of electrons in the bunch defines its initial length. For 10^{11} electrons, the optimal bunch length is about 4 ns or more, for 10^{10} it is possible to use a bunch length of 1 ns. In this report we will consider the possibility to apply a bunch with maximal initial length. This approach leads to some problems in the engineering of the energy-modulating RF-cavity. The use of an initial bunch length of 1 ns simplifies the buncher significantly.

The bunching system consists of the energy-modulating RF resonator, operating at a sub-harmonic of the main accelerating structure frequency, and the magnetic buncher. In order to reduce the required energy modulation to an acceptable value (less than ±10%) we have to use a high value of the longitudinal dispersion R_{56}. The large energy spread makes a second-order achromat highly desirable.

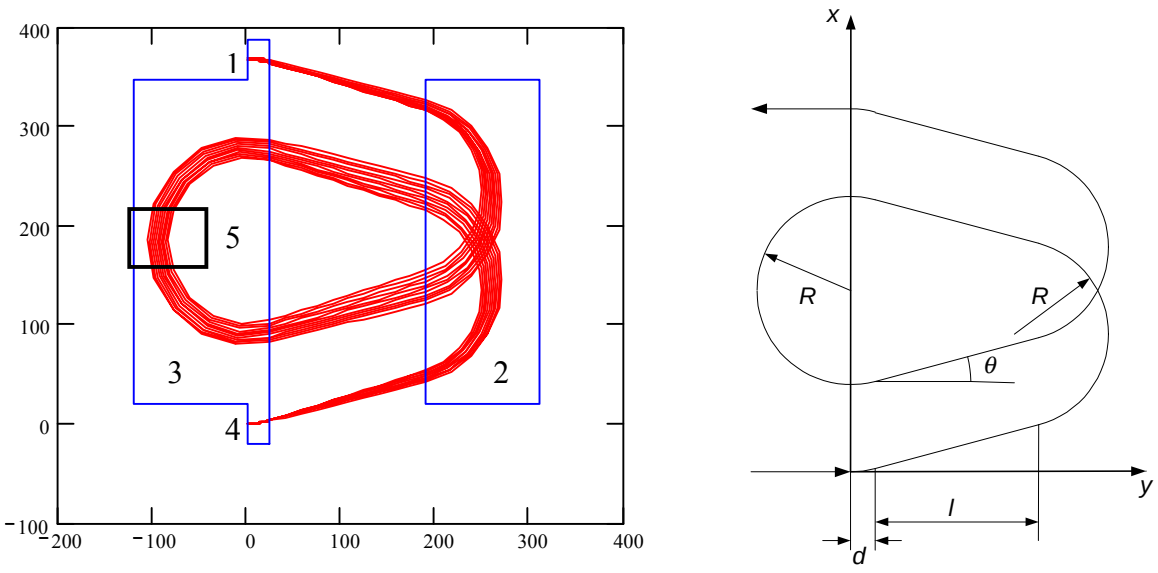

Figure 3.7. Achromatic bend. 1 and 4 – parallel edges magnets, 2 and 3 – magnetic mirrors, 5 – sextupole corrector.

The second-order achromat comprises four homogeneous-field magnets. The first magnet (1), with parallel edges, deflects the beam by an angle θ. Then the beam crosses the gap l and passes through magnetic mirrors 2 and 3 and the second parallel edges magnet 4. As all magnet edges are parallel, the whole 540-degrees bend is a magnetic mirror, i. e., the horizontal output (reflection) angle is equal to the input (incidence) one. Mechanically magnets 1, 3 and 4 are joined to one block. The longitudinal dispersion is

$$R_{56} = E\frac{d}{dE}\left(\frac{L}{v}\right) = -\frac{L}{c\beta^3\gamma^2} + \frac{p}{c\beta^3}\frac{dL}{dp}, \qquad (1)$$

e.f.g.

where c is the velocity of light, E, p, v and γ are the electron energy, momentum, velocity and relativistic factor, respectively, and $\beta = v/c$. The total length of a trajectory in the buncher, (see Figure 3.7), is given by

$$L = 3\pi R + 4\frac{l}{\cos\theta} \text{ h.} \qquad (2)$$

where $R = \frac{pc}{eB}$ is the bend radius, e is an electron charge, and B is the value of magnetic induction in the magnets. The horizontal beam displacement can be expressed as

$$x = 2R + 4l\tan\theta\,. \qquad (3)$$

For the parallel edge magnet of length d, the angle θ is given by $\sin\theta = \frac{eBd}{pc}$. Then the first-order achromaticity condition is:

$$0 = p\frac{dx}{dp} = 2R + 4l\frac{\tan\theta}{\cos^2\theta}. \qquad (4)$$

To satisfy Eq. (4) one can choose the gap between magnets as

$$l = R\frac{\cos^2\theta}{2\tan\theta}. \qquad (5)$$

Calculating the longitudinal dispersion with Eqs. (1, 2 and 5) one obtain

$$R_{56} = \frac{R}{c\beta^3}\left[-\frac{1}{\gamma^2}\left(3\pi + 2\frac{\cos\theta}{\tan\theta}\right) + 3\pi - 2\sin\theta\right]. \qquad (6)$$

i.

To provide the necessary value of R_{56}, the bending radius R was chosen to be 1m. The calculated beta- and eta- functions used at this case are shown in Figure 3.8.

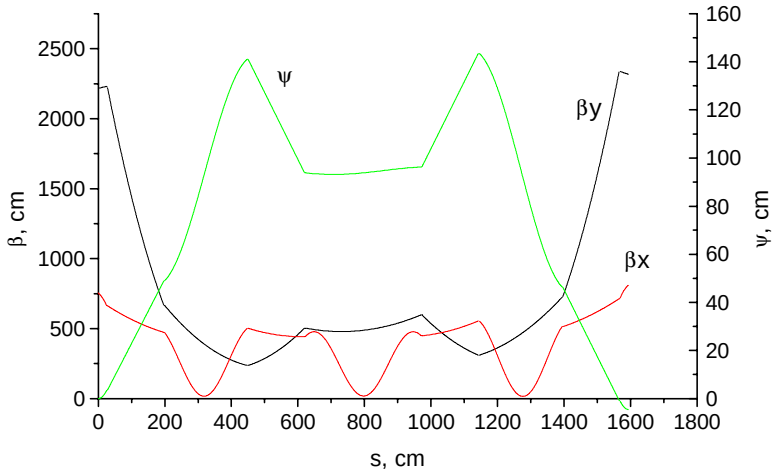

Figure 3.8. Beta- and eta- functions of the bunching system.

The second order chromaticity coefficient $\Delta x(\Delta p/p)^{-2}$ is

$$\frac{1}{2}p^2\frac{d^2x}{dp^2} = R\left(\frac{3}{\cos^2\theta} - 1\right). \qquad (7)$$

j.This chromaticity leads to the increase of radial size of beam after bunching system. Let the set of particles have the initial condition Y=0,Y'=0 and 10% spread of energy before bunching system. Than the transverse position of particles after the bunching system is as shown at figure 3.9.

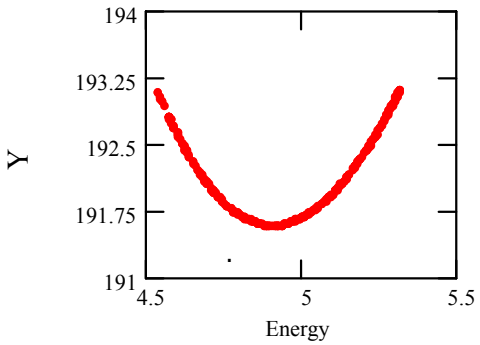

Figure 3.9. The transverse position of electron versus energy ($\gamma=E/mc^2$).

The estimation shows that the effective emittance ε_{nx} gains about 1.5 times at $(\Delta p/p)\approx 0.1$ and radius of beam about 5cm. To make it zero it is enough to install the sextupole field coils (see Figure 3.7.) in the median point of the equilibrium trajectory (in the middle of magnet 2). The calculation of the necessary sextupole strength gives

$$\frac{l_s}{BR}\frac{\partial^2 B}{\partial x^2}=\frac{d^2x'}{dx^2}=\frac{2}{R^2}\left(\frac{3}{\cos^2\theta}-1\right), \qquad (8)\text{k.}$$

where l_s is the length of sextupole, and x and x' means the transverse horizontal deviation from the equilibrium trajectory (in contrary to the meaning of x in Figure 3.7. and in all previous equations) and the corresponding angle deviation. The problem of this approach is the strong non-linearity of particle motion in X and Y-direction. Thus it needs or more complicated system of sextupole or may be it is possible to agree with some gain ε_{nx} in case without sextupole.

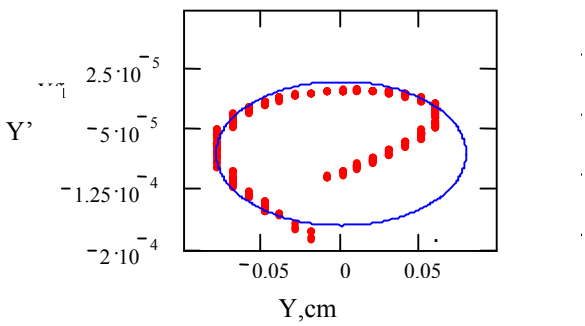

Figure 3.10. The phase diagram of particle after bunching with correction by sextupole. The initial condition for the particles is Y=0,Y'=0 and 10% energy spread

The energy-modulating RF resonator can be a capacitive loaded coaxial line. A schematic drawing of such a device is shown in Figure 3.11. This construction provides a long RF

wavelength with a small resonator size. The length of the resonator and its wavelength are related by the equation:

$$\tan\left[\frac{\omega}{c}L_{cav}\right] = \frac{1}{Z_0 \omega C}, \qquad 1.(9)$$

where Z_0 is the impedance of the coaxial line, C is the value of the shunting capacitor, ω is the resonance frequency of the resonator and L_{cav} is its length.

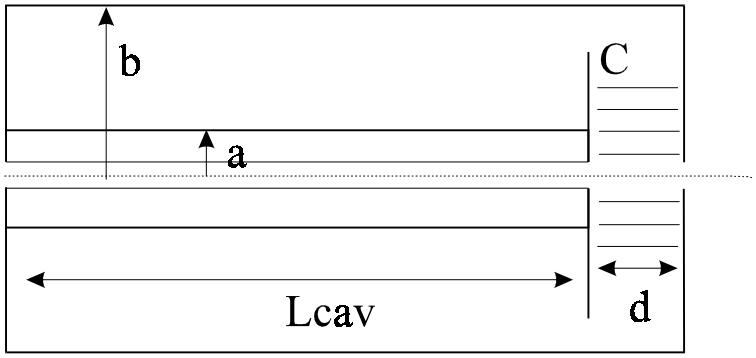

Figure 3.11. Schematic diagram of the energy-modulating RF cavity.

In order to linearize the functional dependence of the momentum increment on the longitudinal position it is necessary to use a harmonic combination of such resonators. The value of the final length of the bunch imposes constraints on the energy-modulating system of resonators. The non-linearity of the momentum increment cannot exceed $2 \cdot 10^{-3}$. This may be determined by observing the spread of electron longitudinal positions due to the non-linearity of the longitudinal momentum, which is approximately

$$\Delta s = 3\pi R \frac{\Delta p'}{p} \qquad (10)$$

where Δs is the final length of the electron bunch and Δp' is the nonlinear momentum increment. This requirement is easily achieved with two harmonics (the third harmonic has a relative amplitude of 0.05) for a phase interval of ±50°. The suggested parameters of the RF-system are shown in the table below. For the fundamental we use two resonators, with a voltage of 360 kV each.

Table 3.4. Suggested parameters of the RF system.

a, cm	b, cm	D, cm	L_{cav}, cm	λ, cm	f, MHz	P, kW	U, kV
5	30	5	56	432	70	60	720/2
5	12	5	30	144	210	1	36

For bunching of beam it is possible to eliminate the high-order term in the equation for time of path via bunching system depending on particle energy.

$$T(\gamma) = T(\gamma_0) + T'(\gamma_0)\cdot\Delta\gamma + \frac{1}{2}T''(\gamma_0)\cdot\Delta\gamma^2 + \dots \quad .$$

This is possible by proper choice of a set of higher harmonics in the cavity. The amplitude and frequency of harmonic are V_1=310 kV f_1=70 MHz, V_2=60 kV f_2=140 MHz, V_3=10 kV f_3=210 MHz.

The phase diagram of particles after passing such bunching system is shown in Figure 3.12. The bunch length shrinks to 0.2 cm.

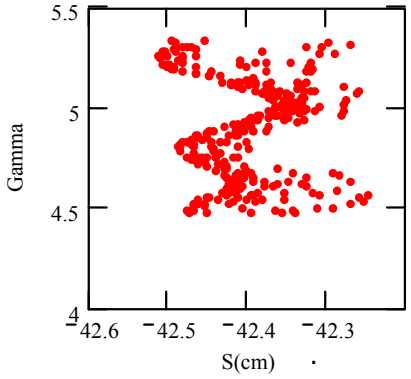

Figure 3.12. The phase diagram γ - s after passing a bunching system with three harmonics of RF-modulation.

One of problems in a low energy electron beam transport is the influence of space charge. A beam is space-charge dominated if the charge-dependent term is comparable to emittance term or to focusing term of the envelope equation.

$$\frac{\partial^2 x}{\partial s^2} + \frac{1}{\beta_x{}^2}x - \frac{\varepsilon_x{}^2}{x^3} - \frac{4N_e r_e}{\gamma^3\beta^2(x+y)\Delta s} = 0$$

$$\frac{\partial^2 y}{\partial s^2} + \frac{1}{\beta_y{}^2}y - \frac{\varepsilon_y{}^2}{y^3} - \frac{4N_e r_e}{\gamma^3\beta^2(x+y)\Delta s} = 0 \qquad \text{m.(11)}$$

where x,y are the transverse r.m.s. sizes of the beam, Δs is the r.m.s. length of beam, N_e is the number of electrons in a bunch, ε is ther.m.s. emittance and r_e is the classical electron radius. Taking the parameters of the bunching system as β_x=500cm, β_y=500cm, $\varepsilon_{nx}=2.2*10^{-2}$ cm, , $\varepsilon_{ny}=2.2*10^{-3}$ cm, and defining

$$K1_x = \frac{4N_e r_e \beta_x^2}{\gamma^3\beta^2(x+y)x\Delta s} = \text{<space charge term>/<focusing term>}$$

n.(12)

$$K2_x = \frac{4N_e r_e x^3}{\gamma(x+y)\Delta s \varepsilon_{xn}^2} = \text{<space charge term>/<emittance term>}$$

o. (13)

we calculate the values of the beam size and space-charge strength terms for a couple of bunch charges:

Table 3.5. Beam size and space-charge strength terms for two representativebunch charges.

Ne	E(MeV)	Δs (cm)	x	y	$K1_x$	$K2_x$
10^{11}	2	30	1.5	0.5	2.7	2.9
10^{10}	2	30	1.5	0.5	0.27	0.29
10^{10}	1	30	1.5	0.5	1.4	0.5

One can see that the electron beam dynamics is space-charge dominated, and for transporting a beam bunch with Ne=10^{11} electrons we need a strong focusing system with beta-functions of about 50-100 cm. The r.m.s. beam parameters are shown in Figure 3.13. for various values of the number of electrons in a single bunch (Ne=10^9, 10^{10} and 10^{11}).

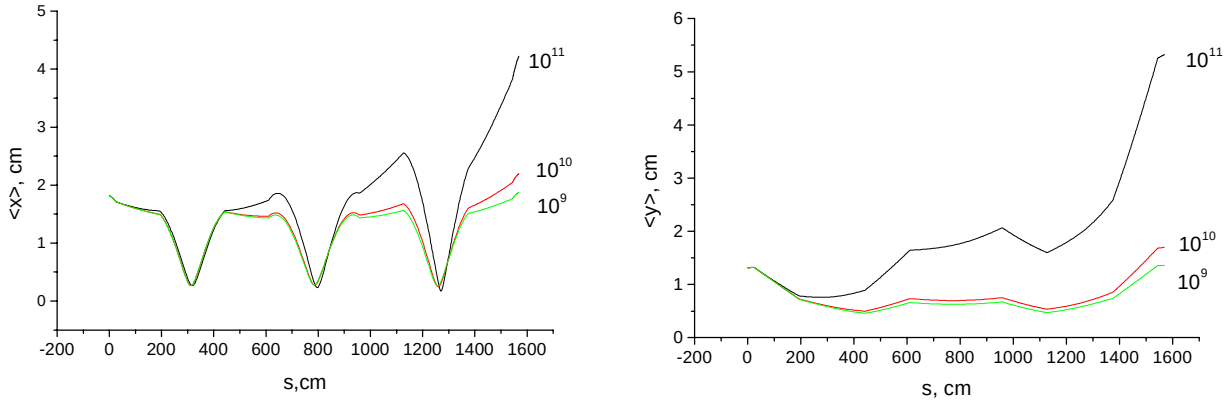

Figure 3.13. The r.m.s. parameters of the electron beam vs. the longitudinal coordinate.

We can see that the effect of the space-charge isn't significant for Ne=10^{10} , but it is crucial for Ne=10^{11}. For transporting Ne=10^{11} in a single bunch, it is necessary to provide a stronger focusing system with β-function of about 50-100 cm or increase the injection energy.

It was shown in [1] that the emittance growth is related to the difference of the field energy of the bunch and an equivalent bunch with uniform density. For the case of a highly space-charge dominated beam, a special form is required for the charge distribution of the bunch in order to preserve the density distribution. For that reason, additional studies of the emittance growth in intense electron bunch are very desirable.

Another problem for high-charge bunch is the physics of such a bunch in a dispersion element (bend). The space-charge force can add a correlation between the horizontal position of electron and its longitudinal momentum. This effect vanishes at a high electron energy.

1. I. Hofmann and J. Struckmeier. Generalized three-dimensional equations for the emittance and field energy of high-current beams in periodic focusing structures. Particle Accelerators, 1987, Vol.21., pp.69-98.

3.5 Main linac

For electron cooling of RHIC we need an electron beam with an energy of 52 MeV, more than 10^{10} electrons in a single bunch, an energy spread of $\Delta\gamma/\gamma=10^{-4}$ or better and a transverse momentum spread of $\Delta p_{\perp}/p=4\cdot10^{-4}$ or better. The main factors affecting the energy and momentum spread of the electron beam in a linear accelerator are the following:

1. Wake field produced by higher-order modes of the cavity on the energy spread of particles.
2. The time dependence of the accelerating RF voltage during the passage of a short electron bunch.
3. The influence of a space-charge field on the energy spread of particles.
4. The influence of inhomogeneity of the magnetic and transverse electric components on the particle's motion.

The bunch is placed at a phase of $\theta= -10°$ in order to produce a linear correlation between the longitudinal momentum and position in the bunch (chirp). This chirp will later serve for debunching of the electrons.

1. The longitudinal wake fields for LEP (350 MHz) and CEBAF(1.5 GHz) accelerating structures were calculated.

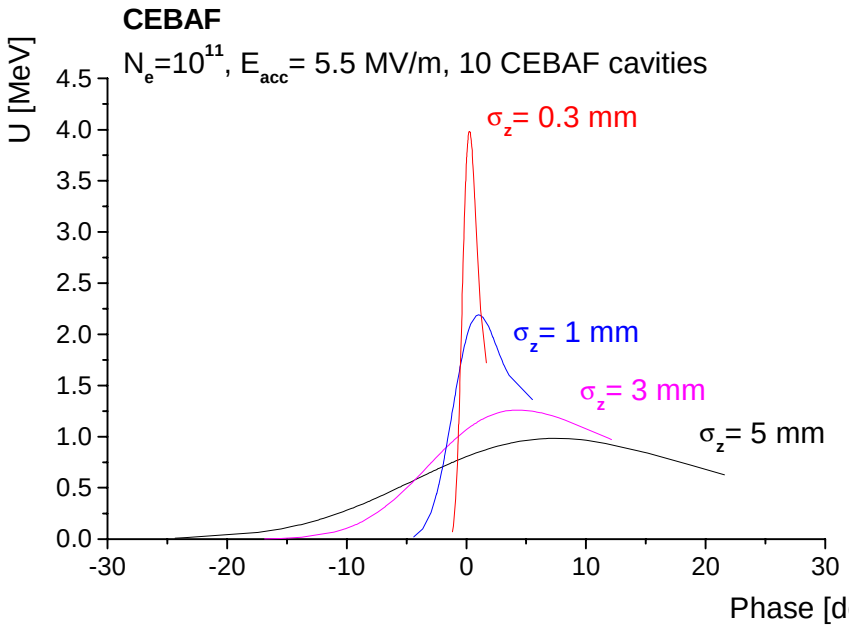

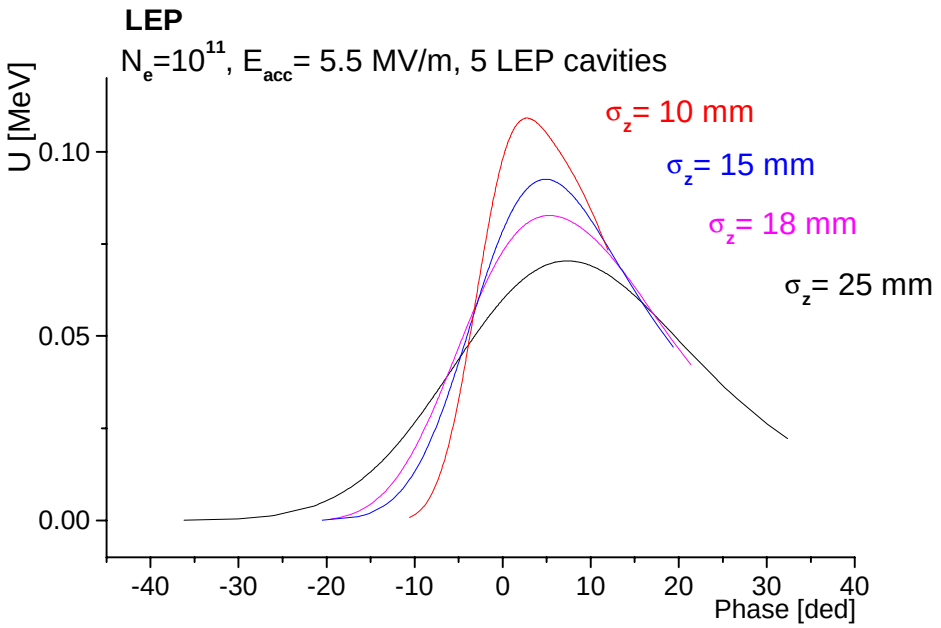

Figure 3.14. The longitudinal wake fields for LEP and CEBAF accelerating structures.

The LEP and CEBAF accelerating structures consist of 5 and 10 cells, respectively. The average accelerating gradient is E=5.5 MeV/m. The results of calculation are shown in Figure 3.14. The increment of particle energy spread as a result of the wake field is given for various values of bunch length. For the CEBAF structure, $\Delta\gamma/\gamma$ is larger than 0.02, which is a large value. For the LEP accelerating structure, this value is more attractive ($\Delta\gamma/\gamma \approx 0.002$). So, the results of the above estimation show that a longer wavelength linac is more appropriate. Of course, there are a few alternatives. One is to use TESLA structures, which have an improved wakefield performance and can be operated at 20 to 25 MV/m. The bunch length may be made longer than 1 mm (requiring a more careful linearization) and the wake field may be largely compensated against the curvature of the accelerating field, as done in the SLC. Yet another way to decrease the wake field effect is using the bunch with a smaller number of electrons, a few times 10^{10}. For the time being we will assume the LEP structure for the design of the machine.

2. The method to increase the linearity of the RF voltage in a cavity during the passage of a short bunch through the accelerating gap is well known. To this end, one needs to add a harmonic component of particular amplitude. For this purpose, a third-harmonic

RF-cavity is placed following the linac, with a relative amplitude approximately -0.11 (the exact value depends on the bunch length). With that we can obtain an energy spread of $\Delta\gamma/\gamma \approx 4 \cdot 10^{-4}$. For the LEP structure, it is possible to use a CEBAF section as the third harmonic cavity. Then, from Figure 3.14 one can see that the wake field from this additional cavity does not add appreciably to the longitudinal spread of momentum (the bunch length is now 18mm). Figure 3.15 shows the distribution of the particles after acceleration, taking into account the wake field. For the LEP structure, the energy spread is $1.3 \cdot 10^{-4}$ at a bunch length of 1.8 cm. Using a longer bunch increases the energy spread (see upper diagram in Fig.3.14). Thus, the bunching system located before the linac should compress the bunch down to less than 2 cm.

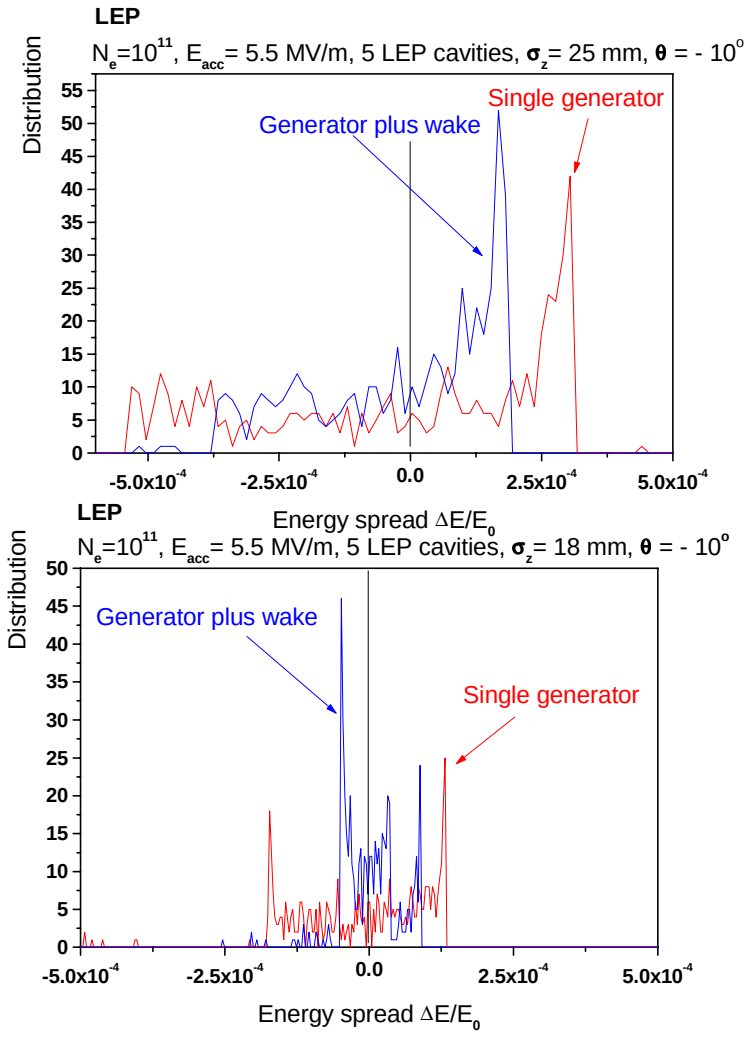

Figure 3.15. The distribution of the particles as function of energy.

3. The particles can suffer an additional transverse and longitudinal momentum spread due to space-charge forces. Let us estimate the magnitude of the space-charge effects. Let the bunch have a normal longitudinal distribution (σ_z=18 mm that is equivalent to σ_t= 0.06 ns) and a uniform transverse distribution. The transverse shape of the bunch is

an ellipse with semi-axis rx, ry. Such a bunch can be approaximated as a three-dimensional ellipse with length of z semi-axis $lz = \frac{3}{4}\sqrt{2\pi}\sigma_z$. The number of particles in the range lz of the ellipse is 94% of the total and the particle distribution along the z-axis is close to normal. The difference between the RF-field at the edge of a bunch and at the center of a bunch is

$$\Delta E_z(\varphi_c, s) = E_{acc}\left(\cos\left(\varphi_c + \frac{2\pi s}{\beta\lambda}\right) - \cos(\varphi_c)\right). \quad (1)$$

The effective longitudinal electric field of the space-charge is

$$\Delta E_{qz}(s,\gamma,lz,rx,ry) = \frac{3Q}{4\pi\varepsilon_0}\cdot\frac{1}{\gamma^2}\cdot\frac{s}{lz}\cdot F_z\left(\frac{rx}{lz},\frac{ry}{lz}\right), \quad (2)$$

where $F_z\left(\frac{rx}{lz},\frac{ry}{rx}\right) \equiv F_z(a,b) = \frac{1}{2}\int_0^\infty \frac{d\xi}{\sqrt{(a^2+\zeta)\cdot(a^2b^2+\zeta)\cdot(1+\zeta)^3}} = 1.261.$ (3)

For the following parameters

$\varepsilon_{ing} = 1$ MeV, $\gamma_{ing} = 2.96$. $\varepsilon_{out} = 50$ MeV, $\gamma_{out} = 98.8$.

$N_e = 10^{11}$, $Q = 16$ nC. $E_{acc} = 5.3$ MeV/m.

σ_z=18 mm ($lz \cong 34$ mm), $rx = 15$ mm, $ry = 1.5$ mm.

and $\varphi_c = 0$, $s = lz$, we have

$\Delta E_z \cong 0.17$MV/m.

$\Delta E_{qz}(\gamma = \gamma_{ing}) \cong 5.5\cdot10^{-2}$ MV/m,

$\Delta E_{qz}(\gamma = \gamma_{out}) \cong 4.8\cdot10^{-5}$ MV/m ($\sim 1/\gamma^2$). (4)

This means that the space-charge force along the z-axis is just 0.3 (at the linac input) or $3\cdot10^{-4}$ (at the linac output) compared to the inhomogeneity of leading RF-fields. Thus, the final increase in longitudinal emittance is dominated by the wake-fields and leading RF-field.

Now let us estimate the transverse dynamics of the electron due to space charge. The transverse RF- and charge dependent electric fields are:

$$E_x(\varphi_c,s,x,\lambda) = E_{acc}\frac{x}{2\gamma^2}\cdot\frac{2\pi}{\beta\lambda}\sin\left(\varphi_c + \frac{2\pi s}{\beta\lambda}\right), \qquad E_y(\varphi_c,s,x,\gamma) = E_{acc}\frac{y}{2\gamma^2}\cdot\frac{2\pi}{\beta\lambda}\sin\left(\varphi_c + \frac{2\pi s}{\beta\lambda}\right).$$

(4)

$$E_{qx}(x,\gamma,lz,rx,ry) = \frac{3Q}{4\pi\varepsilon_0}\cdot\frac{1}{\gamma^2}\cdot\frac{x}{rx(rx+ry)lz}, \qquad E_{qy}(y,\gamma,lz,rx,ry) = \frac{3Q}{4\pi\varepsilon_0}\cdot\frac{1}{\gamma^2}\cdot\frac{y}{ry(rx+ry)lz}.$$

(5)

For $\varphi_c = 0$, $s = lz$, $x = rx$, $y = ry$ we have

$E_x(\gamma = \gamma_{ing}) \cong 9.4\cdot10^{-3}$ MV/m, $E_y(\gamma = \gamma_{ing}) \cong 9.4\cdot10^{-4}$ MV/m,

$E_x(\gamma = \gamma_{out}) \cong 7.5\cdot10^{-6}$ MV/m, $E_y(\gamma = \gamma_{out}) \cong 7.5\cdot10^{-7}$ MV/m ($\sim 1/\gamma^2$).

(6)

$E_{qx}(\gamma = \gamma_{ing}) = E_{qy}(\gamma = \gamma_{ing}) \cong 9.1\cdot10^{-2}$ MV/m,

$E_{qx}(\gamma = \gamma_{out}) = E_{qy}(\gamma = \gamma_{out}) \cong 7.9\cdot10^{-5}$ MV/m ($\sim 1/\gamma^2$).

(7)

In contrast to the case of longitudinal dynamics, the space-charge force dominates the transverse dynamics of the electrons.

The calculation above shows that the accelerating rate of 5.3 MeV/m is sufficient to insure the invariability of the bunch length during acceleration considering the space-charge force.

Note that at a first glance, it would seem that the range of short wave length is more attractive, as its overall dimensions are relatively small as well as its cost. But $\Delta p_{\|}/p \sim \sigma_z^3 \sim \omega_0^3$, where ω_0 is the main frequency. Thus the difficulties related to the effect of space-charge force are sharply increased with an increase in the accelerator working frequency. Therefore we should use the minimum RF frequency.

3.6 Debunching system after linac.

The length of electron bunches is very short (Lbunch~1cm). However, for electron cooling we need bunches with a length of about 30 cm. The debuncher is similar to the buncher device at low energy (section 3.4). It consists of the energy-modulating RF and the magnetic buncher. The buncher with a high value of the longitudinal dispersion is required for decreasing RF voltage needed for the reduction of momentum spread of electron. In this report we use a 4% modulation of energy for debunching. It is also possible to use 1-0.5% but this variant will have a magnet of large size. In the intermediate report we considered the variants with a half-turn bend bunching system. Similar bunchers have the large size and we have now chosen the α- magnet system as a dispersion element.

We use the result of the section 3.4. The total length of trajectory in a buncher (Fig.3.7. in section 3.4.) is:

$$L = 3\pi R + 4\frac{l}{\cos\theta} \qquad (1)$$

This system produces a bunch of about 30 cm in length for a bend radius 1 m and a relative momentum spread of $\Delta p/p_0 = 0.04$.

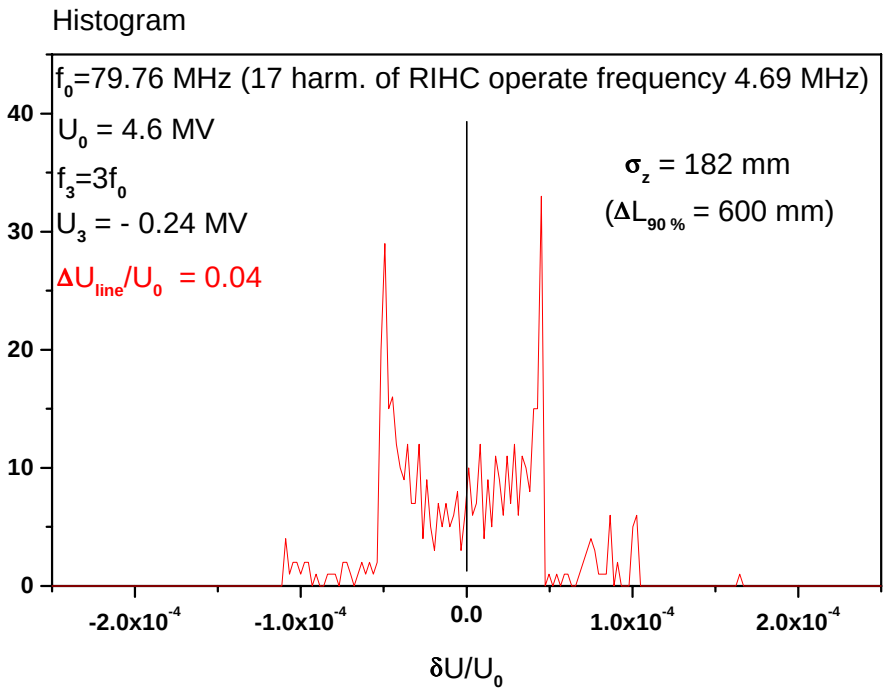

Fig.3.16. The particle distribution as a function of energy after reduction of momentum spread.

The momentum spread of electrons is defined by the choice of the acceleration phase. A system of superconducting RF-cavities is used for the reduction of momentum spread. The first harmonic is 80 MHz with amplitude 4.6 MV; the third harmonic is 240 MHz with amplitude 0.24 MV. The distribution of electrons after the reduction of momentum spread is shown in Fig. 3.6.1. We can see that the requirement $\Delta\gamma/\gamma=10^{-4}$ is satisfied.

3.7. Injection of the electron beam into the field of solenoid

Since we have a very strict limit on the transverse emittance of the electron beam inside the solenoid, a non-destructive method of injection of electrons into the field of the solenoid is very important. We will consider two possible methods of nondestructive injection of electrons into the field: (1) Injection of a flat electron beam using quadrupoles as the focusing elements [1-3]; (2) injection of the round electron beam generated by a magnetized cathode.

3.7.1. Injection of a flat electron beam using quadrupoles.

For injecting a beam into the field of a solenoid we assume the optical system shown in Figure 3.17. The radius of the electron beam is a_e=0.06 cm in the magnetic field B_{cool}=10kG of the cooling section. Let the magnetic field on the cathode of the electron gun be B_{gun}=100 G, then the radius of the electron beam is a_{egun}=0.6 cm. After acceleration to an energy of eU_0=2 MeV, the electron bunch exits the magnet field and then is transformed from a round beam to a flat beam. Before entering the main solenoid, the beam is transformed back to a round beam by the inverse operation.

Let the wavelength of the Larmor spiral in the gun solenoid be λ. Then we choose the distance between skew-quadrupoles SKW1 and SKW2 to be πλ. The focal lengths of SKW1 and SKW2 are 2λ and –4λ, respectively. For the main solenoid we adopt a similar notation.

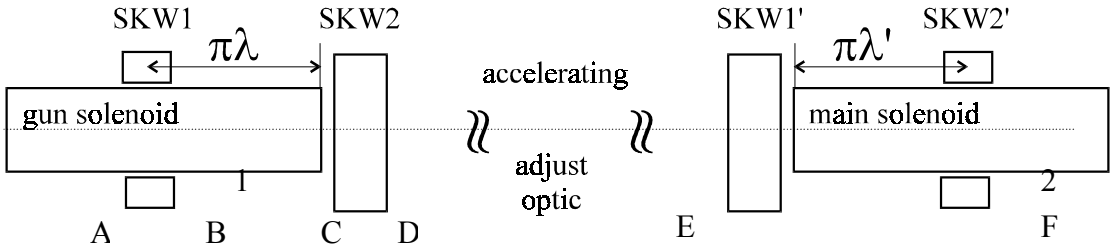

Figure 3.17. Schematic diagram of a matching transition of the electron beam between solenoids.

The value of the transverse momentum in the main solenoid can be evaluated from the invariance of the magnetic flux in the Larmor circle

$$r_{L1}^{\,2} \cdot B_1 = r_{L2}^{\,2} \cdot B_2 . \qquad (1)$$

Hence

$$\frac{\Delta p_2}{p_2} = \frac{\Delta p_1}{p_1}\frac{\gamma_1}{\gamma_2}\sqrt{\frac{B_2}{B_1}} . \qquad (2)$$

Thus, the initial spread of the transverse momentum in the injector should not exceed $\Delta p_1/p=1.3\cdot10^{-3}$ ($\gamma_2=100$, $\gamma_1=5$, $B_2=10^4$ G, $B_1=100$ G, $\Delta p_2/p\approx6.4\cdot10^{-4}$) This is not a severe restriction.

The features of beam transport from one longitudinal magnetic field to another is as follows. If we consider the invariance of emittance as an invariance of the phase-space volume then the proper variables are {$P_x = p_x+eA_x/c$, $Q_x=x$, $P_y = p_y+eA_y/c$, $Q_y=y$, }, where P is the generalized momentum and A the vector-potential of the magnetic field. As can be seen by the choice $A_x=-B\cdot y/2$, $A_y=B\cdot x/2$ for the gauge, there is a nonzero "magnetic emittance" for a beam generated in a longitudinal magnetic field. Note that this "magnetic emittance" isn't related to the spread of transverse momentum of the particles ($p_x=0$, $p_y=0$). After transition of beam from the zone with magnetic field to the zone without magnetic field, the "magnetic emittance" converts to a real emittance and a spread of the transverse momentum of the particles appears (Busch's theorem). However, with the special optics described below, it is possible to convert the "magnetic emittance" to the real emittance of just one component of particle motion, for example x. In this case, the correlation between x and y is eliminated and the beam can be transported with a standard optical system. The emittance of the y-component in the magnetic field free zone is defined by the thermal spread of transverse momentum in the magnetic field and the radius of the Larmor circle. Thus,

$$\varepsilon_{yn} = \left[\frac{\varepsilon'_n}{a_e}\right]^2 \frac{m_e c^2}{e B} \qquad (3)$$

where ε'_n is normalized emittance in the injector. For the injector parameters of $T_{e\perp}$=0.1 eV, a_e=0.6 cm, B=100 G we have $\varepsilon_{yn} \approx 7 \cdot 10^{-6}$ cm·rad and the beam is flat with $\varepsilon_x >> \varepsilon_y$. This value ε_{yn} is very small and therefore problematic, since the y-size of beam is very small and space charge forces will dominate the dynamics. But we have observed above that a momentum spread of $\Delta p_l/p = 1.3 \cdot 10^{-3}$ in the injector is good enough for maintaining the tolerance on $\Delta p/p$ in the main solenoid. Thus the $T_{e\perp}$=10 eV, a_e=0.6 cm, B=100 G and $\varepsilon_{yn} \approx 7 \cdot 10^{-4}$ cm·rad leads to a satisfactory beam in the main solenoid and the discrepancy between ε_{xn} and ε_{yn} is not very large.

The phase space diagrams shown in Figure 3.17. illustrate the beam propagating through the first solenoid. The first pair of diagrams (marked "A") shows a round beam with zero spread of transverse momentum ($\{p_\alpha, q_\alpha\}$ - coordinates). After passing the skew-quadrupole SKW1 with focal length of 2λ, the phase space diagram is shown in the second pair (B). Next, the result of a drift space with length $\pi \cdot \lambda$, followed by the solenoid edge. (C) and the skew-quadrupole SKW2 (D) are shown. After SKW2 the beam has a horizontal plane emittance of 1.2 cm *0.0035 radians and 0 for vertical plane. The normalized beam emittance is $\varepsilon_{xn} = \gamma\beta x x' = 0.022$cm-radians. If the transverse distribution of electron current is flat then all electrons moved inside this emittance. This way the "magnetic emittance" is transferred to the real emittance of the x-component of the electron motion. Before the main solenoid this operation is done in reverse order.

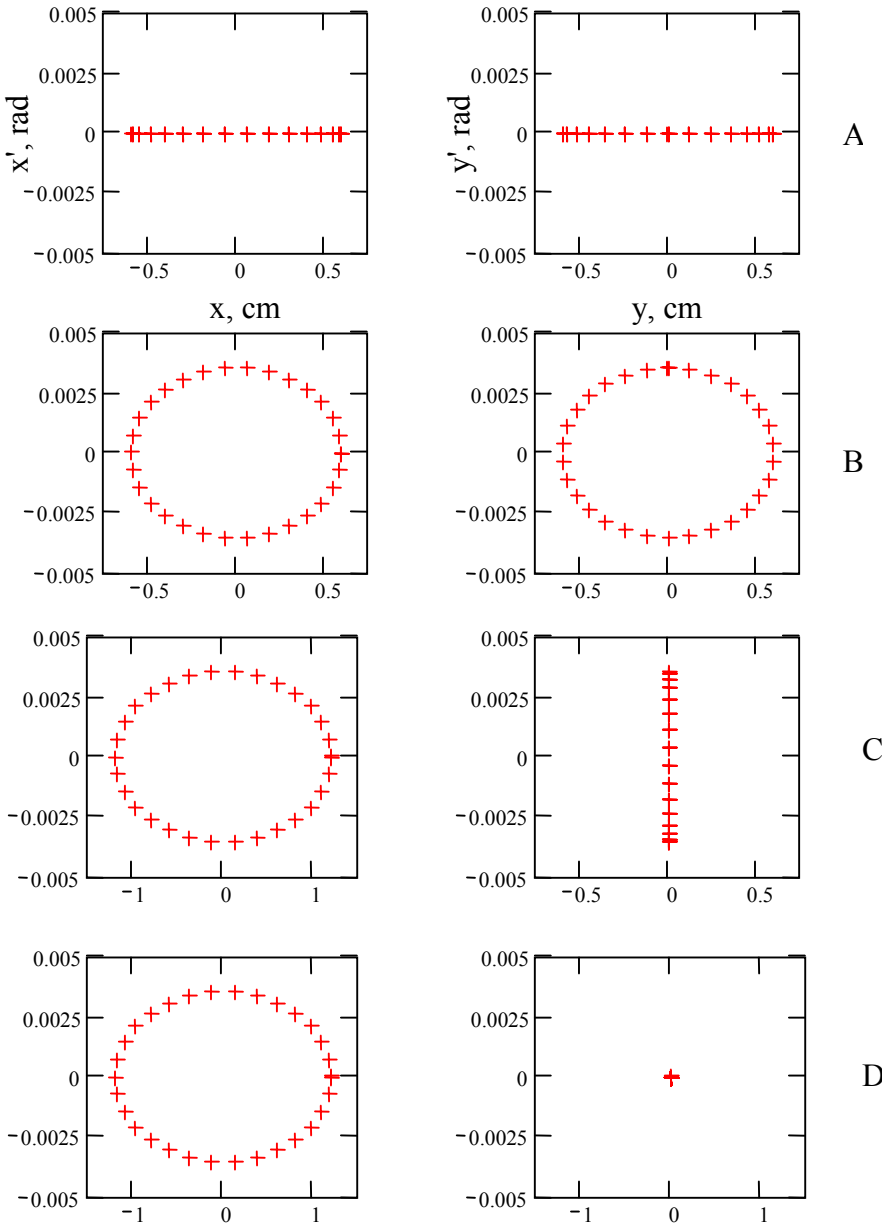

Figure 3.18. The phase diagram for optics matching a solenoid, a conventional optic channel and another solenoid.

The matrix of transformation from the round to the flat beam is the product of a skew quadrupole, solenoid, solenoid edge and another skew quad. We can write it as:

$$\begin{bmatrix} 2 & 0 & 0 & 2\lambda \\ 0 & \frac{1}{2} & -\frac{1}{2\lambda} & 0 \\ 0 & -2\lambda & 0 & 0 \\ 0 & 0 & 0 & -\frac{1}{2} \end{bmatrix} \begin{bmatrix} x \\ x' \\ y \\ y' \end{bmatrix} = \begin{bmatrix} 1 & 0 & 0 & 0 \\ 0 & 1 & -\frac{1}{4\lambda} & 0 \\ 0 & 0 & 1 & 0 \\ -\frac{1}{4\lambda} & 0 & 0 & 1 \end{bmatrix} \cdot \begin{bmatrix} 1 & 0 & 0 & 0 \\ 0 & 1 & -\frac{1}{2\lambda} & 0 \\ 0 & 0 & 1 & 0 \\ \frac{1}{2\lambda} & 0 & 0 & 1 \end{bmatrix} \cdot \begin{bmatrix} 1 & 0 & 0 & 2\lambda \\ 0 & -1 & 0 & 0 \\ 0 & -2\lambda & 1 & 0 \\ 0 & 0 & 0 & -1 \end{bmatrix} \cdot \begin{bmatrix} 1 & 0 & 0 & 0 \\ 0 & 1 & \frac{1}{2\lambda} & 0 \\ 0 & 0 & 1 & 0 \\ \frac{1}{2\lambda} & 0 & 0 & 1 \end{bmatrix} \cdot \begin{bmatrix} x \\ x' \\ y \\ y' \end{bmatrix}$$

The evolution of the beam envelopes as a function of longitudinal position is shown in Figure 3.18. Point A is the starting point of the transformation and point D is the finish. The edges of a vertical line segment represent the beam envelope. The continuous lines are the trajectories of four test particles (two shown in the x-z plot and two in the y-z plot).

Another illustration of the beam transformation is shown in Figure 3.19. All particles are starting inside the solenoid. The starting points are located on a circle indicated by the dash line. The initial transverse momentum of particles is zero. SKW1 impacts the transverse impulse and the electrons move as is shown by the "+" points. After turning by half Larmor cycle they appear on the straight line Y=0. SKW2 and the edge field of the solenoid eliminate the transverse momentum of the y-component. The finish points are located on the solid line Y=0.

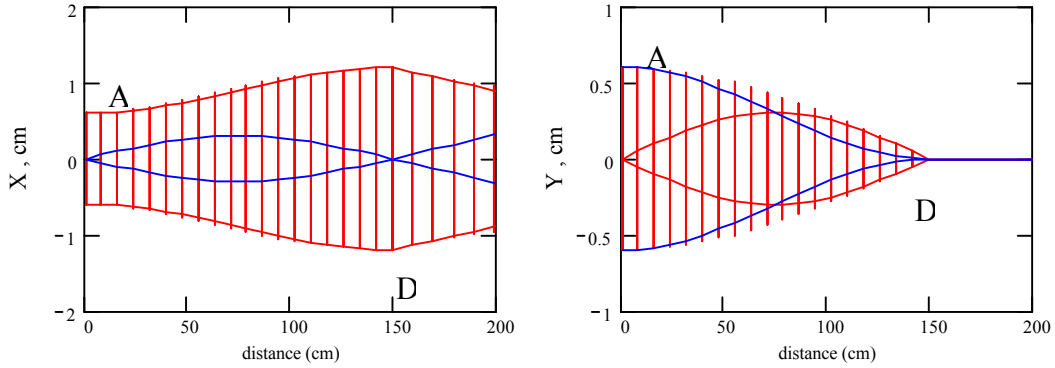

Figure 3.19. The x-y dynamics of test particles and beam envelopes along the path. The edges of a vertical line segment represent the beam envelope. The continuous lines are the trajectories of test particles.

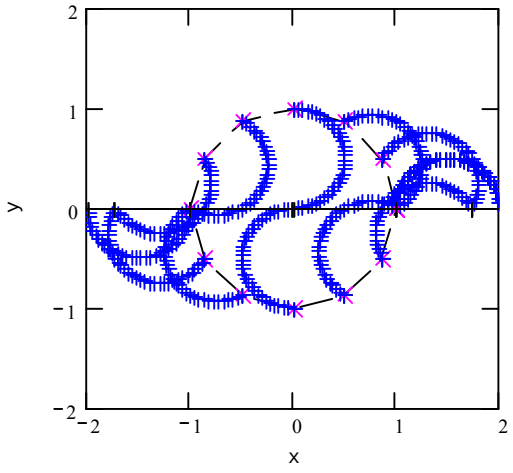

Figure 3.20. The illustration of conversion of round beam into a flat beam.

The calculation above was done assuming a zero initial emittance (no thermal, space charge or similar emittances included.) Next we include the effect of an additional emittance, as shown in Figure 3.21. A small value of noise is added to the transverse momentum in various places of the system in Figure 3.21. The noise has a normal distribution. The first phase space diagram in Figure 3.21. shows the influence of the momentum spread in the injector (A, D, E). According to Equation 2, a transverse temperature of 0.2 eV ($\Delta p/p \approx 1.8 \cdot 10^{-4}$) at the injector (point A) leads to an increase in the transverse momentum of particle into the main solenoid of $\Delta p_2/p \approx 9 \cdot 10^{-5}$. A noise level of $\Delta p/p = 1.8 \cdot 10^{-4}$ after SKW2 (point D) leads to a transverse momentum into the main solenoid of $\Delta p_2/p = 1.6 \cdot 10^{-4}$. This result illustrates the restriction on the emittance growth in the electron beam transport system. Consider that at point D the beam size in one dimension is very small. Since it is essential to transport a bunch containing a large number of electrons, the space-charge dominated bunch may acquire an additional emittance due to the nonlinear part of the electric field. Another cause for increase in transverse momentum is RF induced transverse kick by the exit from an accelerating cavity.

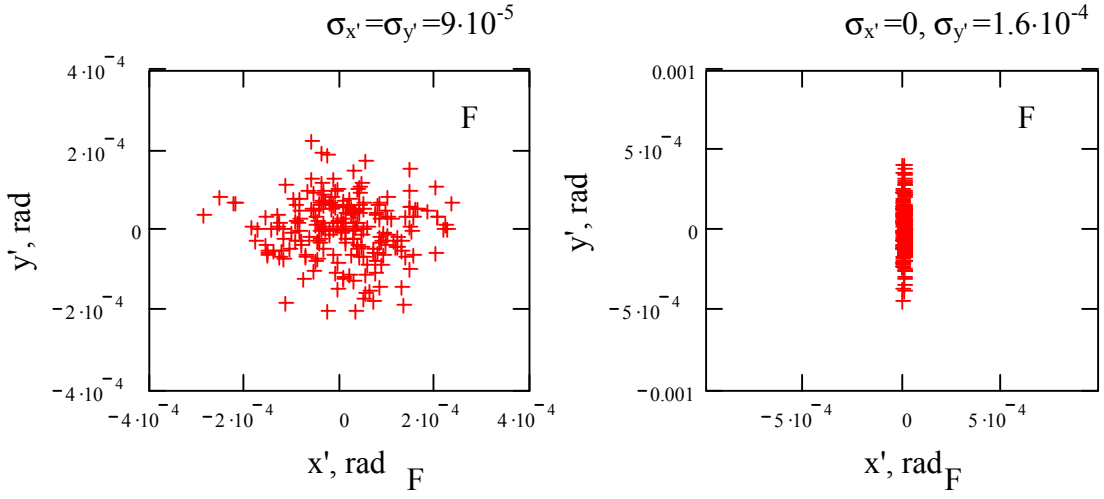

Figure 3.21. The influence of emittance growth along the transport channel on the resulting momentum spread sent to the main solenoid. The left and right diagrams deal with the additional transverse momentum spread into the injector (A) and before accelerating (D), respectively . The magnitude of the noise is $\Delta p/p = 1.8 \cdot 10^{-4}$ for both cases.

3.7.2. Injection of round electron beam generated by a magnetized cathode

It is possible to realize a non-destructive injection of an electron beam into the magnetic field of the solenoid if one can prepare the vortex like state of the electron beam with the azimuth component of momentum of the particles proportional to the distance from the axis. In this case, the edge field of the solenoid may cancel the azimuthal

component of the momentum and the particles will move inside the solenoid with zero transverse velocities. This vortex like state of the beam can be obtained by using an electron gun immersed in a magnetic field (Figure 3.22.).

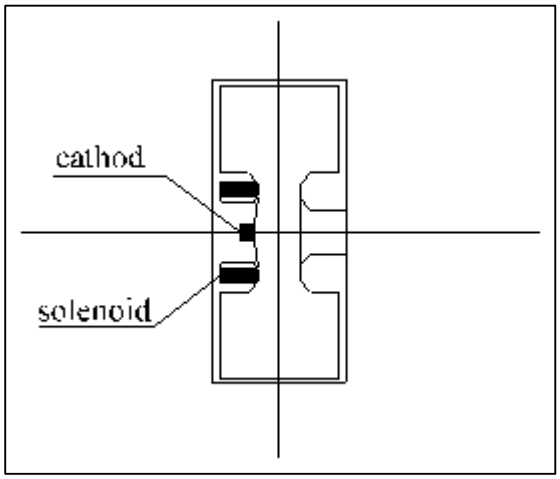

Figure 3.22. Electron gun with a cathode immersed in a magnetic field.

Let us discuss this possibility. The law of conservation of the generalized momentum for azimuth component is:

$$p_\varphi \cdot r + \frac{1}{2}\cdot\frac{e}{c} Hr^2 = const$$

From this law the condition of the correct injection of the particles into the solenoid is

$$H_g R_g^2 = H_s R_s^2,$$

$$H_g = H_s \frac{R_s^2}{R_g^2}$$

Where (H_g, R_g) and (H_s, R_s) are the magnetic field and radius of the beam at the gun and solenoid, respectively. (at the presence of a space charge, this expression is modified but not significantly).

$$\omega = \frac{eH}{mc} \qquad \frac{\omega}{c} = 0.578 \times H\,(kG)\,(1/cm)$$

If the magnet field at cooling solenoid H_s=10 kG, the radius of electron beam R_s=0.06 (cm), the radius of electron beam at the electron gun R_s=0.6 (cm) then:

$$H_g = H_s \left(\frac{R_s}{R_g}\right)^2 \qquad H_g=100\ (G)$$

If the energy of the injector is $\gamma f := 5$, the energy of accelerator $\gamma a := 100$, then the angle of divergence of the beam after the injector:

$$\alpha_f = \frac{1}{2}\frac{\omega R_g}{c\sqrt{\gamma_f^2 - 1}} = 0.006$$

the angle of divergence of the beam after the accelerator :

$$\alpha_s = \frac{1}{2}\frac{\omega R_s}{c\sqrt{\gamma_a^2 - 1}} = 3\times 10^{-4}$$

The transmission of such a beam through a transport channel and creation of appropriate properties of the beam at the entrance of the solenoid by an appropriate system of lenses is known but a detailed calculation of the complete optical system of this scheme is required.

References

[5] V.I. Kudelainen, I.N.Meshkov, V.V.Parkhomchuk, R.A.Salimov, A.N.Skrinskii, V.G.Fainstein. "Deep deacceleration of electron beam at a system with longitudinal magnetic field" Journal of Techical Physics, Vol.46 (1976), N8, p.1678-1686.

[6] **A.N.**Sharapa. Ph.D.Thesis "Experimental investigation of recuperation of intensive electron beam" Novosibirsk, BINP, 1982.

[3] A.Burov, Ya.Derbenev, S.Nagaitsev, A.Shemiakin. "Optical principles of beam transport for relativistic electron cooling". Phys.Rev. Special topics – Accelerators and beams, Vol.3, (094002), 2000.

3.8. Cooling straight section parameters

There are a few reasons why the cooling section for RHIC should have a large length:

a. Magnetized-electron cooling requires a long interaction time at the beam reference frame, satisfying $\omega_L*\tau >>1$, and maximal impact parameter should be $\rho_{max}=V*\tau >>\rho_L$ -Larmor radius of transverse motion of electrons, where $\tau =l_{cool}/(\gamma\beta c)$- time of flight cooling section at beams rest reference system.

b. A longer cooling length allows us to use a smaller electron beam current.

c. The cooling time is proportional to the ion's transverse velocity to the third power and inversely proportional to electron beam density. A larger value of the ion's beta function in the cooling section, β_{cool}, decreases the transverse ion velocity. Thus, an increase in β_{cool} leads to decreasing cooling time as $\beta_{cool}^{-1/2}$.

d. The coherent damping decrement of an ion beam fluctuation is proportional to τ^4.

As long as the cooling parameter is far from dangerous limits, it is advantageous to have faster coherent cooling by increasing the length of the cooling section.

The long straight sections near the RHIC interaction points permit to have a cooling solenoid length of about l_{cool}=30 m and this value will be used in this report.

The magnetic field for obtaining a sufficiently long lifetime due to radiative electron capture is estimated in the introduction as 1 Tesla. It means that the solenoid for

the cooling section should be superconducting. The action of this solenoid on the ion motion at RHIC should be the subject of a special study.

The main requirement imposed to the solenoid by the electron cooling mechanism is parallelism of the direction of the magnetic field lines along the beam orbit. This parallelism should be a few times better than the angular spread of the ion beam:

$$\Delta\theta = \sqrt{\frac{\varepsilon_{ni}}{\beta\gamma\beta_{cool}}} \qquad \Delta\theta = 1.25\times 10^{-5}$$

3.8.1. The effect of gap between sections of the main solenoid.

The main solenoid can be made as one unit or as a modular structure. In the first case, the main solenoid is placed to one cryo-volume. The value of gap is determined by manufacture of the long solenoid and it can be minimal (1-2 cm). In the case of a modular structure of the main solenoid, we must deal with the problem of the variation of the electron beam parameters while passing through the gap.

The magnetic field in the gap has a radial component that generates an additional azimuthal velocity of the electron. This leads to two harmful effects. The first is related to an increase in the Larmor radius that leads to decrease in the cooling rate by a factor (see Section 4)

$$\varepsilon = \frac{\lambda_1}{\lambda_0} = \frac{Ln(1+\frac{\rho_{max}}{\rho_{L1}})}{Ln(1+\frac{\rho_{max}}{\rho_{L0}})} \qquad (1)$$

where ρ_{max} is the maximal impact parameter of an ion-electron collision, ρ_{L0} and ρ_{L1} is the Larmor radius for both cases, λ - cooling rate for the ion oscillation with the amplitude about zero.

The second effect is related to a drift of the center of the Larmor circle. During its interaction time with the electron beam, the ion has time to cover a distance smaller than the electron beam radius. Thus, the maximal impact parameter is $\rho_{max} = Vi*\tau$. Moreover, an arbitrary shift of the center of the electron Larmor circle leads to appearance of an effective drift velocity of the electron relative to the ion. The ratio of cooling rate in the case of main solenoid with gap to the case without gap is

$$\varepsilon = \frac{\lambda_1}{\lambda_0} = \frac{V_{eff\,0}^3}{V_{eff\,1}^3} \qquad (2)$$

where V_{eff} is the effective velocity between ion and the Larmor center of an electron induced by any of several mechanisms: The drift in crossed ExB fields in the parallel line of magnetic field, the error in the parallelism of magnetic field line, the longitudinal temperature of electron and gap effects.

Let us estimate the value of the effects when the length of gap δ is smaller than the longitudinal Larmor length λ_L . The increase in transverse momentum upon passing a single gap is approximately

$$\Delta p_{\perp} = \int F_{\perp} dt \approx \frac{1}{2} eB_0 \frac{a_e}{c} \frac{\delta}{\lambda_L} \qquad (3)$$

where a_e is the electron beam radius. The average drift momentum of electron in the gap is estimated as

$$\Delta p_D \approx \frac{1}{2} eB_0 \frac{a_e}{c} \frac{\delta}{l_{section}} \qquad (4)$$

For the gap of δ=4 cm and length of sections $l_{section}$ =200 cm losses the cooling rates decrease factor as ε_1= 0.8 for the effect of Larmor radius growth and ε_1= 0.072 for the effect of Larmor circle drift. Thus, the drift of the Larmor circle center induces the more harmful effect. The worse case is shown in Figure 3.23. In this case, the length of one section of the main solenoid is taken as $4*\pi*\lambda_L$ and the shifts of the Larmor center induced by all gaps are added together. The trajectory in the transverse plane x-y is shown in Figure 3.23(left) and the shift of the Larmor center is shown on the right. The drift velocity leads to the angle between electron and ion velocities of $\Delta\theta = 2.332\times 10^{-5}$ that is larger than the angle related to the magnetic field error $\Delta\theta_B=10^{-5}$. The cooling rate decreases by factor 100 (ε_1= 0.01). That is unacceptable.

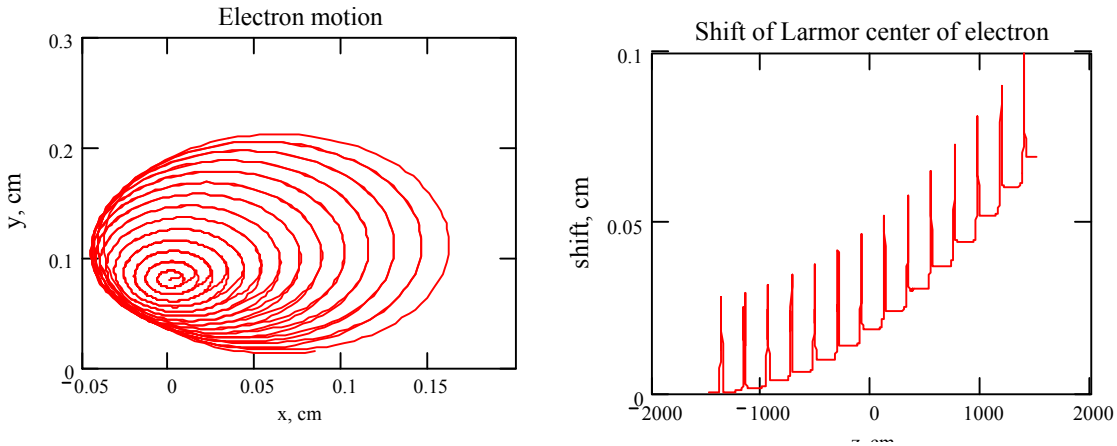

Figure 3.23. The trajectory of the electron for the solenoid section with parameters: the length - 208 cm, the gap between solenoids - 4cm, the solenoid radius - 7.5cm.

In order to minimize this effect we propose two ways. The first method is to select a special length of the solenoid section, and the second method uses a special correction coil.

3.8.2. Choice of section length.

If one choose the length of solenoid section as $(2*n+1)\pi\lambda_L$where n is the integer then the contributions of even and odd gaps are cancelled. In this case, electrons move with alternating large and small Larmor circles ρ_L in the adjacent sections but the centers

of Larmor circles do not drift very much. The trajectories of the electron motion are shown in Figure 3.23.

The angle between electron and ion velocities is much less than the angle induced by error in the magnetic field. The resultant decrease in cooling force is $\varepsilon = 0.834$. This solution can be used to decrease the negative effect of a short gap (for the version with main solenoid being one unit with small gaps).

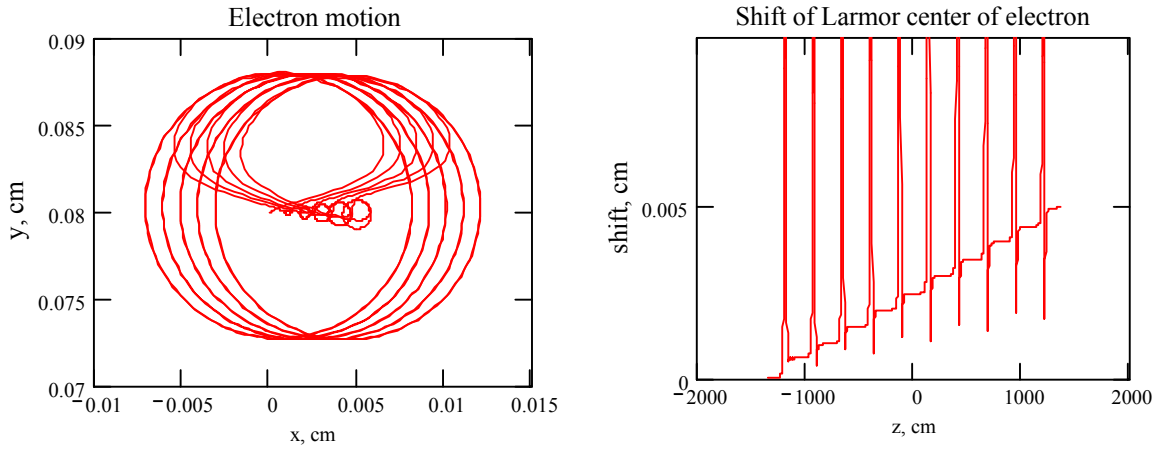

Figure 3.24. The electron motion for the solenoid section with parameters: the length - 261 cm, the gap between solenoids – 4 cm, the solenoid radius - 7.5 cm.

3.8.3. A coil for the compensation of the gap effect.

When passing the gap, the azimuthal momentum of an electron acquires impulses of opposite sign at the entrance and exit. Since the electron has time to change its radial location while passing the gap, the two impulses do not cancel. In order to compensate this effect, a special coil system can be used. By creating a domain with a higher magnetic field it is possible to have positive and negative radial magnetic field in both output and input. A proper choice of the current in the compensation coil reduces the increment of azimuthal velocity very significantly. In this case, the drift of the Larmor circle center is very small too. The general view of the gap with the compensation coil and corresponding longitudinal magnetic field is shown in Figure 3.25.

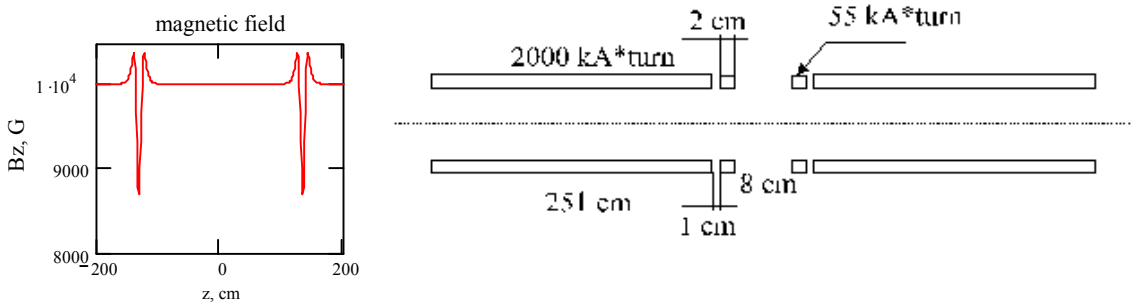

Figure 3.25. The compensation coil scheme and the magnetic field.

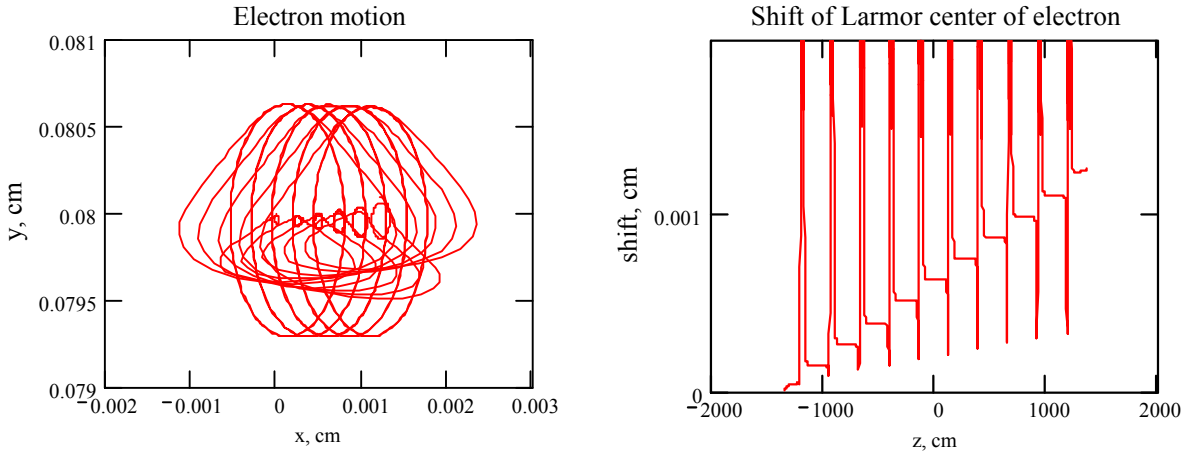

Figure 3.26. The electron motion for the solenoid with compensation coils.

This method provides an even smaller disturbance of electron motion while traversing the gap than the previous method. The decrease in the cooling rate is $\varepsilon = 0.993$ and the angle between ion and electron velocities is $\Delta\theta = 4.685 \times 10^{-7}$.

In summary, we have shown that two methods for compensation of gap effects are possible. The features of the first method are a very simple design and the slight dependence on the electron energy. The features of the second method are the possibility to have the large gap at the wide range of the electron energy. The energy dependences of the two approaches are shown in Figure 3.27.

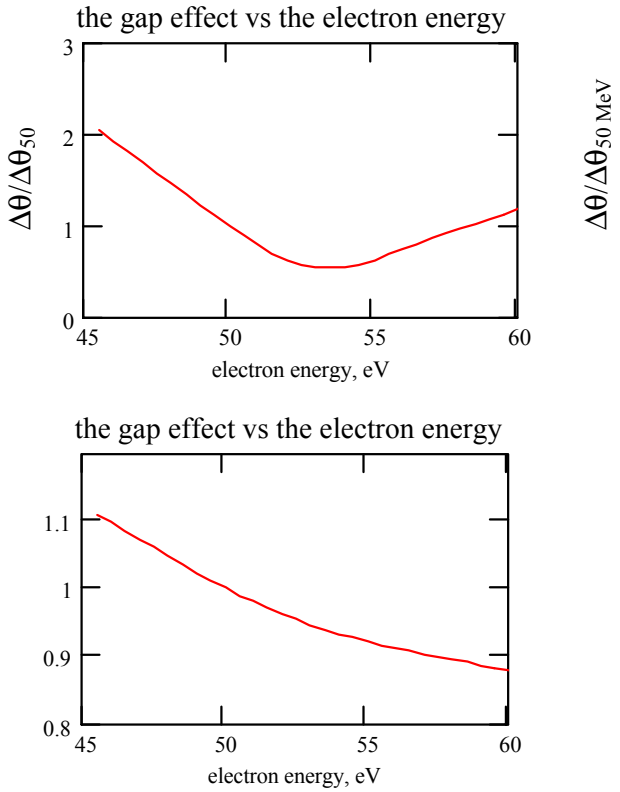

Figure 3.27. The angle between the effective electron velocity and the ion velocity vs. the electron energy. The angle is normalized by the angle corresponding to the electron energy 50 MeV.

3.8.4. A coil for the correction of the magnetic field error.

A basic technical question of this cooling project is the production feasibility of the main solenoid. The magnetic field in the solenoid must be a straight line so that the drift velocity of an electron may not exceed $\beta_{eff}=v_{drift}/c=10^{-5}$.

For modeling, the error of magnetic field was chosen as the sum of constant magnetic field and 8 harmonic sine wave with length $2\pi*i*l$, where i - integer number i=[1..7], l=11 cm. The resonance harmonic with the length of $2\pi\lambda_L=2\pi\gamma mc^2/eB$ is additionally added. The case of one transverse component of the magnetic field was examined. The longitudinal magnetic field is homogeneous and equal to 10^4 G. The length a section is 600 cm. The correction of the error of the magnetic field is carried out with the dipole coil. The length of the coil is 15 cm and radius 7.5 cm. The number of correction coils is 40.

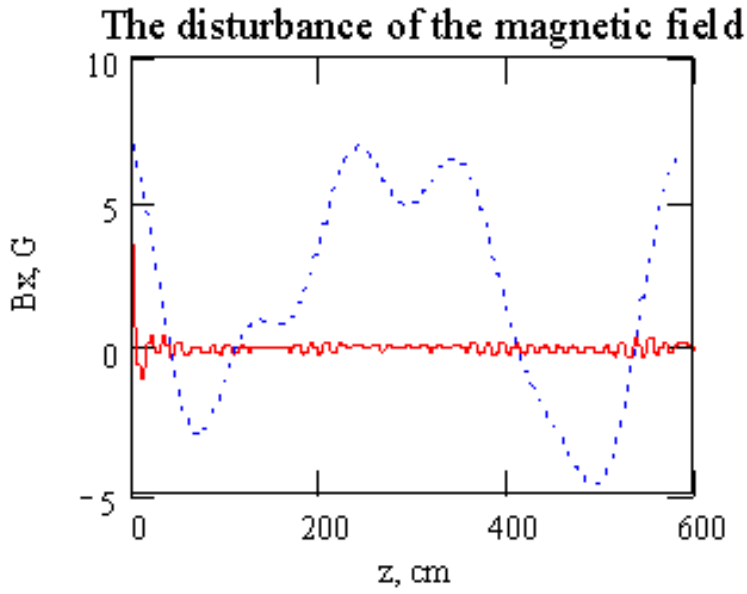

Figure 3.28. The x-component of magnetic field before and after correction.

One can see that the correction leads to decrease in the maximum transverse magnetic field from MaxError1 = 6.97 G to MaxError2 = 0.465 G and decrease in mean square error of magnetic field from RMSError1 = 4.018 G to RMSError2 = 0.136 G. This result can probably be further improved.

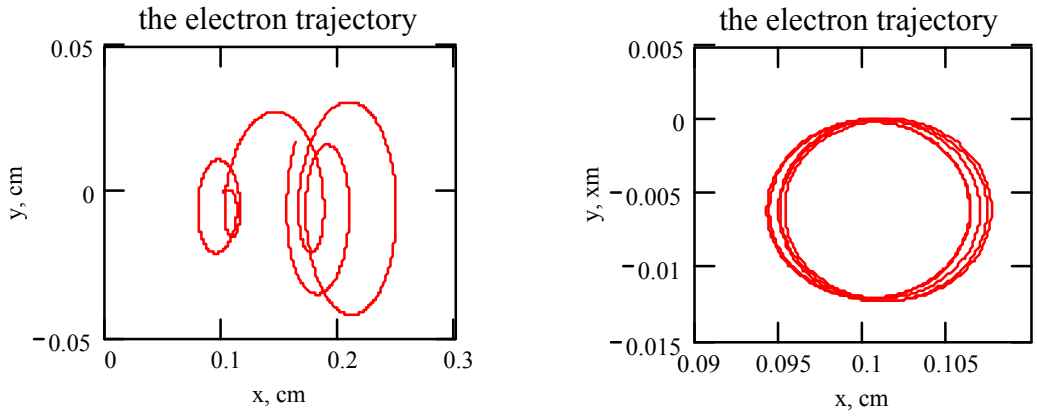

Figure 3.29. The electron trajectory without and with correction of the error of the magnetic field.

The shift of center of the Larmor circle is shown in Figure 3.30. The resulting drift velocity of electron is about $\beta_{eff} = 2.438\times 10^{-6}$ that is a very good result.

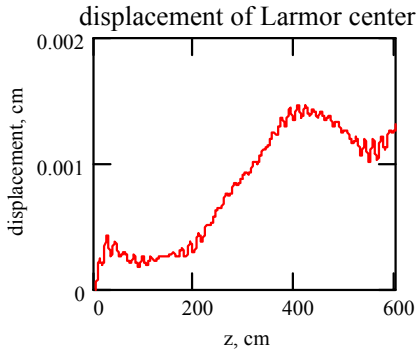

Figure 3.30. The shift of center of Larmor circle after correction of the magnetic error.

The magnetic field should be measurement with accuracy better than $\Delta B=\pm 0.1G$ ($\Delta B/B=10^{-5}$). A lower accuracy will lead to a decrease in the cooling force by a factor of 0.1 or worse. In reality the accuracy 10^{-5} is desirable. Precision of this cooling section at the level 10^{-5} means the accuracy near 0.01 mm at a distance of 1 m. That is hard but attainable accuracy, in principle. Usually, manufacture is performed with maximum possible accuracy (from economic point of view) but special coils distributed along the cooling section make final correction. The main problem for this procedure is a precise measuring of the field direction. For this purpose a compass with mirror reflecting laser light [1,2] is used.

[1] L. Arapov, N. Dikansky, V. Kokoulin, V. Kudelainen, V, Lebedev, V. Parkhomchuk, B. Smirnov, B. Sukhina, Precise solenoid for electron cooling, 13 International conference on high energy accelerators v.1 p.341-343 1986.
[2] V. Bocharov, A. Bublei, V. Parkhomchuk, V. Tupikov, S. Nagaitsev, A. Shemiakin. Precision measuring device of magnetic field in solenoid for electron cooling. National 17-th Conference on Accelerators, Protvino, Russia, October 16-20, 2000.

3.9 Recuperating the energy of the electron beam in the main linac

The maximal intensity of the electron beam that is considered for electron cooling at RHIC is $Ne=10^{11}$ electrons per bunch at a repetition frequency of f_{rep} =4.6 MHz. These values correspond to an average current of 75 mA. At an energy of 52 MeV,

the beam power is 3.9 MW. After passing the cooling section, the electron beam increases the momentum spread and the emittance, but not too much. The ion beam temperature (at the beam rest-reference system) at the initial moment T_i =38 keV and energy transferred to single electrons is:

$$\Delta E_i = \frac{T_i N_i}{N_e} \frac{1}{N_{cturns}},$$

where $N_{cturns}=f_0*\tau_{cool}$ is the number of revolution turns during the cooling time. For τ_{cool}=100 s, N_{cturns} =7.4 10^6 and we see that the additional random energy of the electron beam is extremely small, ΔE= 5 10^{-5} eV. Therefore the electron beam can be recuperated by recovering the most part of the energy of 52 MeV in the RF cavity. An example of this recuperation was made at Jefferson Laboratory for an FEL device. After passing the main linac we will have an electron beam at the injection energy of 2 MeV. This beam can be dumped at absorber and the power of this beam 150 kW is not too high. But a more elegant approach is to return this beam at the DC accelerator for final recuperation.

3.10 Recuperating the energy of the electron beam in the DC accelerator

The final recuperation of the electron beam energy is useful not only from the point of view of the recirculation energy but mainly due to decreasing radiation problems of stopping a 75 mA beam at an energy of 2 MeV. The radiation produced at 2 MeV * 75 mA stopped in a copper target at a distance of 1 m is 22 krad/min. This amount of radiation, even though it generated no activation (being just x-rays) requires a substantial degree of shielding.

The minimal energy for stopping the electron beam is defined by the momentum spread in the electron beam after recuperation at the main linac. Assuming the energy spread at cooling section 10^{-4} and bunch length 60 cm $\varepsilon_l=10^{-4}$ 60 *γ*β, after recuperation the electron beam with the same longitudinal emittance will have an energy spread of ΔE=2 MeV*εl/(γ_{inj} β_{inj})/200= 20 eV. This low energy spread suggests that a successful recuperation may be done at a final energy of a few keV, same as the many low energy electron coolers, starting with the pioneering electron cooler NAP-M. In these coolers, the minimal potential on the electron collector is defined by the potential of the space charge from the electron current at the collector:

$$\Delta U = 500 J_{epeak}^{2/3}$$

where J_{epeak} is the peak electron current (A) and ΔU is the space-charge potential of the electron beam. From this equation we can see that for 1 A range electron current it is possible to decelerate electron beam down to the potential 1-2 kV with a safety factor of 2-4 for the tail of the electron distribution at the energy spread and for ripple. There is typical value of the potential for low energy coolers. The power of this beam 1A*1kV = 1 kW becomes very low and does not cause any problems. But this recuperation of a bunched beam should be studied at a later stage in more detail.

4. KEY-PHYSICAL PROCESSES

Fundamentals of electron cooling theory

4.1 The drag force in the absence of a magnetic field

The electric field produced by ions moving in an electron gas causes a perturbation of the electrons by imparting a fraction of the ion's energy of motion to them. In moving path an electron with an impact parameter ρ at a velocity V, a particle with a charge $Z_i e$ transfers to the electron a momentum

$$\Delta p_{\perp} = \frac{2Z_i e^2}{\rho V} \qquad (1)$$

The momentum transfer is enhanced in close collisions, and for the minimal impact parameter

$$\rho = \frac{Z_i r_e}{(V/c)^2} \qquad (2)$$

where r_e is the classical electron radius, the transferred momentum reaches its largest possible value 2mV, where m is the mass of the electron. Various effects may limit the maximal impact parameter. In the case of a high-density electron beam, the electron motion has to be taken into account. If the time $\tau_i = \rho/V$ it takes the particle to pass by the electron approaches the time for which the Debye shielding is established owing to plasma oscillations with a frequency $\omega_e = c\sqrt{4\pi n_e r_e}$, the interaction efficiency is reduced for $\rho > \rho_{max} = V/\omega_e$. For an electron beam that is not too dense, the time of flight through the cooling section τ_{flight} (at beam reference system) limits the interaction time $\tau_i < \tau_{flight}$ and as result, the impact parameter is bound by $\rho_{max} = V\tau_{flight}$ (Provided that $\omega_e < 1/\tau_{flight}$). For the range of allowed impact parameters $\rho_{min} < \rho < \rho_{max}$, it is easy to calculate the mean energy loss of a particle moving in an electron gas:

$$\frac{dE}{dt} = -\int_{\rho_{min}}^{\rho_{max}} \frac{\Delta p_{\perp}^2}{2m_e} n_e V 2\pi\rho d\rho = -\frac{Z_i^2 e^4 n_e L n_c}{m_e V} \qquad (3)$$

where the Coulomb logarithm

$$Ln_c = \ln\left(\frac{\rho_{max}}{\rho_{min}}\right)$$

and thus we obtain the drag force (defined through the energy loss by FV=dE/dt) [1]:

$$F = -\frac{Z_i^2 e^4 n_e L n_c}{m_e V^3} V \qquad (4)$$

If it is necessary to take into account the proper thermal motion of electrons in a beam, the drag force is averaged over the velocity distribution f_e (V_e). Such integrals are most

readily computed by applying the Coulomb analog of force in velocity space (neglecting the change in the Coulomb logarithm Ln_c).

Assume the velocity distribution of electrons to have the shape of a flat disk with a transverse radius $V_{e\perp}$ and longitudinal width $V_{e\|}$, and consider $V_{e\|} << V_{e\perp}$. In this case, longitudinal drag force takes the form

$$F_{\|} = -\frac{8\pi Z_i^2 e^4 n_e L n_c}{m_e V_{e\perp}^2} \begin{cases} \dfrac{V_{\|}}{V_{e\|}} & |V_{\|}| < V_{e\|} \\ \dfrac{V_{\|}}{|V_{\|}|} - \dfrac{V_{\|}}{\sqrt{V_{\|}^2 + V_{e\perp}^2}} & |V_{\|}| >> V_{e\|} \end{cases} \qquad (5)$$

At ion velocity $V_{\|} < V_{e\|}$ within the electron distribution, the longitudinal drag force increases linearly; in the region $V_{e\|} < V_{\|} < V_{e\perp}$ it falls weakly, and when $V_{\|} > V_{e\perp}$, it decreases rapidly (in proportion to V^{-2}). The transverse drag force in the case $V_{\perp} < V_{e\perp}$ $F \propto V_{\perp}/V_{e\perp}^3$ is seen to fall rapidly (in proportion to $V_{e\perp}^{-3}$) at high electron beam temperature, and the possibility of attaining high cooling rate is limited by the fast motion of electrons (with velocity $V_{e\perp} >> V$).

4.2 The drag force in a magnetic field

The longitudinal magnetic field B accompanying the electron beam in the cooling zone alters the drag force significantly. The reason for such a phenomenon is that owing to the thermal motion, the Larmor radius of the electron spiral movement

$\rho_L = \dfrac{m_e V_{e\perp} c}{eB}$ may be significantly smaller then the maximum impact parameter

$\rho_L << \rho_{max}$. The transverse thermal motion of electrons in the "magnetized" zone of impact parameters exerts an influence on the ions-electrons interaction kinetics, while the contribution of electrons from this region of impact parameters to the drag force increases strongly and becomes predominant. The next figure shows the change in momentum of a proton passing by an electron at a distance ρ in case of magnetic fields B being equal to 0,100,1000G. This result was calculated by direct computer simulation of electron-ion interaction. The single charge of ion (proton) moves transversely to magnetic field direction with velocity $3\ 10^6$ cm/s. Multiplication of the change in proton momentum by ρ^2 permits the more correct comparison of contributions of different impact parameters to the total drag force with due regard for the change in number of electrons present in the volume element $n_e\ V\tau_{flight}\ 2\pi\rho\ d\rho$:

$F = \int (\Delta p \rho^2) n_e V 2\pi \frac{d\rho}{\rho}$. The constancy of the product $\Delta p \rho^2$ within the range of impact parameters (ρ_1,ρ_2) indicates that contribution of this region of impact parameters to the drag force is $(\Delta p \rho^2) n_e V 2\pi \ln(\frac{\rho_2}{\rho_1})$

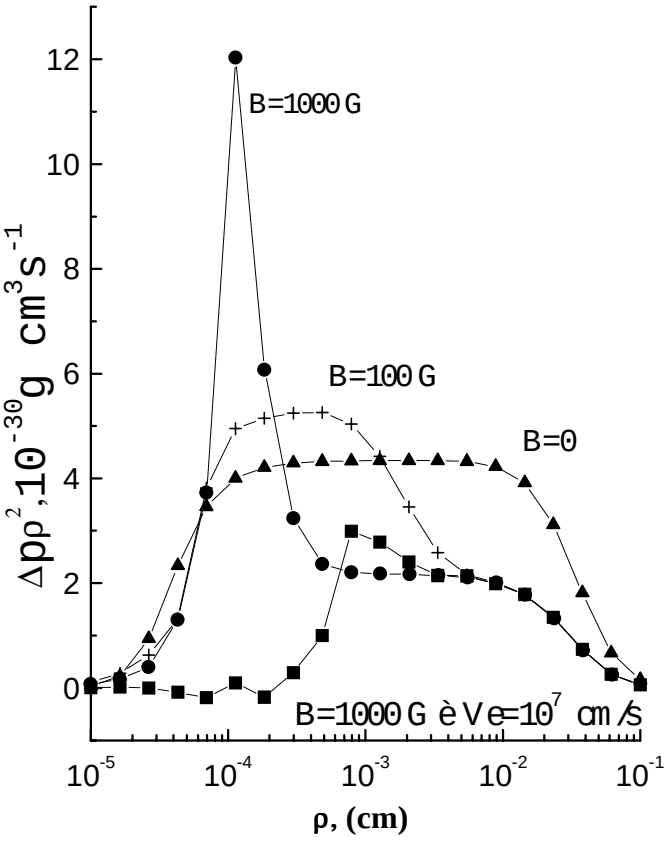

Figure 4.1. Contribution of collisions with electrons to drag force versus the impact parameter in the case of motion transverse to magnetic field. The momentum transverse for an electron beam of zero temperature are shown for various magnetic fields, as well as the influence of the transverse electron velocity at B=1000 G (curve marked by squares). The proton velocity V=3 10^6 cm/s, the interaction time with electron beam τ_{flight} =4 10^{-8} s.

From Figure 4.1. one can see that in the case of collision with electrons at rest (without their proper thermal motion), the magnetic field suppresses by a factor of two the energy transverse at impact parameters exceeding V/ω_L (ω_L=eB/m_ec). This is because the electrons are capable of free motion only along the magnetic field lines and the averaging of energy transfers over the electrons location at identical distances ρ from the ion trajectory, but with different azimuthal angles, suppresses the transfer of energy from proton to an electron in proportion to $\langle\cos^2(\phi)\rangle$, where ϕ is the angle between the momentum transferred from the proton and magnet field line. When electrons have a

noticeable velocity owing to transverse temperature in the region of small impact parameters ($\rho << V_{e\perp}/\omega_L$), where the action of magnetic field is insignificant, the energy transfer becomes small:

$\Delta p \rho^2 = \frac{2Z_i^2 e^4}{m_e V_{e\perp}^3}$ and for the parameters in the calculated example, the force is only 10^{-31} gcm^3/s. But for large impact $\rho > \rho_L = V/\omega_L = 5.6\ 10^{-4}$ cm, the contribution increases up to $2*10^{-30}$ g cm^2 s, that is close to the contribution for the electron beam with zero temperature. The magnetic field maintains a large energy transfer within the range of impact parameters from $5\ 10^{-4}$ up to $3\ 10^{-2}$ cm (ρ_L--ρ_{max}). As a result, the drag force for small proton velocities ($V << V_{e\perp}$) in the presence of a magnetic field turns out to be many times higher than that without the magnetic field, and it depends weakly ($\ln(\rho_{max}/\rho_L)$) on the velocity of transverse electron motion instead of falling as $(V_{e\perp})^{-3}$.

For the description of the drag force in real experiments, it is convenient to have an analytical expression that allows for numerical computation for comparison with experimental results. Reflection on this issue have resulted in a drag force determined by the formula [2]:

$$\vec{F} = -\frac{4Z_i^2 e^4 n_e \vec{V}}{m_e (\sqrt{V^2 + V_{eff}^2})^3} \ln\left(\frac{\rho_{max} + \rho_L + \rho_{min}}{\rho_L + \rho_{min}}\right) \quad (6)$$

and the cooling rate at the beam-reference system is:

$$\lambda = -\frac{F}{M_i V} = \frac{4Z_i^2 e^4 n_e}{m_e M_i (\sqrt{V^2 + V_{eff}^2})^3} \ln\left(\frac{\rho_{max} + \rho_L + \rho_{min}}{\rho_L + \rho_{min}}\right) = \frac{4 r_e r_i c n_e}{(\sqrt{V^2 + V_{eff}^2}/c)^3} \ln\left(\frac{\rho_{max} + \rho_L + \rho_{min}}{\rho_L + \rho_{min}}\right)$$

(7),

where V_{eff} –is the effective velocity of motion of the Larmor circles related both to the longitudinal electron velocity and transverse drift motion caused by the magnetic and electric fields owing to the space charge of beams and inaccuracies in the creation concomitant magnetic field at cooling section.

The argument of logarithm makes it possible to extend the application of these expressions to parameter ranges that are clearly not logarithmic. Thus, at small velocity of motion, when $\rho_{min} = Z_i e^2 / m_e V >> \rho_{max} = V/\omega_e >> \rho_L$ for the electron gas with zero temperature ($V_{eff}=0$), the drag force is assumed to have the form:

$$F = -4Z_i e^2 n \frac{V}{\omega_e} \quad (8)$$

and force linearly increased up to its maximum as the ion velocity increases up to $V_{max} = c\ (4\pi\ Z_i^2\ r_e^3\ n_e)^{1/6}$, after which it drops in according to formula ( ) as V^{-2} . The maximal cooling rate at this linear range of velocity is equal to:

$$\lambda_{max} = \frac{F}{M_i V} = \frac{m_e Z_i}{M_i \pi} \sqrt{\frac{4\pi e^2 n_e}{m_e}} = \frac{m_e}{M_p} \frac{Z_i}{A_i} \frac{\omega_e}{\pi} \quad (9),$$

and at this case the drag force and cooling rate increase with electron beam density in proportion to $(n_e)^{1/2}$ as was measured at MOSOL experiments.

4.3 Stationary parameters of an ion beam after cooling

Cooling of the ion beam continues until equilibrium is established between the heating (energy supply) and cooling (energy extraction) processes. The main source of heating at low intensity of the ion beam is diffusion caused by random kicks of the ions owing to the thermal motion of the beam electrons and in the case strong magnetization case we can use equation in the form:

$$\frac{dp^2}{dt}_{heat} = -\frac{8Z_i^2 e^4 n_e \vec{V}}{\sqrt{V^2 + V_{eff}^2}} \ln\left(\frac{\rho_{max} + \rho_L + \rho_{min}}{\rho_L + \rho_{min}}\right) \quad (10).$$

The equation of balance between cooling and heating has the form:

$$\frac{dp^2}{dt} = -2\lambda(V)p^2 + \frac{dp^2}{dt}_{heat} \quad (11),$$

where $\lambda(V)$ cooling rate determined by Eq.7. As easy to see, Eq.11. leads to a simple condition for equalizing the ion and electron beam temperatures:

$$\langle V^2 \rangle = \frac{m_e}{M_i} V_{eff}^2, \quad T_i = T_{eff} \quad (12).$$

In a strong magnetic field, the effective motion of Larmor circles in an ideal cooler (magnetic field lines are parallel to orbit of the ion beam) depends only on the longitudinal repulsion between the electrons distributed randomly in space after acceleration. The effective temperature can be estimated by the formula:

$$T_e = \frac{m_e V_{eeff}^2}{2} = 2e^2 n_e^{1/3} \quad (13).$$

When the electron density is about $n_e=10^8$ cm^{-3}, this estimate yields the value T_e =1 K. Many coolers, starting from NAP-M, actually achieved such low temperatures for the longitudinal motion of the ions.

For the transverse motion of ions in a storage ring (betatron oscillations) there are additional heating mechanisms (especially, in the case of heavy-charge ions) due to the formation of quasi-recombined weakly bound electron ion pairs in the cooling zone, which break up upon exit from the electron cooler. Here, a strong magnetic field acts on the electron, thus resulting in additional diffusion due to the randomness of the moment when the electron is captured by ions entering the electron cooler.

Figure 4.2 shows evaluation of the ion beam profile calculated for a statistical model (1000 samples taken) which takes into account the electron cooling, IBS and capture of electrons in the cooler. These equations are for single particle motion, but with a large number of ions in the calculation can show a more realistic distribution without using a Gaussian model.

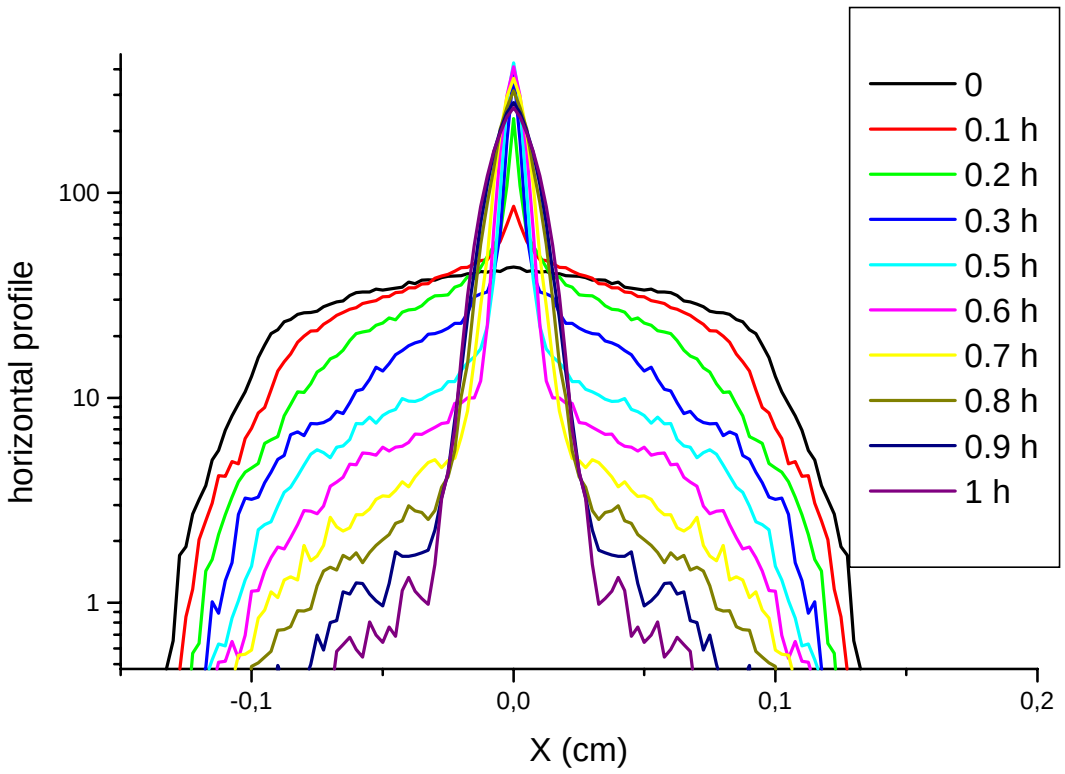

Figure 4.2. Transverse ion beam profiles (horizontal) in the cooling section. The profiles are shown at time intervals of 0.1 hour.

From this figure we can see first of all cooled ions with small amplitude. At center of beam we see at formation the cooled ion beam core just at the first stage of cooling. The ions with large amplitude cooled slowly and the tail of the distribution is drawn into the cooled core only in 1 hour. This code was written at Fortran and was verified on the experimentally measured results from the electron cooling of high charge ions in the SIS cooler.

4.4 The space charge tune shift (Laslett tune shift)

The strongest additional heating in the transverse direction is due to the influence of machine resonances. The field of the cooled ion beam space charge results in the shift and spread of the frequencies of betatron oscillations, and the largest possible tune-shift $\Delta\nu_{max}$ serves as a good characteristic. At the same time, the smallest transverse emittance achievable in cooling is limited by the value:

$$\varepsilon_{min} = \frac{\sigma_\perp^2}{\beta_\perp} = \frac{N_i R r_i}{\pi l_b \beta^2 \gamma^3 \Delta\nu_{max}} \quad (14),$$

where l_b is the ion bunch length, $r=(Z_i e)^2/(A_i M_p)$ is the classical ion radius, $\beta_\perp$ is the beta function, and R the average radius of storage ring.

The experiments have revealed that the most typical tune shift, obtained under conditions of electron cooling amounts to $\Delta\nu_{max}$=0.1-0.2. Usually, the ion beam size decreases until the tune shift reaches the value indicated and this results was obtained at NAP-M experiments with the proton beam and at SIS cooler with heavy ion beam (see ECOOL99 proceeding, page 179, fig.7).

4.5 The Intra Beam Scattering

Ion scattering within the ion beam is a factor determining the longitudinal momentum spread in the beam for ion currents that are not too small. As a rule, the decrement of the longitudinal electron cooling is significantly higher than the transverse one (the reason is flatness of the electron beam distributions in velocity space) and, consequently, the longitudinal spread of ion momentum is significantly lower in the co-moving frame of reference than the transverse momentum spread. At the beam reference system the Intra Beam Scattering can be described as relaxation in the ion gas. The time of this relaxation in the beams reference system can be written in the form:

$$\frac{1}{\tau_{ibs}} = \frac{1}{\left\langle \Delta p^2 \right\rangle} \frac{d\Delta p^2}{dt} = \frac{4\pi (Z_i e)^4 n_i L n_{ibs}}{M_i^2 \left\langle V^3 \right\rangle} \quad (15)$$

where $n_i = \frac{N_i}{2\pi\varepsilon_\perp \beta_\perp l_b \gamma}$ is the ion beam density at beam system, Ln_{ibs} is the Coulomb logarithm for IBS.

As a result, for flat velocity distribution in the ion beam (in the beam reference system $V_\parallel << V_\perp$) the IBS leads to an enhancement of the longitudinal momentum spread at a heating rate:

$$\frac{d}{dt}\left(\frac{\Delta p_\parallel}{p}\right)^2 = \frac{2 r_i^2 N_i c L n_{ibs}}{\gamma^3 \beta^3 \varepsilon^{3/2} \left\langle \sqrt{\beta_\perp} \right\rangle l_b}, \quad (16)$$

where ⟨⟩- mean averaging along the ring circumference. For example, this equation allows a comparison to HERA measurements from report M.-P. Zorzano, R. Wanzenberg, “Intrabeam scattering and the coasting beam in the HERA proton ring”, CERN-SL-2000-072 AP, fig.2 meas.3)[0.5]

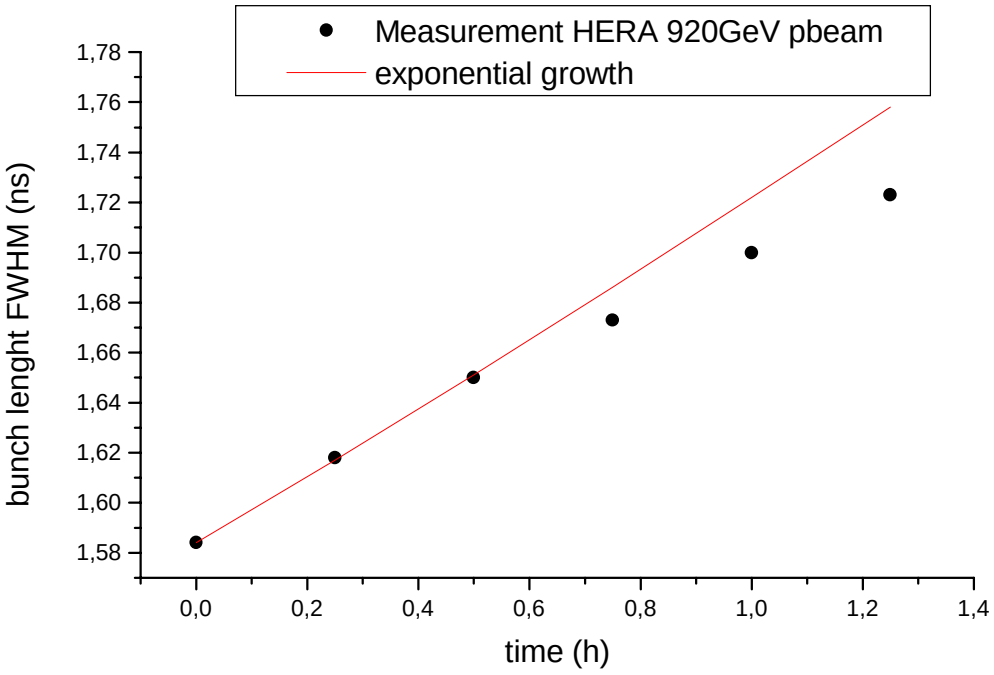

Figure 4.3. Comparison between the measured bunch length FWHM (ns) (HERA, 29 July,2000) and the expected growth from IBS according to equation 17.

We take the HERA parameters of γ=980, N=7.3 10^{10}, $\varepsilon n=\varepsilon\gamma\beta=5\ 10^{-4}$cm, $\beta_\perp$ =31m, $\delta p/p$=0.00015 and use the definition of the bunch length $l_b=(2\pi)^{0.5}$ c τFWHM/2.36. The line shows the expected growth of the bunch length from Eq.16. as:

$$\tau_{FWHM} = \tau_{FWHM\,0}\sqrt{\exp(\lambda_{\|ibs}t)} \quad (17)$$

where $\lambda_{\|ibs}$ is

$$\lambda_{\|ibs} = \frac{2r_i^2 N_i c Ln_{ibs}}{\gamma^3\beta^3\varepsilon^{3/2}\left\langle\sqrt{\beta_\perp}\right\rangle l_b(\delta p/p)^2}, \quad (18)$$

τ_{FWHM0} is the bunch length at start of storage, Ln_{ibs}=10. The agreement looks too good for such a simple (smooth approximation) equation for IBS. It provides hope that using this equation we will not make too big a mistake in the calculation of IBS for RHIC.

Let us now take the cooling rate. The bunched electron beam is taken to be at the same length and radius as the ion bunch. Then, for case V_{eff} <<V, we can write the cooling rate from equation (7):

$$\lambda_{lab} = \frac{2r_e r_i c N_e \eta_e \sqrt{\beta_\perp} Ln_c}{\pi\gamma^5\beta^3\varepsilon_\perp^{5/2} l_b} \quad (19)$$

The equation of balance between cooling and heating by IBS for longitudinal momentum spread has the form:

$$\frac{d}{dt}\left(\frac{\Delta p_{||}}{p}\right)^2 = -2\lambda_{lab}\left(\frac{\Delta p_{||}}{p}\right)^2 + \frac{d}{dt}\left(\frac{\Delta p_{||}}{p}\right)^2_{ibs} = \lambda_{lab}\left(-2 + \frac{\pi N_i m_e Z_i^2}{N_e \eta_e M_p A_i g_f}\frac{Ln_{ibs}}{Ln_c}\right)\left(\frac{\Delta p_{||}}{p}\right)^2, \quad (19)$$

where $g_f=(V_{||}/V_{\perp})^2=(\Delta p_{||}/p)^2/(\gamma^2\ \varepsilon_{\perp}/\ \beta_{\perp})$ is a flatness parameter for the ions' velocity distribution. As easy to see, this equation shows really the threshold number of electrons that can be used to suppress IBS but not the equilibrium momentum spread. The decrease of beam emittance and momentum spread increase in the cooling and heating at the same proportion. The calculation of equilibrium cooled ion beam parameters is possible if we fix, for example, the electron beam radius. The threshold electron beam number in a bunch is (assuming $Lnibs=Ln_c$):

$$N_{eth} = N_i \frac{\pi}{2\eta_e g_f}\frac{m_e}{M_p}\frac{Z_i^2}{A_i}. \quad (20)$$

For cooling at RHIC Gold ions parameters ($g_f=1$), $N_{eth}=3.5\ 10^9$ is the minimal number of electrons per bunch which is useful for improving ion beam parameters by electron cooling. But as can easily be seen from Eq.19. the gain that can be achieved by cooling with this electron bunch intensity depends on the accuracy fabrication of cooling section solenoid. The cooling will stop when the ion beam velocity at the ion beam system of reference will reach V_{eff} and the increase in the cooling rate gets saturated. For this purpose $V_{eff}=\gamma\beta c\,\Delta\theta$ where $\Delta\theta$- angle inaccuracies in the direction of magnetic force line in the cooling section.

For a fixed electron beam radius, the real number of electrons that effectively interact with the ions can be written as:

$$N_e^* = N_e\frac{\varepsilon}{\varepsilon_0}, \quad (21)$$

where ε_0 is the initial ion beam emittance, ε- the equilibrium emittance with IBS and cooling. After cooling starts, the ion beam emittance and N_e^* decreases until $N_e^*=N_{eth}$, and that gives the simplest estimate for the equilibrium emittance of the ion beam under cooling:

$$\varepsilon = \varepsilon_0\frac{N_i}{N_e}\frac{\pi}{2\eta_e g_f}\frac{m_e}{M_p}\frac{Z_i^2}{A_i}, \quad (22)$$

For a more careful calculation of the equilibrium one should take into account the local variations of the beta function and dispersion function of the RHIC lattice.

4.6 Ion beam loss rate by capture of electrons at cooler

Ion charge exchange by the electron beam recombination is a source of ion beam loss. The value of radiative recombination coefficient α is given by the equation:

$$\alpha_{rec} = 3.02\times10^{-13}\frac{Z_i^2}{\sqrt{T_e}}\left[\ln\left(\frac{1132 Z_i}{\sqrt{T_e}}\right) + 0.14\left(\frac{T_e}{Z_i^2}\right)^{1/3}\right] (\mathrm{cm^3 s^{-1}}), \quad (23)$$

where T_e is the electron beam temperature in eV (M.Bell, J.S.Bell Particle Accelerator 12 p.49 (1982) , A. Wolf, G. Gwinner et al., Recombination in electron coolers, Nuclear Instruments and Methods in Physics Research A **441** p.183-190 (2000)).

Let us demonstrate the recombination action at the real electron coolers with using lifetime measurements.

At NAP-M coolers recombination of proton beam was measured in wide range of the electrons temperatures. For exciting the transverse electrons temperature, a short electrostatic kicker was used. The kick generated a transverse Larmor rotation of the whole electron beam. Changing the potential on the kicker's plates controlled the magnitude of this rotation. Fig.1 shows results of the measurement of the recombination rate coefficient (cm^3 s^{-1}) versus the energy of this Larmor motion (eV) in the beam reference system.

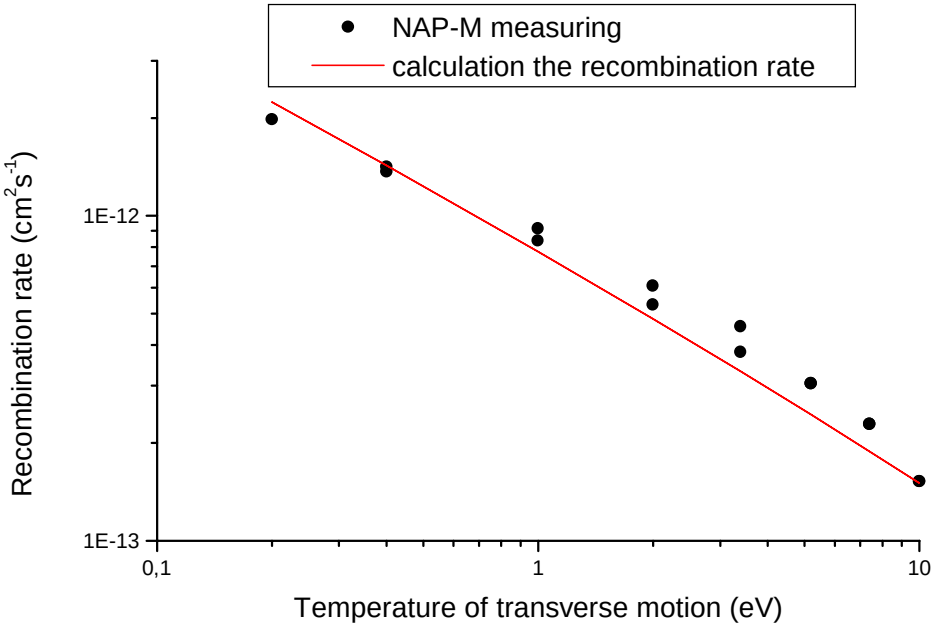

Figure 4.4. Measuring on NAP-M recombination rate coefficient (cm^3 s^{-1}) versus the energy of the electron transverse motion (eV) at the beam reference system.

This figure 4.4 shows that an increase in the temperature of the transverse motion by 2 orders of magnitude decreased the recombination losses by one order of magnitude. For RHIC, the transverse temperature should be increased by 4 orders of magnitude from 0.1 eV to 1000 eV.

The measurement of the recombination rate for heavy, highly charged but not fully stripped ions, shows an interesting phenomenon of strong variation of the recombination versus the residual number of electrons in the ion shell.

At LEAR, operating with lead ions Pb^{+q} , q=52-54, anomalously short beam lifetime of only 8s was observed during electron cooling of Pb^{+53} , while the lifetimes for Pb^{+52} and Pb^{+54} 40-50 s were close to the predictions.

The results of measuring life-time of the Bi^{+67} ions under electron cooling conditions at SIS synchrotron (GSI) are shown in the figure 4.5. For calculation of lifetime we used the equation:

$$\frac{1}{\tau_{life}} = \frac{n_e \alpha_{rec} \eta_e}{\gamma} Fit + \frac{1}{\tau_0}, \quad (24)$$

where parameters Fit used for fitting data and show how the recombination rate is far from simple radiative model (Eq.23.) . For this measurement, the electron beam size was expanded by a factor √3 times and the electrons temperature was 0.03 eV.

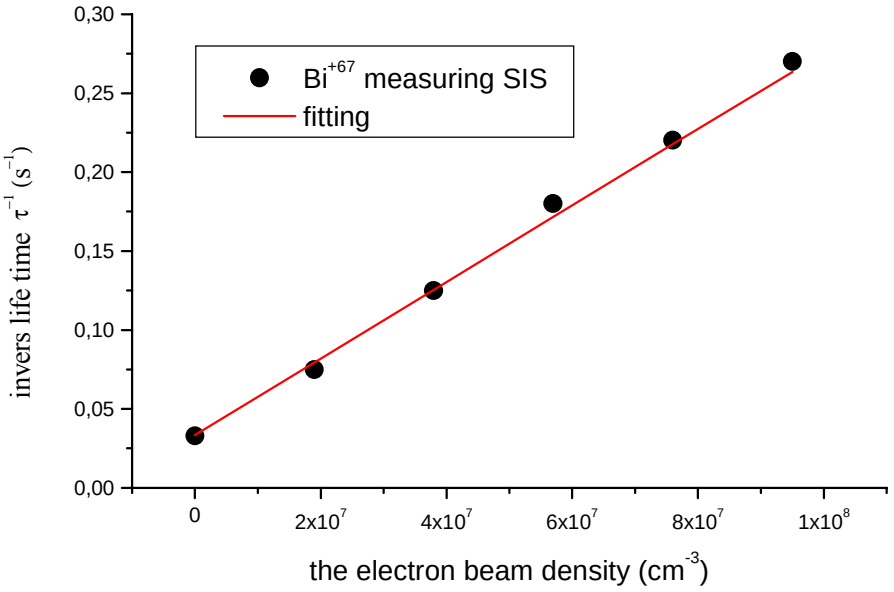

Figure 4.5. The result of measurements of Bi^{+67} lifetime in the SIS synchrotron (GSI) and a best fit line from equation (2).

The fitting gives: Fit=2, τ_0 =30 s – lifetime by charge exchange on the residual gas. It means that gain by dielectronic recombination stimulated the residual electrons nearly by a factor of 2 for this ion. For density of electron beams of 10^8 cm^{-3}, it is possible to calculate the lifetime of Au^{+79} ions using Eq.22.

4.7 Noise and growth of the ion beam emittance

Various sources of noise can produce random fluctuation of the position of the orbit at the Interaction Point. There can be noise of various kicker magnets, electrostatic plates, high frequency vibration of quadrupole magnets and the vacuum chamber. As a result,

the ion bunch will receive a random kick at the IP with an amplitude proportional to deflection of the counter rotating bunch from central position x:

$$\Delta\theta(x) = 2\pi\xi_{ii}\frac{x}{\beta_{IP}}, \quad (25)$$

where $\xi_{ii} = r_i N_i /(4 \pi \varepsilon_n)$ is the parameter of beam-beam interaction at single collision. This kick excites a coherent oscillation of the ion bunch for the decoherence time of RHIC. During the decay, the coherent oscillation of the energy of this motion can be damped by coherent interaction with cooling electron beam or with a standard feedback system. Otherwise this energy passes on to the chaotic thermal motion of the ions. If we neglect the coherent damping, the heating rate of the beam emittance by this process is

$$\frac{d\varepsilon}{dt} = f_0 n_{IP}\frac{(2\pi\xi_{ii})^2}{\beta_{IP}}\langle x^2\rangle \quad (26)$$

For the process of cooling, the increase in density of the ion beam and possible ξ_{ii} increase reach an equilibrium state when cooling balances against this source of heating. The simulation code sicool.mcd takes into account this process. Time of decay of coherent oscillation after singe kick can be estimated (V. Lebedev, V. Parkhomchuk, V. Shiltsev, G. Stupakov, Emittance growth due to noise and its suppression with feedback system in large hadron colliders, Particle Accelerators, V44, pp.147-264, 1994) as:

$$\Delta\nu \approx 0.2 n_{IP}\xi_{ii}, \quad N_{turns} = \frac{1}{\Delta\nu} \quad (27)$$

When ξ_{ii} =0.006, n_{IP} =6 number of turns for decoherence ion bunch oscillation become very short N_{turns} =160. The coherent oscillation damping system should be powerful for damping the oscillation in a very short time.

4.8 Requirement on impedance after cooling

In low energy coolers when the transverse emittances and longitudinal momentum spread decreases by a few order magnitude as a result of cooling, the beam may become unstable. The "Keil-Schnell" threshold of ion beam current can be written in the form [3]

$$\left|\frac{Z_n}{n}\right| \le F_L \frac{A}{Z_i}\frac{\beta^2\gamma(M_p c^2/e)|\eta|}{I_0}\left(\frac{\delta p}{p}\right)^2, \quad (28)$$

where $F_L \approx 1$ and $I_0 = eZ_i f_0 N$ is the average ion beam current for a coasting beam. For a bunched beam, the local (peak) current can be used for a rough estimate, $I_{peak} = eZ_i \beta c/l_b$. For RHIC with Gold*Gold collision, I_0= 60mA and I_{peak}=5 A, the impedance is limited as $Z/n<10\ \Omega$ and thus is not really a problem. The process of cooling should be controlled such that the transverse cooling (decreasing the ion beam emittance) would not produce simultaneously a large decrease of the longitudinally momentum spread. In this case, the requirement on the longitudinal coupling impedance after cooling is not higher then without cooling. The question of coherent interaction of the ion bunch with cooling electron beam will discussed at section 5.2.

[1] G.I. Budker, A.N. Skrinsky “Electron cooling” Uspekhi Fizicheskikh Nauk, v/124, 4 p.561, 1978.
[2] V.V. Parkhomchuk, A.N. Skrinsky “Elaectron cooling: 35 years of development” Physics-Uspekhi 43(5),pp. 433-452,2000
[3] J.Bosser,. C.Carli, M.Chanel, N.Madsen, S.Maury, D.Mohl, G.Tranquille, “Stabillity of cooled beams”, ECOOL’99, Nuclear Instrum. And Methods in Physics Research A441 (2000) pp.1-8

5. COLLECTIVE EFFECTS

5.1 Laslett tune shift

The collective space charge field manifested itself in low energy coolers by a halt of the cooling taking place when the tune shift becomes larger than 0.01-0.1. The value of the Laslett tune-shift can be written in the form:

$$\xi_L = \frac{r_i N_i R}{2\beta\gamma^2 \varepsilon n_i (2\pi)^{1/2} \sigma_s}, \quad (1)$$

where R is average ring radius, σ_s is bunch length, εn is the normalized ion beam r.m.s. emittance. The effect drops down with energy and for initial parameters RHIC on top energy ξ_L =0.001 is far from the dangerous region of 0.01-0.1. But after cooling, if the beam emittance is decreased by one or two orders of magnitude it can become a real limitation. It is interesting that for high rate electron cooling when the Laslett tune shift reaches 0.1-0.2 it is not clear what is the real mechanism of heating, nonlinear resonances or IBS. The value of the Laslett tune-shift is a good characteristic of the quality of cooling. In powerful coolers, the ion beams can be cooled down to large values of $\xi_L \cong$0.1-0.2 but if ξ_L <<0.01 it means that there may be some problems with alignment of the ion and electron beams or same other cooler problem.

5.2. Electron-beam ion interaction problems

The electron cooling method uses energy exchange between ions and electrons, taking place during their joint motion in a special section of the ion ring. The interaction between the ions and electrons is governed by a long-distance Coulomb force. It is convenient to represent the resulting action of this force to a single particle as a sum of two parts. The first part is related to the short-range part of interaction. The action of this short-range interaction is manifested as direct collision between particles when the distance from one to the other is less than the Debye length, $r<<r_D$. The second, long-range part of the interaction is manifested as the action of a self-consistent electric field. In the case of a closed system, the motion resulting from this long-range part is reversible in time and doesn't lead to the growth of entropy and bunch phase space volume. In our case, the system is open and the electron beam is renewed. Thus, this situation calls for a special analysis.

5.2.1 The longitudinal-longitudinal coherent interaction

First let us consider the effect of the short-wave longitudinal fluctuation of space charge in the ion and electron beams. If the phase velocity of a fluctuation excited in the ion bunch is greater than the dispersion of azimuthal velocity, then a hydro-dynamical model can be applied. For a very cold electron beam this requirement is satisfied

automatically. Within this boundary of validity we can formulate the equation describing the dynamics of the fluctuation with a wavelength much less than the beam radius as

$$\frac{d^2 s_i}{dt^2} + \omega_{pi}^2 s_i = \omega_{ie}^2 s_e$$

$$\frac{d^2 s_e}{dt^2} + \omega_{pe}^2 s_e = \omega_{ei}^2 s_i$$

where s_i,s_e are the longitudinal shift of the ion and electron, respectively, from an unperturbed location,

$\omega_{pe} = \sqrt{\frac{4\pi n_e e^2}{m_e}}$ is the electron plasma frequency, ω_{pe}=6.2 10^8 1/s

$\omega_{pi} = \sqrt{\frac{4\pi n_i Z_i^2 e^2}{M_i}}$ is the ion plasma frequency, ω_{pi}=1.8 10^7 1/s

$\omega_{ie} = \sqrt{\frac{4\pi n_e Z_i e^2}{M_i}}$ is the ion oscillation frequency due to the electron's space charge, ω_{ie}=9.1 10^6 1/s

$\omega_{ei} = \sqrt{\frac{4\pi n_i Z_i e^2}{m_e}}$ is the electron's oscillation frequency in the ion's space charge field, ω_{ei}=1.21 10^9 1/s

All values are given in the beam reference frame. The determinant of the ion transport matrix corresponding to the above equation (at zero initial condition for electron $s_e(t=0)=0$, $ds_e/dt(t=0)=0$) is

$$Det = 1 + \frac{2\omega_{ei}^2\omega_{ie}^2}{\omega_0^4}(\cos(\omega_0\tau) - 1) + \frac{\omega_{ei}^2\omega_{ie}^2}{\omega_0^4}\omega_0\tau\sin(\omega_0\tau)$$

where τ is the flight-time of an ion through the cooling section in the beam reference frame, and

$$\omega_0 = \sqrt{\omega_{pe}^2 + \omega_{pi}^2}$$

The determinant is not equal to 1. This system is not closed, and the electron beam can either absorb or increase the energy of the charge fluctuation in the ion beam. Figure 5.1. shows the deviation of the determinant from unity, (Δ(Det)=Det-1) as a function of the electron beam density.

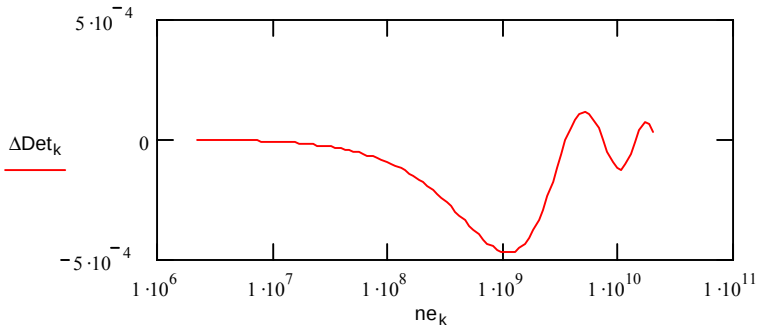

Figure.5.1. Longitudinal-longitudinal interaction of the ion and electron beams.

One can see that the determinant value is Det < 1 for small electron beam density, but the determinant value is Det > 1 for large electron beam density $\omega_{pe}\tau > 2\pi$. It is shown that in our case, the heating caused by the effect is important only for a large electron beam density $n_e=10^{10}$ cm^{-3}, corresponding to current density $j_{e\ peak} \cong 5$ kA/cm^2 . At a smaller density, the interaction with the electron beam leads to damping of the coherent oscillation mode in the ion beam. Note that the damping rate of the fluctuations under discussion is much larger than the damping rate associated with the usual single-particle friction force (see section 4).

5.2.2. The transverse-longitudinal coherent interaction

The second effect, related to the interaction of the short wavelength transverse betatron oscillation n >> 1 and the longitudinal oscillation of the electron column with k_S a_e << 1. The electron motion is strongly magnetized. In the reference frame of the co-moving beams the system of equations describing the phenomena is:

$$\frac{d^2x_i}{dt^2}+\frac{1}{2}\omega_{ie}^2x_i=\frac{i}{2}(k_sa_1)\omega_{ie}^2s_e$$

$$\frac{d^2s_e}{dt^2}+(k_sa_1)^2\omega_{pe}^2s_e=-\frac{i}{2}(k_sa_1)\omega_{ei}^2x_i$$

The left-hand side of the first equation describes the transverse oscillation of the center of mass of the ion beam under the space-charge field of electron beam. The left-hand side of the second equation describes the longitudinal oscillation of the first radial mode $a_1 \cong a_i=a_e$ (it is assumed that the beam radii are roughly equal in the cooler section) of the electron beam with a wave-vector k_S. The right-hand side of the system of equations ties these oscillations via the electrostatic fields induced in the electron medium by electric field of the betatron wave. Actually many radial modes may be excited, making the problem very difficult, but it is possible to restrict the solution to the dynamics of only the first radial mode.

The determinant value for the transfer matrix is

$$Det = 1 + \frac{1}{2}\frac{(k_s a_1)^2 \omega_{ie}^2 \omega_{ei}^2}{\left(\omega_{ie}^2 - (k_s a_1)^2 \omega_{pe}^2\right)^2 + 4(k_s a_1)^2 \omega_{ie}^2 \omega_{ei}^2}(\cos(\omega_1 \tau) - 1) +$$

$$\frac{1}{4}\frac{(k_s a_1)^2 \omega_{ie}^2 \omega_{ei}^2}{\left(\omega_{ie}^2 - (k_s a_1)^2 \omega_{pe}^2\right)^2 + 4(k_s a_1)^2 \omega_{ie}^2 \omega_{ei}^2}\omega_1 \tau \sin(\omega_1 \tau) \qquad \omega_1^2 = \omega_{ie}^2 + (k_s a_1)^2 \omega_{pe}^2$$

The value of Det as a function of the electron beam density is plotted in Figure 5.2. As in the case of the interaction of the longitudinal charge waves, a damping of the coherent mode is observed. The rate also can exceed the single-particle friction rate for betatron fluctuation with sufficiently short wavelength in a high ion density.

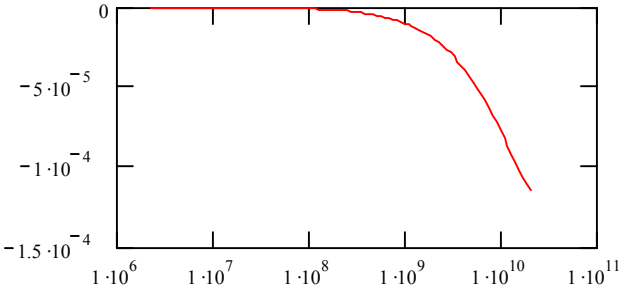

Figure 5.2. Transverse-longitudinal interaction of space charge fluctuation of ion and electron beams.

6. CONTROL OF THE ION BEAM DISTRIBUTION IN 6-D PHASE-SPACE

The electron cooling has an extremely sharp dependence on the drag versus the difference at the velocity of ions and electrons. The cooling electron beam (with practically zero temperature) generates a situation that may be thought of as a "black hole" in 6-dimensional phase-space that attracts all nearby ions and, once they enter the cold electrons phase-space, they are trapped. Let us demonstrate the longitudinal motion of the ions for the case of electron cooling of RHIC with an electron beam density $n=10^8$ cm^{-3}. The drag force is equal to:

$$F(V) = -m \frac{4r_e^2 Z_i^2 n_e \eta_e c^4 L n_c}{((V - V_e(t))^2 + V_{eff}^2)^{3/2}} (V - V_e(t)) \quad (1)$$

where $V_e(t)$ is the electron velocity as a function of time at the beams' reference system. In this case, the equation of the ion oscillation along the beam can be written in the form:

$$\frac{d^2x}{dt^2} - \frac{4r_i r_e n_e \eta_e c^2 L n_c}{((\frac{dx}{dt} - V_e(t))^2 + V_{eff}^2)^{3/2}} (\frac{dx}{dt} - V_e(t)) + \Omega_s^2 x = 0 \quad (3)$$

where Ω_s is the frequency of longitudinal oscillation in the beams' system of reference. Without the drag force the ions execute a linear synchrotron oscillations with circular motion in the x,V plane. Figure 6.1 shows how a single ion cools down in the beam reference system in the case of $V_e(t)=0$.

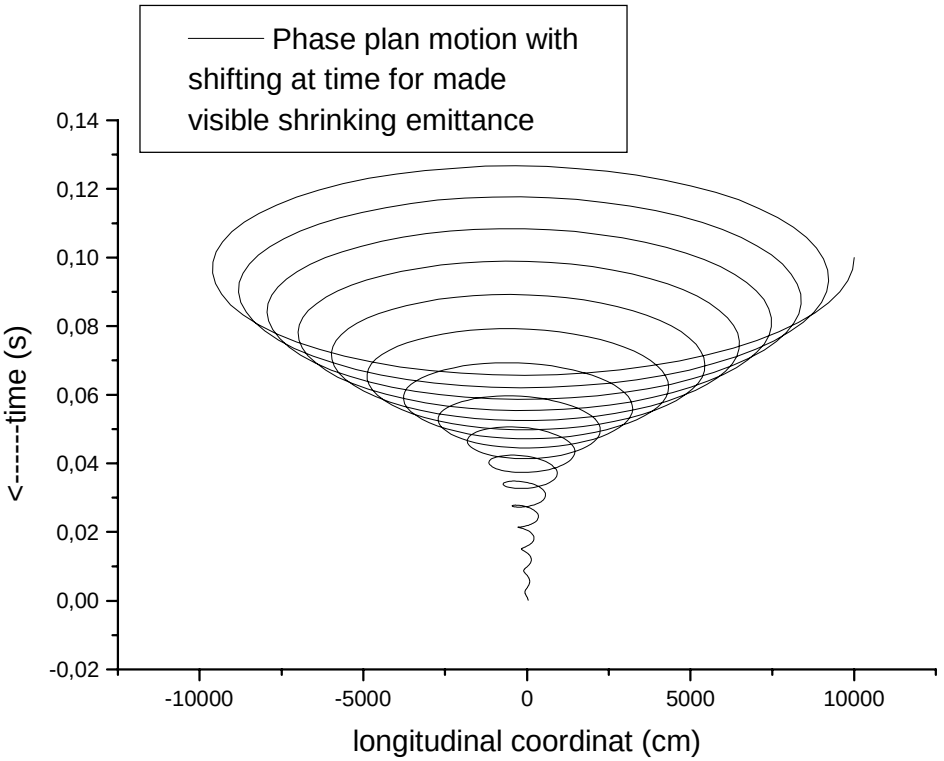

Figure 6.1. The longitudinal motion of a single ion under the combined action of the drag force and synchrotron oscillations. After 0.14 seconds (at beam system) the ion is captured at the center of the phase space.

In the simplest case (one dimensional), the time-averaged (for a stationary solution) coasting-beam distribution of the ions in velocity space is given by the Equation (3):

$$\frac{df(V)}{dV} D + f(V) \frac{< F(V,t) >}{M_i} = 0 \quad (3)$$

where $D=\Delta V^2/\tau_{dif}$ is the coefficient of diffusion in velocity space, F(V,t) is the drag force and the time dependence allows for a possible variation of the electron beam velocity $V_e(t)$ from equation 1. In this case in order to obtain the velocity distribution we can average the drag force over time, provided that the time variation of V_e is faster than the cooling time:

$$f(V) = const \cdot e^{-\int_{-\infty}^{V} \frac{\langle F(V,t) \rangle}{DM_i} dV} \quad (4)$$

where const is defined by the normalization of the velocity distribution.
When the electron velocity has a rectangular modulation (half time $-V_e$ and the rest half time $+V_e$) the average drag force can be written as:

$$\langle F(V) \rangle = \frac{F(V+V_e) + F(V-V_e)}{2} \quad (5)$$

Figure 6.2 shows the distribution, calculated according to Eq.4., for a few values of the amplitude of modulation V_e (V_{eff}=0.5 10^7cm/s, D=1.5 10^9 cm^2/s^3). This figure demonstrates that the final ion velocity distribution is similar to the case when cooling is done with two electron beams each with half of intensity but with different velocities.

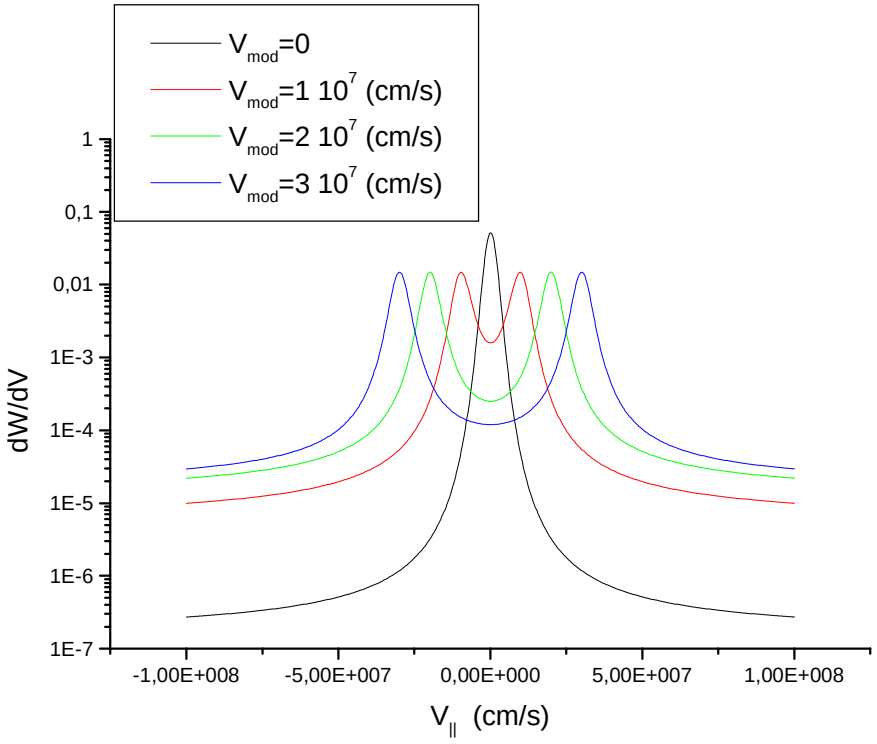

Figure 6.2. The ion beam velocity distribution at the beam reference system for fast rectangular modulation of the electron beam energy.

If the distribution of the electron's velocity is modified in time, the next question is what should we use for the modulation waveform of the electron beam's energy.
A linear modulation (saw-tooth form) can produce a flatter ion beam distribution, as shown in figure 6.3.

An experimental demonstration of the application of electron energy modulation can be seen in a report from the CELSIUS team (L. Hermansson, D. Reistad, Electron cooling at CELSIUS, ECOOL'99, Nuclear Ins. And Methods in Physics Research A 441 (2000), pp. 140-144).

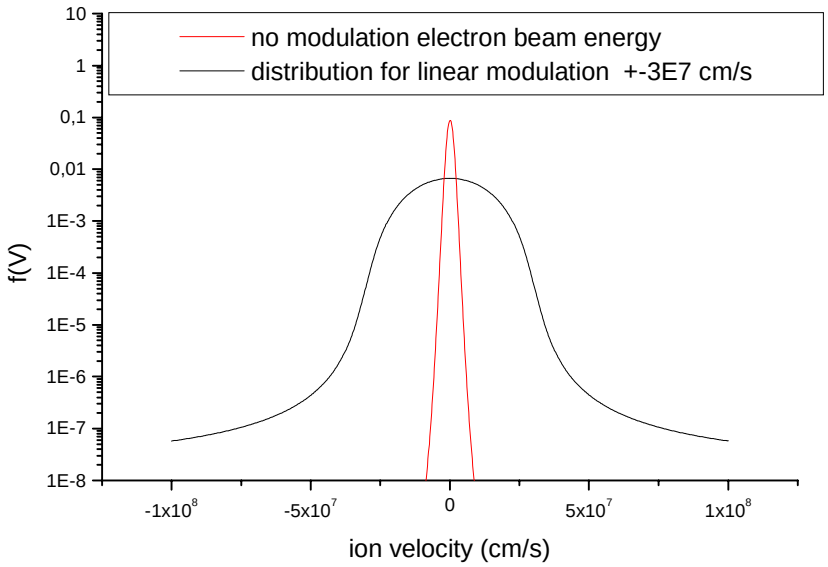

Figure 6.3. The velocity distribution of ions for a linear modulation of the electron beam's energy

At CELSIUS this modulation helped to stop overcooling of the momentum spread and thus prevent the development of a coherent instability.

The one-dimensional example discussed above was provided as a simple demonstration of the principle of the modulation technique. Fast painting of an electron beam over 6 dimensional coordinates along the same principles can produce any distribution of the average friction force and as result to control the 6-dimensional density distribution of the ion beam. The calculation of the average drag force should use equation 1 and this is relatively easy. But for a calculation of the distribution in a 6-dimensional coordinate system requires a clear understanding of the diffusion coefficient. The simplest approach is to measure the diffusion experimentally at RHIC and then reconstruct the necessary distribution of the drag force.

To accomplish this "painting" of the electron beam in momentum coordinates, we need to modulate fast the energy of electron beam and the angles (horizontal and vertical planes). For the space coordinates it is useful to have rapidly varying horizontal, vertical and longitudinal positions of electron beam at the cooling section.

What is the meaning of fast in this context? If the cooling time is a few hundred seconds, fast means about 1 second at each position, so that the change of the distribution function in a single time step is near a few percent. For magnetic steering elements to modify angles and position it is rather straightforward. For phase and energy modulation we have to use the main RF linac. The phase control can be done easily and fast by low-level, electronically controlled phase-shifters. The modulation of the energy is a bit trickier and requires some study.

7. STOCHASTIC COOLING SYSTEM.

In this section we discuss the usefulness of a bunched beam betatron stochastic cooling at RHIC. A functional scheme of a feedback system for a stochastic cooling of the particle betatron oscillations is presented in Figure 7.1. It comprises a pickup, subtracting transformer, amplifier, power splitter and kicker. The pickup and kicker are identical and perform as 50 Ohm matched striplines. The length of striplines is chosen to be equal to a quarter of the wavelength corresponding to the central frequency of the operating frequency band. The pickup and kicker are placed so to provide a betatron phase advance between them equal to an odd multiple of $\pi/2$ and a particle signal delay time by the feedback circuit equal to particle travel time from the pickup to the kicker.

An analysis of the kinetics of the betatron stochastic cooling of a bunched beam as well as estimates of the maximum decrement and required power of the feedback amplifier are given below.

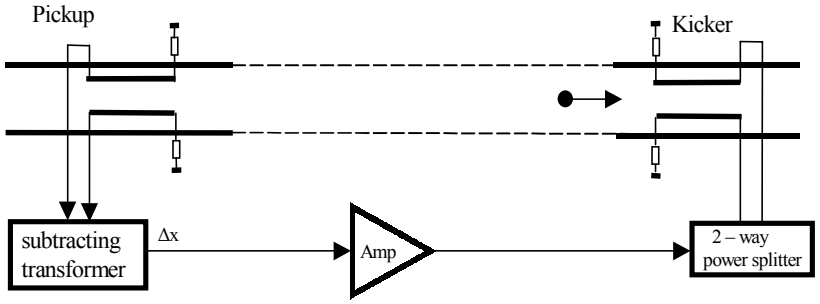

Figure 7.1. Block - diagram of the betatron stochastic cooling system.

Input equations. We will follow here techniques advanced in the references below [1,2]. The behavior of charged particles in a storage rings can be described by equations of the microscopic phase density of the particles. By definition, the phase density in a four-dimension space, in our case, can be written as

$$F(J,\omega,\varphi,\vartheta,t)=\frac{1}{N}\sum_{i=1}^{N}\delta[J-J_i(t)]\delta[\omega-\omega_i(t)]\delta[\varphi-\varphi_i(t)]\delta[\vartheta-\vartheta_i(t)].$$

where $J-\varphi,\omega,\vartheta$ are the transverse variables action in angle, revolution frequency and longitudinal azimuth, respectively, in the rest system of the equilibrium particle, and N is the number of particles. Note that the transition to the rest system from the laboratory system and back is performed by a simple replacement $\vartheta_L=\vartheta+\omega_0 t$, where ϑ_L is the azimuth in the laboratory system and ω_0 is the angular frequency of revolution. The value $FdJd\omega d\varphi d\vartheta$ - defines the real (not average) share of the particles in the space element $dJd\omega d\varphi d\vartheta$. This value, of course, is a random one. The ensemble-average phase density value $F(J,\omega,\varphi,\vartheta,t)$ coincides with the single-particle distribution function $f_1(J,\omega,\varphi,\vartheta,t)$.

The phase density evolution is determined by the equation

$$\frac{\partial F}{\partial t}+\dot{\varphi}\frac{\partial F}{\partial \varphi}+\dot{\vartheta}\frac{\partial F}{\partial \vartheta}+\dot{\omega}\frac{\partial F}{\partial \omega}+\dot{J}\frac{\partial F}{\partial J}=0 \qquad (1)$$

Let us designate the phase density deviations from their average values as

$$\delta f(J,\omega,\varphi,\vartheta,t)=F(J,\omega,\varphi,\vartheta,t)-F_1(J,\omega,\varphi,\vartheta,t).$$

After averaging the ensemble, equation (1) gives the equations for the distribution function F_1 and δF

(2)

$$\frac{\partial \delta f}{\partial t}+\dot{\varphi}\frac{\partial \delta f}{\partial \varphi}+\dot{\vartheta}\frac{\partial \delta f}{\partial \vartheta}+\dot{\omega}\frac{\partial \delta f}{\partial \omega}+\dot{J}\frac{\partial f_1}{\partial J}=-\dot{J}\frac{\partial \delta f}{\partial J}+\overline{\dot{J}\frac{\partial \delta f}{\partial J}} \qquad (3)$$

Model of the interaction. The particle motion equations, written down in the rest system of the equilibrium particle, are of the form:

$$\dot{\varphi}=\Omega$$
$$\dot{J}=q\sqrt{\frac{2J}{M\Omega}}(E_x-vB_y)\cos\varphi=2q\sqrt{\frac{2J}{M\Omega}}E_x\cos\varphi \qquad (4)$$
$$\dot{\vartheta}=\omega$$

where M,q,Ω are the mass, charge and angular betatron frequency of the particle, respectively. We assume here that the main mechanism of the particles-mixing is the revolution frequency spread of particles.

The transverse electric field created by a kicker, $E_x(\vartheta+\omega_0 t,t)$, is expressed by the Fourier expansion:

$$E_x(\vartheta+\omega_0 t,t)=\frac{L}{2\pi R_0}\frac{U(t)}{2a}\sum_m a_m e^{im(\vartheta+m\omega_0 t)} \qquad (5)$$

where $L,R_0,a,U(t)$ are the kicker length, ring average radius, kicker half-aperture and voltage between kicker striplines, respectively. The coefficients a_m take into account the field distribution in the kicker. For simplicity, let a_m be equal to unity.

Let us assume that the particle interaction via feedback is small and that the decisive role in the interaction is provided by beam azimuth harmonics with length much less than the azimuth bunch length. Under this assumption, upon the integration of equation (3), it is possible to take ignore the t,ϑ dependence of the single-participle distribution function.

We suppose also that the correlation time of the feedback signal is much less than the period of particle synchrotron oscillations and $\dot{\omega} = 0$. Neglecting non-linear terms, we can write down (3) as follows

$$\frac{\partial \delta f}{\partial t} + \dot{\varphi}\frac{\partial \delta f}{\partial \varphi} + \dot{\vartheta}\frac{\partial \delta f}{\partial \vartheta} = -\dot{J}\frac{\partial f_1}{\partial J}. \qquad (6)$$

Equation (6) is a usual linear equation with respect to fluctuations. Its complete solution is, as known, the sum of the free solution, determined by the initial condition, and of the forced one. However, it is more convenient to consider the initial conditions being zero and to introduce into (6) a source, equivalent to them. Taking into account (4), (5) we have

$$\left(\frac{\partial}{\partial t} + \dot{\varphi}\frac{\partial}{\partial \varphi} + \dot{\vartheta}\frac{\partial}{\partial \vartheta}\right)(\delta f - \delta f^{src}) = -\frac{qL}{2\pi R_0}\frac{U(t)}{a}\sqrt{\frac{2J}{M\Omega}}\frac{\partial f_1}{\partial J}\cos\varphi \sum_m e^{im(\vartheta+\omega_0 t)} \qquad (7)$$

The source fluctuations δf^{src} are the free fluctuations δf when there is no interaction. The source correlation function is determined by the relation [1]

$$\overline{\delta f^{src}(J,\omega,\varphi,\vartheta,t)\delta f^{src}(J',\omega',\varphi',\vartheta',t-\tau)} =$$
$$= \frac{1}{N}\delta(J-J')\delta(\omega-\omega')\delta(\varphi-\varphi'-\Omega\tau)\delta(\vartheta-\vartheta'-\omega\tau) f_1(J,\omega,\varphi,\vartheta). \qquad (8)$$

The solution of the equation (7) can be presented after Laplace transformation in following form

$$\delta f_{m,\pm 1}(J,\omega,s) = -\frac{qL}{2\pi R_0}\sqrt{\frac{2J}{M\Omega}}\frac{U(s-im\omega_0)}{2a}\frac{\partial f_1}{\partial J}\frac{1}{s+im\omega \pm i\Omega} + \delta f^{src}_{m,\pm 1}, \qquad (9)$$

where $\delta f_{m,\pm 1} = \frac{1}{(2\pi)^2}\int d\varphi d\vartheta \delta f(J,\omega,\varphi,\vartheta,s) e^{-im\vartheta \mp i\varphi}$, and s is a variable in a Laplace image.

Taking into account the relative position of the pickup and kicker and the betatron phase advance between them, the feedback voltage on the kicker is of the form

$$U(s) = K(s)\sum_m x_m(s+im\omega_0), \qquad (10)$$

where $$x_m(s) = \int\sqrt{\frac{2J}{M\Omega}}\cos\varphi\,\delta f_m\, dJ d\omega d\varphi = \pi\int\sqrt{\frac{2J}{M\Omega}}(\delta f_{m,1} + \delta f_{m,-1})dJ d\omega$$

and $K(s)$ - a gain from the pickup to the kicker. From (9),(10) one can obtain that

$$x_m = \frac{x^{src}_m}{1 - K(s-im\omega_0)\eta_m(s)}, \qquad (11)$$

$$\eta_{m(s)} = -\frac{qL}{2aR_0 M\Omega}\int J\frac{\partial f_1}{\partial J}\left(\frac{1}{s+im\omega+i\Omega}+\frac{1}{s+im\omega-i\Omega}\right)dJd\omega =$$

$$= -\frac{qL}{2aR_0 M\Omega}\int f_1\left(\frac{1}{s+im\omega+i\Omega}+\frac{1}{s+im\omega-i\Omega}\right)d\omega. \quad (12)$$

Cooling decrement. Return to equation (2). Assuming that there is no influence of the particle transverse motion on the longitudinal one in the left-hand side of (2) only a time derivative should be left. Writing down the right-hand side of (2) in detailed form we have

$$\frac{\partial f_1}{\partial t} = -\overline{\frac{qL}{2\pi R_0}\frac{U(t)}{a}\sqrt{\frac{2J}{M\Omega}}\cos\varphi\sum_{m,m'}e^{im(\vartheta+\omega_0 t)}\frac{\partial}{\partial J}\delta f_{-m,}e^{-im'\vartheta}}$$

Averaging the right-hand side of the last equation over φ,ϑ one can obtain

$$\frac{\partial f_1}{\partial t} = -\overline{\frac{qL}{2\pi R_0}\frac{U(t)}{2a}\sqrt{\frac{2J}{M\Omega}}\sum_m e^{im\omega_0 t}\frac{\partial}{\partial J}\left(\delta f_{-m,1}+\delta f_{-m,-1}\right)} \quad (13)$$

Substitute (9) in (13), then multiply (13) by J and carry out integration over J,ω. The result can be written down in the following form

$$\frac{\partial}{\partial t}\int Jf_1 dJd\omega = \frac{\partial}{\partial t}\langle J\rangle(\vartheta,t) = -\frac{3}{2}\overline{\frac{qL}{2\pi R_0}\frac{1}{2\pi a}\sum_{m,m'}L^{-1}\left[K(s-im'\omega_0)x_{m'}(s)\right]_{-m}(t)}, \quad (14)$$

$L^{-1}[.$ - a Laplace inverse transform.

Under the assumption made above, the interaction process can be considered as a stationary one and ensemble averaging in (14) can be replaced by time averaging. Let m_{max} be maximum number of operating azimuth of harmonics and $m_{max}\Delta\omega \le 0.5\omega_0$ (a weak mixing), $\Delta\omega$ - the particles revolution frequency spread. In this case there is no correlation between the center of gravity harmonics with different numbers and in (14) one should left the terms with $m = m'$. Following [1] it can be shown that

$$\overline{L^{-1}\left[K(s-im\omega_0)x_m(s)\right]_{-m}(t)} = \int_{-\infty}^{\infty}d\phi S_{x,m}(\phi)K(i\phi-im\omega_0),$$

where $S_{x,m}$ is a spectral density of the center of gravity fluctuations. For the stationary process

$$S_{x,m}(\phi) = \frac{S_{x,m}^{src}(\phi)}{\left|1-\eta_m(-i\phi-im\omega_0)K(-i\phi-im\omega_0)\right|^2},$$

$S^{src}_{x,m}$ is the spectral density of free fluctuations of the center of gravity. Taking into account (8), (10) one can obtain that

$$S^{src}_{x,m}(\phi)=\frac{1}{2M\Omega N}\int Jf_1(J,\omega,\vartheta)\left[\delta(\phi+m\omega-\Omega)+\delta(\phi+m\omega+\Omega)\right]dJd\omega.$$

Summing these results, we write down the final equation described the betatron stochastic cooling of a bunched beam

$$\frac{\partial}{\partial t}\langle J\rangle(\vartheta,t)=\frac{qL}{2\pi R_0\pi aNM\Omega}\int Jf_1(J,\omega,\vartheta,t)dJd\omega\sum_m\frac{\mathrm{Re}\left[K(i\Omega+im\omega-im\omega_0)\right.}{\left|1-\eta_m(i\Omega+im\omega)K(i\Omega+im\omega-im\omega_0)\right|^2} \qquad (15)$$

So as one can see the cooling decrement is equal to the sum of partial decrements of the betatron sidebands around the harmonics of the revolution frequency.

Estimates. Assuming that the length of striplines is chosen to be equal to quarter of the wavelength corresponding to a central frequency of a operating frequency band and operating frequency band is of the order of a few GHz

$$K(i\Omega+im\Omega-im\omega_0)\approx K(-im\omega_0)=\frac{qN\omega_0\rho K_{fb}(-im\omega_0)}{a},$$

$K_{fb}(im\omega_0)$ is the voltage gain of the feedback, including the pickup and kicker transmission coefficient and feedback amplifiers gain, ρ is the kicker and pickup striplines wave impedance. Taking into account only resonance term in the expression for $\eta_m(i\Omega+im\omega)$ we have

$$\eta_m(i\Omega+im\omega)=\frac{qL}{2aM\Omega R_0}\left[\frac{\pi f_1(\omega,\vartheta)}{|m|}-i\int\frac{f_1(\omega',\vartheta)d\omega'}{m\omega+m\omega'}\right] \qquad (16)$$

For an estimate, let us leave in (16) only the first term

$$\eta(i\Omega+im\omega)\approx\frac{\pi qL}{2aM\Omega R_0}\frac{f_1(\omega,\vartheta)}{|m|}\approx\frac{\pi qL}{2aM\Omega R_0}\frac{1}{|m|2\pi\Delta\omega\Delta\vartheta}, \qquad (17)$$

where $\Delta\omega,\Delta\vartheta$ are the bunch revolution frequency spread and azimuth length, accordingly.

The frequency bandwidth of the feedback is determined by the bandwidth of the pickup and kicker and in our case is, approximately, one octave ($m_{max}/m_{min}=2$). Then let L be R_0/m_{max}. As a result, equation (15) takes the form

$$\frac{\partial\langle J(\vartheta,t)\rangle}{\partial t}\approx\langle J(\vartheta,t)\rangle\frac{2}{N}\sum_{\frac{m_{max}}{2}}^{m_{max}}\frac{\lambda_m}{(1+\lambda_m\frac{2\pi}{m\Delta\vartheta\Delta\omega})^2}, \qquad \lambda_m=\frac{1}{2\pi}\frac{q^2N\rho}{Ma^2\Omega}\frac{K_{fb}}{m_{max}}.$$

It is clear that a maximum decrement δ_{max}, is obtained when $\lambda_m \frac{2\pi}{\Delta\vartheta\Delta\omega m} = 1$. In this case

$$\delta_{max} = \frac{m^2_{max}\Delta f\Delta\vartheta}{2\pi N} \qquad (18)$$

This expression determines the possibility of using a feedback system for cooling the particles' transverse oscillations. It can be shown that the same expression defines the possibility of the stochastic cooling of the particles' longitudinal motion as well. This is understandable because in both cases the mixing mechanism is the particles revolution frequency spread.

In conclusion, let us make an estimate of a noise power of the beam particle center of gravity fluctuations on the pickup output when the feedback is off.

$$P_{in,beam} = \frac{1}{\rho}\left(\frac{Nq\rho\omega_0}{a}\right)^2 \sum_m \overline{x_m^{src}(t)x_{-m}^{src}(t)}.$$

After averaging for the one octave feedback frequency bandwidth we have

$$P_{in,beam} = \frac{N}{\rho}(qf_0\rho)^2 \frac{\langle \Delta x^2 \rangle}{a^2} \frac{2\pi}{\Delta\vartheta} \frac{m_{max}}{2},$$

where $\langle \Delta x^2 \rangle$ - rms of the betatron beam size.]

The noise power of the electronics on the pickup output is determined by the well known expression

$$P_{in,el} = 4kTf_0F_n \frac{m_{max}}{2},$$

where F_n is the electronics noise figure.

The following are the values relevant for RHIC:

Revolution frequency, kHz	78
Tunes, ν_x/ν_y	28.18/29.18
Ion (gold) beam energy spread	$4*10^{-4}$
Ion beam revolution frequency spread	$5*10^{-7}$
Number of the ion per bunch	10^9
Ion energy per nucleon, GeV	100
Ion beam length, m	0.3
Average betatron beam size, m	$4.5*10^{-4}$
Feedback frequency band, GHz	3÷6
Maximum decrement,sec^{-1}	$1/10^5$

$P_{in,beam}$, W	$3*10^{-9}$
$P_{in,el,}$ W	$2*10^{-10}$
Feedback gain	$3*10^{4}$

Conclusion. As one can see the maximum decrement of the cooling of the transverse particles motion as well as longitudinal one is of the order of 30 hours. The beam lifetime in colliding mode at RHIC is about 10 hours. It is obvious that in this case stochastic cooling is not effective.

References

1. N.I. Zinevich, M.M. Karliner. Kinetic equation of the stochastic cooling of the longitudinal momentum spread. 8 international proceeding on high energy accelerators, Protvino, 1982.
2. 2.Yu.l.Klimontovich. Kinetic theory of a non-ideal gas and non-ideal plasma. Moscow, 1975.

8. CONSIDERATIONS TOWARDS A CDR

The electron cooling of RHIC will take a very large step in energy compared with conventional electron cooling. The highest electron energy cooler now is CELSIUS, at about 300 kV. An experiment with a high energy, high current electron beam, but without cooling, was made at BINP many years ago, reaching an energy of 1MeV with an electron current of 1A. The Fermilab electron cooling project for antiprotons, at an electron energy of 5 MeV, is now under development and results should be clear in 3-4 years. RF-type accelerators for FEL experiments with very high brightness electron beam and with energy in the range of 10-50 MeV are now under development in many laboratories. However, for electron cooling we need a magnetized beam and for the generation of this beam in a magnetic field precludes using a superconducting electron gun. At the same time, a high voltage CW copper cavity gun is very large and expensive.

Key items and some comments for the CDR study.

For this project the parameters of the electron gun should be:

a. Repetition frequency 4.6 MHz,
b. Number of electrons per bunch $N_e=10^{11}$, charge 16 nC,
c. Pulse length 1-4 ns,
d. Peak current Je=4-16 A,
e. The cathode of the electron gun should be immersed in a magnetic field of about 100 G.

The electron emission control may be a grid control or a semiconductor photocathode cathode under laser beam control. The laser system for this electron gun needs R&D because of the very high charge of 16 nC. The final decision should be made between the version of injection system based on DC acceleration system or low frequency RF cavity. For low beam intensity of 10^{10} –$3x10^{10}$ electrons per bunch, an energy of 2 MeV is enough but for a high intensity beam, 10^{11}, it is required to upgrade the injection energy to 4-5 MeV.

1. Development of the electron gun and initial accelerator.
   a. Development of the electron DC accelerator.
   b. Development of the low frequency CW cavity for acceleration.
   c. Development of the photocathode of the gun.
   d. Development of the laser system.

2. Development of the accelerator and beam transport elements:
   a. Development of the debuncher - rebuncher beam transport elements and cavities with a detailed 6-D simulation of the electron beam dynamics.
   b. Demonstration of the energy recovery linac at the current of the cooler and with appropriate beam performance.

c. Investigation of feedback techniques for stabilizing the linac.
d. Detail development of magnetized electron generation and transport. The development of alternative approaches for the transport of a flat or a round (magnetized) beam.

3. Development of the solenoid
a. Development of the high-precision superconducting solenoid
b. Development of magnetic field measuring techniques for a superconducting, high precision solenoid
c. Development of the beam matching sections at either end of the solenoid.
d. Development of electron / ion beam diagnostics for the solenoid section.

4. Cooling theoretical studies:
a. Control of the longitudinal / transverse cooling decrement
b. Shaping the 6-D beam by control of the electron beam
c. Optimization of the cooler parameters
d. Beam-Beam effect under electron cooling
e. Coherent effects in the system of ion bunches –the cooling electron beam
f. An experiment with cooling in high magnetic fields and high transverse electron beam temperature in a low energy cooler (if possible to find time for these experiments on existing ring CELSIUS, GSI, Indiana).
g. Theoretical and experimental investigation of IBS.

Electron beam generator in experiment at BINP

A high-power infrared free electron laser is under construction in Novosibirsk. The list of parameter of this device is shown in table1.

Table 1. Main parameters of FEL device at BINP (Novosibirsk)

Machine itself:		
RF accelerating frequency, MHz		180
Number of RF-cavities		16
Amplitude of accelerating voltage per cavity, MV	up to	0.8
Total RF-power, MW	up to	1.2
Injection and extraction energy (full), MeV		2
Accelerated beam:		
Bunch repetition rate, MHz	up to	22.5
Average electron current, mA	up to	50
Electron energy, MeV	up to	100
Electron energy spread (relative)		10^{-3}
Bunch duration, ps		10...20
Peak current, A		100...200

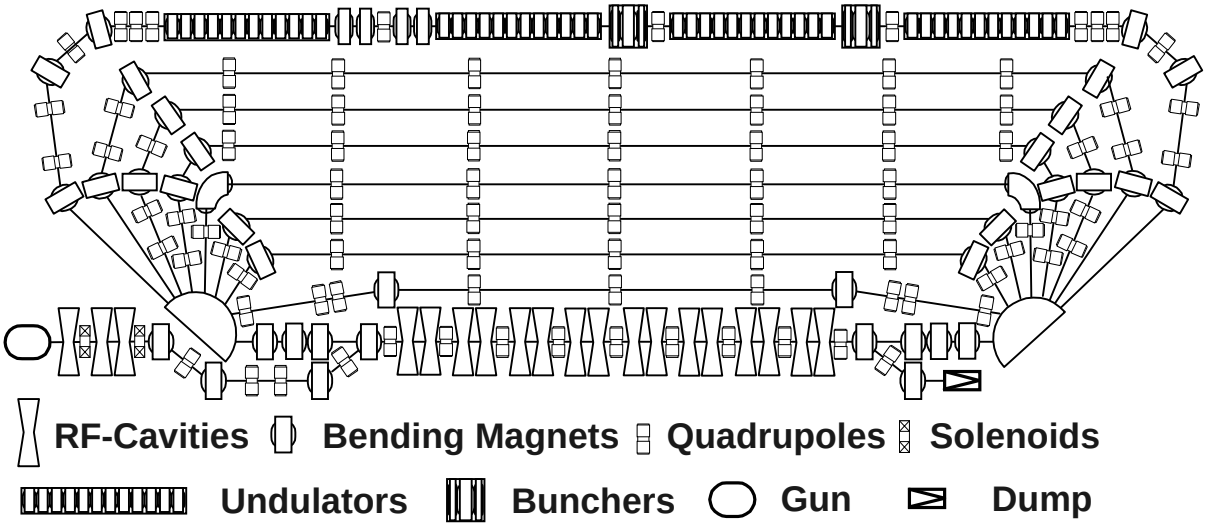

Figure 8.1. The sketch of FEL device at BINP Novosibirsk

The first stage of this project with one turn of electron beam should be commissioned in 2001. Within the frame of this project, it is possible to have collaboration for the development of common elements of BNL cooler system and FEL at BINP:

1. A 2-MeV thermionic electron gun with a solenoid and a beam shape converter.
2. A RF-buncher with bunching RF-cavities, RF-generators, and bending magnets.
3. RF-cavities and RF-generators for compensating the correlated energy spread gained in the main accelerating structure and necessary for debunching.
4. RF-cavities and RF-generators for compensating the cubic term of correlated energy spread gained in the buncher.
5. Magnetic elements (lenses, bending magnets, solenoid) for the whole machine.
6. RF-generators for the main accelerating structure.

R&D according to the mentioned items

1. Gun
    - A prototype of the cathode-grid unit with a manipulator.
    - Beam measurements in the ready machine used as a prototype.
    - A prototype of a 2-MeV power supply and accelerating tube.
    - Numerical simulation of electron motion in the gun and the beam shape converter (3D, transient, space charge effect).
    - A prototype of the beam measurement system (emittance, dispersion function, energy spread, time structure)
2. Buncher
    - Numerical simulation of the bending magnet with gradient and sextupole correction (3D).
    - Numerical simulation of electron motion in the buncher (3D, transient, space charge effect).
    - Prototypes of RF-cavities and RF-generators of the buncher.
3. Prototypes of the compensating RF-cavities and the RF-generators.
4. Prototypes of the compensating RF-cavities and the RF-generators.

5. Numerical simulation of the magnetic elements and electron motion through the whole machine.
6. A prototype of the RF-generators.